CARBON SEQUESTRATION IN CONCRETE

A Thesis

Presented to the Faculty of the Graduate School

of Cornell University

In Partial Fulfillment of the Requirements for the Degree of

Master of Science

by

Wei Cheng

May 2016

ABSTRACT

Concern for the environmental impact of increased carbon dioxide in the atmosphere has focused attention on reducing emissions of both natural and industrial carbon dioxide. This thesis explores a method for inhibiting or preventing the oxidation of carbon in plant material by encapsulating biomass in a mortar composed of portland cement, natural sand, and water. The particular biomass in question is bio-char, a pulverized charcoal produced from the pyrolysis of timber cut down due to insect infestation. While some carbon was oxidized during pyrolysis, unless encapsulated to prevent contact with oxygen, the balance of the carbon would eventually form carbon dioxide. Sequestering carbon in a portland cement binder likewise offsets carbon footprint associated with cement production (an essential ingredient in concrete) However, bio-char is a non-traditional ingredient in mortar and concrete with a heretofore unknown impact on the material performance in both the fresh and hardened states.

To evaluate the impact of bio-char on fresh and hardened cementitious materials, the bio char was first characterized for particle size distribution, density, and absorption. Mortars were prepared with portland cement, natural sand, and water, with varying percentages of replacement of sand with biochar. Workability was measured via the mortar flow test, air content estimated by the Chace Air Indicator, and hardened mortar evaluated at 1 to 56 days via density, compression strength, and splitting tensile strength. For all mixtures water content was adjusted to maintain a fixed mortar flow.

This thesis concentrates on the demonstration and investigation of the impact on mechanical performance including compressive and splitting tensile strength of bio-char mortar when workability of mortar mixture is controlled. The environmental benefit is estimated by means of the author's "carbon sequestration potential", and the trade-off between mechanical performance and environmental benefit demonstrated. Various models are proposed to support hypotheses for the influence of bio-char on mortar behavior.

This work has shown that with the workability controlled, compressive and splitting tensile strength decreased exponentially as bio-char content increases. Carbon sequestration potential increases, however with bio-char content, such that production of cementitious materials for various applications is potentially viable for carbon neutral to carbon negative.

BIOGRAPHICAL SKETCH

The author was born in Taipei, Taiwan on October 22, 1991. His family moved to Shanghai, China a few years later, where he attended Shanghai Weiyu High School, and graduated in 2009. He spent the next four years attending the Hong Kong University of Science and Technology, earning a Bachelor of Engineering in Civil and Structural Engineering. He then was admitted by the Cornell University Graduate School, and moved to Ithaca, New York in the summer of 2013. In the following three years, he studied and worked on his Master of Science thesis in the Civil and Environmental Engineering Department, and in May, 2016 completed his M.S., majoring in Structural Engineering with a minor in Sustainable Design.

ACKNOWLEDGEMENTS

There are a number of people who I would like to thank for their help and support during the completion of my work. First, I would like to give a very special thanks to my committee chair and advisor, Professor Kenneth Hover, for his advice and enthusiasm during my research. He has been a great friend, and gave much time to point me in productive direction for my research. I would also like to thank Professor Jack Elliott, my minor advisor, for without whom, I would never have had the chance to be a part of the project and to complete my degree. He provided the ideas and inspirations, as well as the financial and academic support for this endeavor.

I owe a big thank you to Mr. James Gaspard from Bio-char Now, Berthoud Colorado, who graciously provided and the bio-char product I used for the experimental program. In addition, I would also like to thank Mr. Tim Bond, of the Winter Laboratory, Cornell University, Ithaca, New York. I very much enjoyed my time working in the lab with Mr. Bond who instructed and taught me valuable lessons for performing lab procedures. I would also like to express my appreciation to Dr. Changhoon Lee from Department of Civil and Environmental Engineering, Cornell University, and Mr. Mark Riccio and Ms. Teresa Porri, both from Institute of Biotechnology, Cornell University. Dr. Changhoon Lee provided much insight on concrete studies during completion of my thesis. Mr. Mark Riccio and Ms. Teresa Porri were also extremely helpful in answering my questions on X-ray computed tomography.

The experimental portion of this project was substantial, and its successful completion was only possible because of several people. I would like to thank my classmate Shule Hou, for his help with my experiment that largely eased my burden in completing the experiments within the required timeframe. Thanks also to my officemate Haoran Zhao, for without his help, I would not be able to complete my thesis writing.

Of course I continue to and will always owe thanks to my friends, both those at Cornell and those scattered around the world, and my family for their unconditional love and support. To all of you, my deepest thank-you for always being there.

TABLE OF CONTENTS

LIST OF FIGURES

Chapter 2. Background

Chapter 3. Material Characterization of Bio-char

Chapter 4. Experimental Plan and Methods

Chapter 5. Experimental Results

Chapter 6. Analysis and Interpretation of Results

Chapter 7. Conclusion

Appendix A: Acquire Density Value from CT Scans

Appendix B: Derivation of Absorption

LIST OF TABLES

Chapter 3. Material Characterization of Bio-char

Chapter 4. Experimental Plan and Methods

Chapter 5. Experimental Results

CHAPTER 1

INTRODUCTION

1.1 Research Objectives

Concern for the environmental impact of increased carbon dioxide in the atmosphere has focused attention on reducing emissions of both natural and industrial carbon dioxide. This thesis explores a method for inhibiting or preventing the oxidation of carbon in plant material by encapsulating biomass in a mortar composed of portland cement, natural sand, and water.

Sequestering carbon in a cementitious composite has the duel benefit of likewise off-setting the carbon footprint associated with the production of portland cement. As detailed in Chapter 2, there continue to be many attempts to mitigate the environmental impacts associated with the use of cementitious materials. For example, ground-granulated blast furnace slag, coal fly ash, geopolymers, and crushed glass, among other materials, have been incorporated into cementitious products as cement substitutes to reduce cement content in the mixture, thereby reducing its carbon footprint. Other techniques such as carbon storage by carbonation curing in CMU production, approaches the problem by recycling cement kiln CO_2 in a beneficial manner.

The approach of this thesis is to encapsulate bio-char in mortar. The bio-char in question is a pulverized charcoal produced from the pyrolysis of timber cut down due to insect infestation, which is a carbon-rich substance.

The goal is to sequester carbon in the form of bio-char into portland cement based mortar, to evaluate the mechanical properties of bio-char mortar and to report potential tradeoff between the reduced mechanical properties and the theoretical quantity of carbon that is sequestered into mortar in the study.

1.2 Research Problems

Before this thesis, the physical properties of bio-char as pertain to its use in a cementitious composite material had not been thoroughly investigated. As will be reported in Chapter 2, the properties of bio-char are varied and related to the original biomass material that is made from. The issue of characterizing the bio-char for use in mortar is addressed in this study. The properties including the density and the moisture absorption of bio-char that are crucial to mortar mixtures are quantified by ASTM test standards, or self-developed methods exclusively for charactering the bio-char.

When bio-char, a non-traditional mortar ingredient, is involved, the process of mixing, casting, curing, testing and using bio-char mortar was evaluated and customized to tackle the problems due to the absorption of bio-char in mortar mixture. The details of the experimental procedure are further explained in Chapter 4.

It is also necessary to answer the question of how bio-char affects fresh and hardened mortar behavior, and how much carbon can be encapsulated. Only by reporting the change of mortar properties caused by introduction of the bio-char, can the pros and cons of sequestering carbon into cementitious material be compared.

1.3 Project Scope and Plan

The scope of this project includes:

- Characterizing bio-char materials
- Developing an experimental program for bio-char mortar
- Reporting behaviors of bio-char mortar
- Analyzing effects observed in bio-char mortar

The variables for the experimental program (mixing, casting, curing, and testing) are bio-char content (as a substitute of sand) and curing duration. Mortar specimens are mixed and cast with designed proportions to maintain a constant flow (workability). Bio-char replaces sand in seven increments from 0 to 100%. All specimens are cured in a sealed condition at a constant temperature. The mortar specimens are tested for compression strength and splitting tensile strength at ages-after-casting of 1, 7, 28 and 56 days. The details of the overall plan and the development of the plan are further described in Chapter 4.

1.4 Overall Results

The experiment results shown in Chapter 5 indicate that as the bio-char content increases, more water is required for mortar mixtures to maintain target workability. Also, the density, and compressive and splitting tensile strength of bio-char show a reducing trend as the bio-char content increases. The compressive and tensile strength of bio-char mortar is generally less than that of traditional mortar without bio-char. On the other hand, increasing bio-char content increases carbon sequestration potential. The details of results and interpretation are included in Chapter 5 and Chapter 6.

1.5 Introduction to Applications and Future Work

Given that the introduction of bio-char reduces compressive and tensile strength, structural materials are likely not an ideal application for bio-char mortar. Controlled Low-Strength Material (CLSM) and masonry mortar are more likely examples of successful applications with high carbon sequestration potential.

CHAPTER 2

BACKGROUND

2.1 Sustainable Building Materials

More than any other industry, the building industry is affected by the ongoing sustainability debate [O'Brien, Wallbaum, & Bleischwitz, 2011]. The statistics [EIA, 2008] indicated that, in the United States, building industry accounts for 39 percent of total energy use, 38 percent of the CO_2 emissions. The built environment has a vast impact on the natural environment, human health, and economy. And thus, the sustainability of the building materials is imperative to the well-being of our planet and to the human development.

According to the World Commission on Environmental and Development of the United Nations, sustainability means meeting the needs of the present without compromising the ability of the future generations to meet their own needs [UNFCCC, 2004]. By extension, the sustainable building materials are composed of renewable, that are environmentally responsible because impacts are considered over the life of product [Spiegel & Meadows, 1999].

In the study of Jong-jin Kim [1998], "Sustainable Architecture Module: Qualities, Use, and Examples of Sustainable Building Materials", the green features of sustainable materials were summarized.

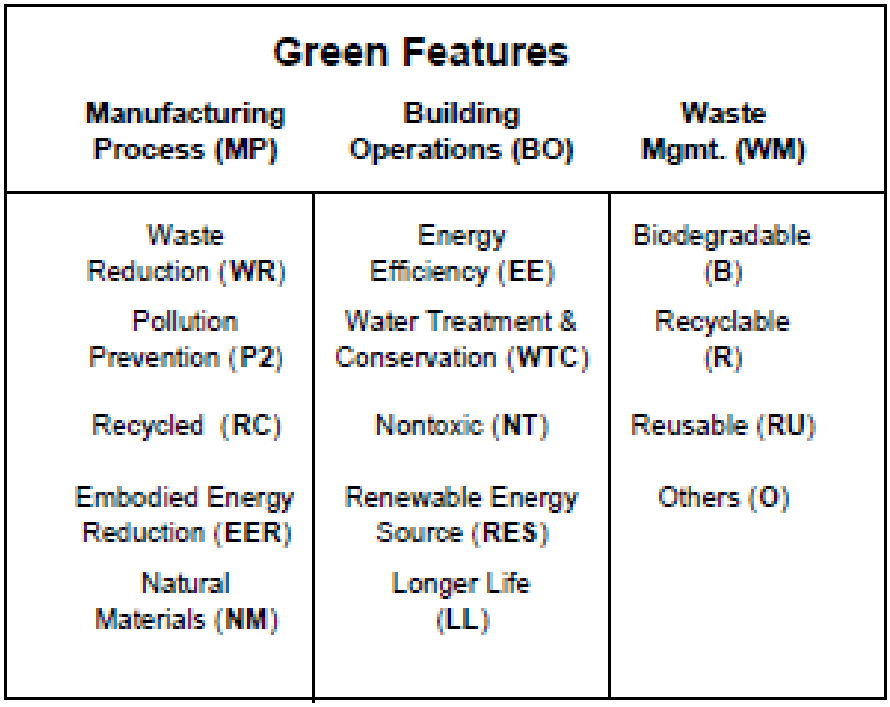

Figure 2.1 Green Features [Kim, 1998]

The environmental material selection criteria recommended by Lynn M. Froeschle [1999], in Environmental Assessment and Specification of Green Building Materials, further refined that low toxicity, minimal emission, low-volatile organic compound (VOC) assembly, recycled content, resource efficiency, recyclability, improving indoor air quality (IAQ), healthfully maintenance, local availability and affordability are the features of sustainable building materials. The presence of one of more of these features in building materials can assist in determining if it is relatively environmentally sustainable.

2.2 Sustainability and Portland Cement and Concrete

As defined by the US Environmental Protection Agency (USEPA)[2009], "portland cement is a fine powder, gray or white in color, that consists of a mixture of hydraulic cement materials comprising

primarily calcium silicates, aluminates, and aluminoferrites." Cements are binding agents in concretes and mortars. Portland cement manufacturing begins with the pyro-processing of clinker followed by fine grinding of the clinker with gypsum and other additives to make the finished cement product [Hover, 2015]. The cement manufacturing flow diagram provided by USEPA is shown as follow.

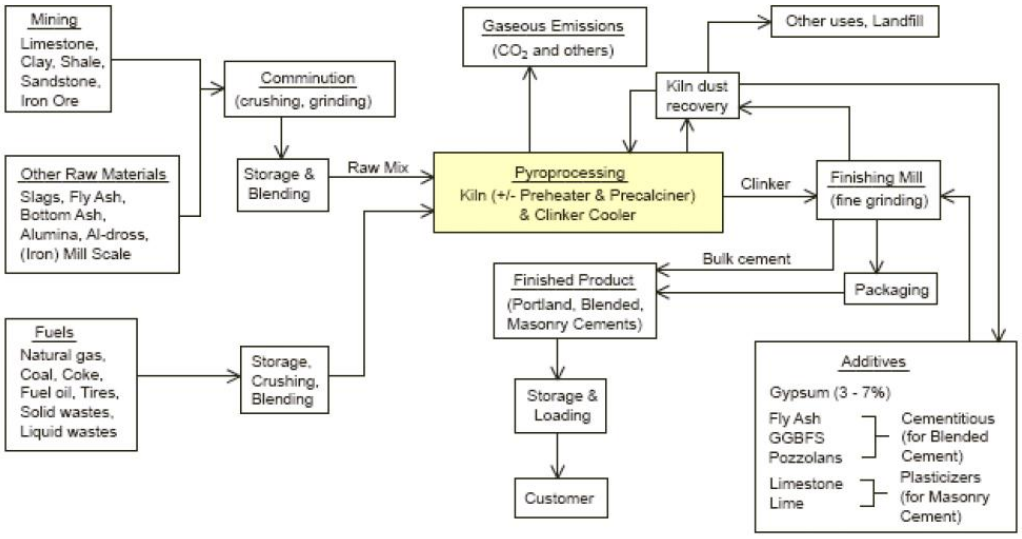

Figure 2.2 Portland Cement Manufacturing Process [USEPA, 1995]

The CO_2 emission from portland cement manufacturing are generated by two mechanisms. As with most high-temperature, energy-intensive industrial processes, combusting fossil fuels to generate process energy releases substantial quantities of CO_2. Substantial quantities of CO_2 also are generated through calcining of limestone or other calcareous material. This calcining process thermally decomposes $CaCO_3$ to CaO and CO_2. In total, the manufacture of cement produces nearly 1 gram of CO_2 for every gram of cement [Nisbet, Marceau, & Van Geem, 2003].

Concrete is an artificial rock-like material produced by mixing coarse aggregate (gravel or crushed stone), fine aggregate (sand), cement, air and water. The cement paste, comprised of cement and

water, binds the aggregate into a solid mass as the paste hardens. The paste hardens because of a chemical reaction between cement and water called hydration. As with any building product, production of concrete also requires energy that in turn results in the generation of CO_2 in addition to that released from production of portland cement.

Water, aggregates, and other ingredients comprise about 95 percent of the volume of a concrete mixture by mass, with the other 5% occupied by air that has become entrapped or intentionally entrained. The amounts of CO_2 embodied in concrete are primarily a function of the cement content in the mix design [NRMCA, 2008].

2.3 Bio-char

Bio-char is a carbon-rich solid residue that is obtained when bio-mass, such as wood or crops, is heated in an enclosed container with little or no air [Lehmann & Joseph, 2009]. Such thermal decomposition of organic material is called pyrolysis [Woolf, Lehmann, Fisher, & Angenent, 2014], during which process the material is heated and decomposed under near zero oxygen (O_2) availability and at relatively low temperatures (<700 °C). This pyrolysis produces non-condensable gases, volatiles, and bio-energy with bio-char as the residual solid.

From a chemical point of view, the defining characteristic of bio-char is its high carbon (C) content, consisting primarily of aromatic compounds characterized by rings of six C atoms linked together without oxygen (O) and hydrogen (H), the otherwise more abundant atoms in living organic matter [Lehmann & Joseph, 2009]. Full and efficient utilization of bio-char has been inhibited due to the

wide range of properties of the output product due largely to the broad range of feedstock and variations in processing [Schmid & Noack, 2000].

The physical properties of bio-char immediately after processing influence use of the material as reported in the book "Bio-char for Environmental Management Science and Technology" [Lehman & Joseph, 2009]. The physical (structural) characteristics are influenced by both the original organic material and the processing conditions. The original structure of most types of feedstock materials is imprinted on the bio-char product [Laine, Simoni, & Calles, 1991] and thus has an overwhelming influence on physical and structural characteristics. During pyrolysis, mass is lost (mostly in the form of volatile organics). Hence, during thermal conversion, the mineral and carbon skeleton retains rudimentary porosity and structure of the original material. The residual cellular structures of botanical origin that are present and identifiable in bio-chars from woods and coals of all ranks contribute the majority of the macro-porosity present [Wildman & Derbyshire, 1991].

Studies of both solid density (true density) and the bulk density (apparent density) were documented in Bio-char for Environmental Management Science and Technology". Solid density is the density on a molecular level, related to the degree of packing of the carbon structure. Bulk density is that of material consisting of multiple particles and includes macro-porosity within each particle and the inter-particle voids. The typical value of solid density of C in bio-chars was reported to range from 1.5 g/cm^3 to 1.7 g/cm^3 [Jankowska, Swiatkowski, & Choma, 1991][Oberlin, 2002]. The maximum value of solid density of C in bio-char was reported to lie between 2.0 g/cm^3 to 2.1 g/cm^3 based on X-ray measurement [Emmett, 1948]. More recent studies [Brown, Kercjer, Nguyen, Nagle, & Ball, 2006] suggested that the Helium-based solid density of bio-char showed direct dependency upon the final pyrolysis temperature, and the solid density was reported to range from 1.4 g/cm^3 to 2.0 g/cm^3.

Byrne and Nagle, [1997] established a linear relationship between the bulk densities of wood and bio-char made from the same material, that bio-char bulk density is 82% of the bulk density of the wood. The bulk densities of bio-char made from different types of woods processed in different types of thermal decomposition processes are reported by Pastor-Villegas et al [2006], and ranged from 0.30 g/cm^3 to 0.43 g/cm^3.

The mechanical strength of bio-char, the ability to withstand wear and tear during use, was reported to be higher than the biomass feedstock that bio-char is made of, supported by the example presented by Byrne and Nagle [1997] that the tulip poplar wood carbonized at high temperature treatment of 1500°C had a 28% increase in strength.

Recent research in the physical properties of bio-char product has been driven by interest in environmental management applications. Focusing on the interaction between physical properties of bio-char and soil systems, and how their properties and influence change over time [Lehman & Joseph, 2009].

The use of bio-char is recommended in various contexts. As early as 1927, Morley [Morley, 1927] wrote in the first issue of The National Greenkeeper that 'Char-coal acts as sponge in the soil, absorbing and retaining water, gases and solutions'. In 2001, Glaser et al, [Glaser, Haumaier, Guggenberger, & Zech, 2001] connected the sustained fertility in soil to bio-char for its high organic C content. Over the past decade, the application of bio-char to soil amendment has acknowledged that the benefits of bio-char go beyond that of merely a fertilizer [Lehman & Joseph, 2009].

2.4 Bio-char and Similar Materials Incorporated into Cementitious Materials

2.4.1 Bio-char in Mortar

Recent research has extended the application of bio-char to promote sustainability and help mitigate the negative environmental impacts caused by carbon emission. A study in Korea [Choi, Yun, & Lee, 2012] has utilized bio-char in the role of a partial replacement for portland cement, in a manner similar to the use of supplementary cementing materials such as coal fly ash, granulated blast furnace slag, or rice-husk ash. The research paper "Mechanical Properties of Mortar Containing Bio-char from Pyrolysis" investigated the experimental results (including the chemical components, microstructure, weight loss, compressive strength and mortar flow) of mortar mixes that varied (mass) replacement rates of cement with hardwood bio-char.

Within all 11 groups of mortar mixes of their study, the mass of sand was kept constant at 3000 grams. The combined mass of cement and bio-char (and fly ash when applicable) was maintained constant at 1000 grams. The rate of bio-char replacement (for cement) was 0%, 5%, 10%, 15% and 20% in terms of mass.

The water cement ratio was set at 0.5, and therefore the mass of water in all the mixes was a constant of 500 grams. The mortar mixes were placed into 2" by 2" cube molds, and cured in moist environment followed by air drying at room temperature. (Details of the curing environment and curing schedule were not included in the paper.) The cube specimens were tested for compressive strength at 14 days, 28 days and 56 days after casting.

The result from the study showed that, firstly, the weight loss (of the mortar cube specimen) over time due to moisture evaporation was found to be less for the mortar mixes that include bio-char

than that for the conventional mix (without no bio-char). The author of the study believed the result indicated that mortar mixes with bio-char replacement (for cement) is more capable of retaining water than mixes that do not include bio-char.

Secondly, it was recognized during the experiment phase that given that the weight of water in the mix design for each study group did not vary with bio-char replacement rate, flow continuously decreased as bio-char content increases. While replacing 5% of the cement with bio-char showed no strength reduction, further increases up to 20% cement replacement led to a 45% reduction in compressive strength. In preparation for the subsequent description of research conducted for this thesis, it must be clear that Choi et al. [Choi et al., 2012] used bio-char as a cement replacement with constant sand content, whereas the work reported in this thesis used bio-char as a sand replacement with constant cement.

2.4.2 Other Material Incorporated into Cementitious Materials

Mortar and concrete can be produced according to various mixture proportions and with different ingredients. Consequently, different production mixture proportions and methods lead to different qualities and different environmental impacts.

According to Slag Cement Association (SGA) [2002], since the late 1800's slag cement has been in worldwide use. Slag, a byproduct of steel manufacturing, can be added to concrete as a cementitious material. Using slag cement in concrete can reduce the amount of Portland cement intended for a specific mixture, depending on application, job requirements and environmental condition. Slag can

replace between 20 to 80 percent of the portland cement used in concrete. The following figure provided by SGA shows the typical ranges of the use of slag cement in concrete.

Concrete Application	Slag Cement as % of Cementitious
Concrete paving	25-50%
Exterior flatwork not exposed to deicer salts	25-50%
Exterior flatwork exposed to deicer salts with w/cm ≤ 0.45	25-50%
Interior flatwork	25-50%
Basement floors	25-50%
Footings	30-65%
Walls & columns	25-50%
Tilt-up panels	25-50%
Pre-stressed concrete	20-50%
Pre-cast concrete	20-50%
Concrete blocks	20-50%
Concrete pavers	20-50%
High strength	25-50%
Alkali-silica reaction mitigation	25-70%
Sulfate resistance: Type II portland equivalence (moderate) Type V portland equivalence (high)	 25-50% 50-65%
Lower permeability	25-65%
Mass concrete	50-80%
Percentages indicate replacement for portland cement by mass. These replacement rates are recommended for individual applications and are based on historical performance. Variations in material sources and environmental conditions may require alternate substitution rates. Consult your slag cement supplier for additional assistance.	

Figure 2.3 Slag Cement Application [SGA, 2002]

The utilization of slag as a cement product substitution recovers the industrial byproduct (slag) when slag is incorporated into concrete, and therefore avoid disposal. From an environmental perspective, the replacement of large proportions of portland cement with slag cement in concrete is beneficial. In the environmental report by SGA, slag cement requires nearly 90 percent less energy to produce than an equivalent amount of portland cement. By substituting 50 percent of portland cement with slag cement, the embodies energy in a cubic yard of concrete is significantly reduced by 30 to 48 percent. In terms of embodied carbon dioxide emissions per cubic yard of concrete, 42 to 46 percent reduction in greenhouse emission occurs. Aside from environmental benefits brought by slag cement, C. Ozyildirim [2010] in his article "Use of Slag Cement for Improved Durability in

Virginia Department of Transportation Structures" indicated that in bridge structures and pavements, slag cement was successfully used to reduce permeability and improve the durability of concrete.

Research led by Clair White at Princeton University [Sustainable Concrete and Carbon Storage Group, 2016] suggests that geopolymers and other alkali-activated cements are low-CO_2 alternatives to ordinary Portland cement-based concretes. The systems use aluminosilicate-rich earth materials (calcined clays such as metakaolin) or waste byproducts (ground granulated blast furnace slag and/or coal-derived fly ash) as main constituents and do not contain any OPC powder in mixture designs. By alkali-activating the aluminosilicate and calcium precursors using hydroxide, silicate and /or carbonated-based activators, the resulting systems possess similar mechanical performance to OPC based systems at a much reduced CO_2 cost to the environment.

Pulverized fuel ash (PFA = "Fly Ash") is another cement admixture. PFA is the ash residue produced by the combustion of powdered coal at high temperature at power station. It is composed of extremely fine, glassy sphere, and looks similar to portland cement. PFA is a pozzolanic material high in silica. The level of PFA replacement in cement is generally not more than 30 percent. PFA will slow the hydration process and the rate of early strength gain, and at the same time beneficially reduce the heat generation of concrete. PFA inclusion can reduce the permeability of concrete and increase sulphate resistance [Bennett, 2010].

Crushed waste glass is also considered as cement replacement. studies by Amirpasha Peyvandi and Parviz Soroushian [2012] indicated that milled glass takes part in a beneficial reaction with cement hydrates, and its reactivity in cementitious systems is enhancing the glass-concrete stronger and

more durable. The use of glass helps reduce the amount of glass that disposes in landfill, and helps to reduce CO_2 emission as well as energy used that is needed to create cement.

CHAPTER 3

MATERIAL CHATACTERIZATION OF BIO-CHAR

3.1 Source of Material

'Bio-char Now' provided all bio-char used in this research project. 'Bio-char Now' is a commercial bio-char processor based in Colorado[1]. The product originated 'Bio-char Now' meets the certification requirements of OMRI (The Organic Materials Review Institute) [OMRI, 2016], USDA (U.S. Department of Agriculture) [USDA, 2016], and EPA (U.S. Environmental Protection Agency).

All bio-char was shipped via UPS to the Winter Laboratory at Cornell University 19.0-liter (0.7-ft^3) plastic bags, packed inside cardboard boxed for protection. The first of two shipments was delivered on 1st May, 2015 and included three bio-char products of different particle sizes classified by the producer as "dust," "small," and "medium." Bio-char products from this first shipment were used for characterization and familiarization. Details of particle size distribution follow.

Figure 3.1 Bio-char Product Stored in 19.0-liter (0.7-ft^3) Plastic Bags

[1] Biochar Now, 1907 Gail, Loveland, CO80537

The second shipment, consisting of 32-kg (70-lb) bio-char "dust" only (of dry "dust" consistency) was delivered on 14th Aug, 2015, just prior to the final mixture experiment. The bio-char "dust" from this second shipment was used for all bio-char mixtures in the final experiment. All the bio-char "dust" from the second shipment came from the same production run to maintain uniformity of the material throughout the final experiment. (Evidence of the consistency of particle size distribution is shown in Table 3.3)

The primary source of timber for the production of all bio-char used in this project was Lodgepole Pine trees from national forests in the mountains of Colorado. The trees had been killed by the Mountain Pine Beetle, and had been cleared from the national forests as part of forest fire fuel reduction stewardship contracts. The timber was converted to charcoal by slow pyrolysis (peak temperature up to 550 °C). Available oxygen during this process was limited to that released from decomposition of biomass. The pyrolysis of each 1.36-tonne (1.5-ton) biomass batch took 8 to 12 hours (longer than industrial average), depending on moisture in the raw feed material and other factors. During pyrolysis, impurities including VOCs and tars were converted to syngas and then removed in an emission control system. There was no chemical treatment applied to the wood. (See Chapter 2 for more background details)

3.2 Storage

The dust, small, and medium bio-char were stored in the Cornell Lab after the shipment, maintained in the sealed plastic bags inside the shipping boxes to minimize change in moisture content or adsorption/desorption of various substances.

3.3 Composition

Compositional analysis of the products from 'Bio-char Now' was performed by Control Laboratory in California[2]. The analytical process for determining the composition of bio-char was certified by International Bio-char Initiative (IBI) [IBI, 2016]. (IBI accredits professional laboratories and has standardized quality control requirements and laboratory procedures.) Analysis results are provided in Table 3.1.

Table 3.1 Composition of Bio-char Product

International BioChar Initiative (IBI) Laboratory Tests for Certification Program

Dry Basis Unless Stated:	Range	Units	
Moisture (time of analysis)	5.6	% wet wt.	ASTM D1762-84 (105c)
Organic Carbon	81.7	% of total mass	Dry Combust-ASTM D 4373
Hydrogen/Carbon (H:C)	0.70 0.7 Max	Molar Ratio	H dry combustion/C(above)
Total Ash	1.2	% of total mass	ASTM D-1762-84
Total Nitrogen	0.32	% of total mass	Dry Combustion
pH value	8.49	units	4.11USCC:dil. Rajkovich
Electrical Conductivity (EC20 w/w)	310 mmhos/cm	dS/m	4.10USCC:dil. Rajkovich
Liming (neut. Value as-CaCO3)	5.1 percent	%CaCO3	Rayment & Higginson

Particle Size Distribution	ASTM D 2862 granular
< 420 um	0.3 percent
420 - 2380 um	8.5 percent
2380 - 4760 um	20.4 percent
> 4760 um	70.9 percent

All units mg/kg dry unless stated:		Results	Range of Max. Level:	Meth. Det. Limit (ppm)	Method
Arsenic	(As)	0.44	12 to 100	0.15	E
Cadmium	(Cd)	0.05	1.4 to 39	0.005	E
Chromium	(Cr)	6.2	64 to 1200	0.015	E
Cobalt	(Co)	< 0.3	40 to 150	0.25	E
Copper	(Cu)	2.4	63 to 1500	0.5	E
Lead	(Pb)	0.22	70 to 500	0.1	E
Molybdenur	(Mo)	< 0.7	5 to 20	0.6	E
Mercury	(Hg)	< 0.2	1 to 17	0.160 ppb	EPA 7471
Nickel	(Ni)	2.6	47 to 600	0.05	E
Selenium	(Se)	0.89	1 to 36	0.25	E
Zinc	(Zn)	6.0	200 to 7000	0.1	E
Boron	(B)	11	Declaration	1	TMECC
Chlorine	(Cl)	842	Declaration	0	TMECC
Sodium	(Na)	72	Declaration	5	E

Basic Soil Enhancement Properties	Results	units	Meth.
Potassium			
Total (K)	703	mg/kg	B
Available (K)	452	mg/kg	C
Phosphorus			
Total (P)	24	mg/kg	B
Available (P)	2.3	mg/kg	C
Nitrogen			
Ammonia(NH4-N)	8	mg/kg	A
Nitrate (NO3-N)	41	mg/kg	A
Organic (Org-N)	3177	mg/kg	Calc.
Volatile Matter	98.8	percent dw	D
Plant Inhibition		See Attached	

Methods

A Rayment & Higginson
B Enders & Lehmann
C Wang after Rajan
D ASTM D1762-84
E EPA3050B/EPA 6010

Analyst: Frank Shields

From the particle size distribution given, the sample tested is similar to the bio-char "small" size shipped to Cornell.

[2] Control Laboratory, 42 Hangar Way, Watsonville, CA95076

3.4 Particle Shape and Size

After pyrolysis, all bio-char products were processed through a "Lump Breaker" followed by sieving over four screens with opening sizes of 3.00, 0.707, and 0.297 mm prior to shipment to Cornell. According to the producer, 100% of bio-char "medium" passes the 3-mm screen but is retained on the 0.707-mm screen. All bio-char "small" passes the 0.707-mm sieve but is retained on the 0.297-mm screen, and all bio-char "dust" passes the 0.297 mm screen. The three bio-char products are shown in Figures 3.2, 3.3 and 3.4.

Figure 3.2 Bio-char "Medium"

Figure 3.3 Bio-char "Small"

Figure 3.4 Bio-char "Dust"

At the author's request, large pieces of bio-char that had not yet been broken and shredded were sent to Cornell for examination. With the help of photography of bio-char products, it can be observed that the bio-char product before breaking and shredding consisted of uniaxial structures. The cleavage of the bio-char block in the picture was apparent.

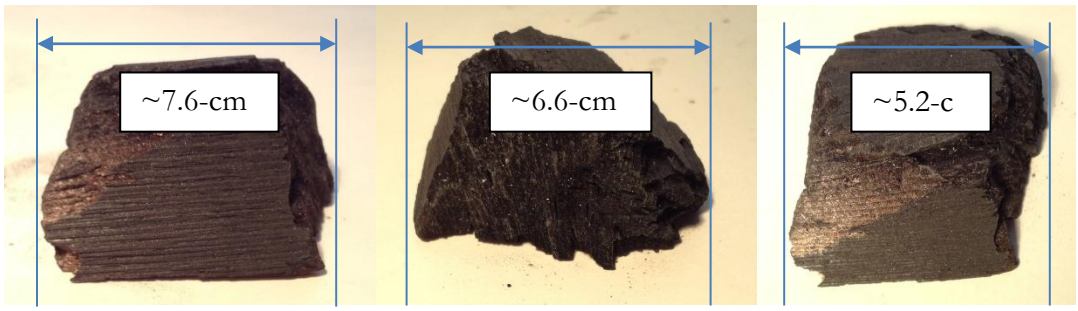

(a) (b) (c)

Figure 3.5 Bio-char Product before Breaking (a) Front View, (b) Side View and (c) Top View

Bio-char "dust" is black, fine "dust". No visible shape or structure can be observed with naked eye. Bio-char "small" and "medium" are black, light, long, thin particles, with visible uniaxial structure. Both bio-char "small" and bio-char "medium" are friable, i.e., easy to break by hand.

The particle size distribution of bio-char "dust", bio-char "small" and bio-char "medium" was determined. Sieve analysis was performed in accordance with ASTM C136 using a mechanical shaker, as shown in Figure 3.6.

Figure 3.6 Mechanical Sieve Apparatus

Initial sieve analysis for materials characterization was performed via ASTM C136. Given the fragility of the bio-char, it was possible that mechanical sieving (a commonly selected option in C136) could break particles and thus modify the particle-size distribution. To examine this hypothesis, 150 to 200g samples were 4 extracted from the bags for each of the 3 sizes of bio-char from the first shipment. These samples were first sieved with relatively gentle hand-shaking only and the results obtained. That entire sample was then returned to the top sieve and the entire sieve-stack was

mechanically shaken. An additional sieve analysis (mechanical shaking only) was performed on the bio-char dust received in shipment #2.

The results of sieve analyses are provided in Tables 5.2 and 5.3. Results are plotted (along with size distribution of the sand used in this study, and the ASTM C33 acceptable range of sizes for concrete sand).

Table 3.2 Sieve Analysis on Bio-char "Dust", "Small" and "Medium"

Sieve #	Particle Diameter (mm)	Sieve Analysis Percent Mass Passing (%)					
		Bio-char "Dust"		Bio-char "Small"		Bio-char "Medium"	
		Hand	Mechanical	Hand	Mechanical	Hand	Mechanical
3/8-in	9.500	100.0	100.0	100.0	100.0	100.0	100.0
4	4.750	99.8	100.0	99.9	100.0	19.0	57.4
8	2.360	99.7	100.0	56.8	94.3	2.7	5.8
16	1.180	93.7	99.7	14.2	51.2	1.0	1.7
30	0.600	38.2	99.3	1.6	12.1	0.2	1.2
50	0.300	7.3	83.3	0.2	4.2	0.0	0.6
100	0.150	0.8	69.0	0.0	3.4	0.0	0.5
200	0.075	0.2	44.6	0.0	2.8	0.0	0.2
Pan	0.000	0.0	0.0	0.0	0.0	0.0	0.0

Table 3.3 Consistency Shown in Bio-char "Dust" Particle Size Distribution

Sieve #	Particle Diameter (mm)	Mechanical Sieve Analysis Percent Mass Passing for Bio-char "Dust" (%)			
		Sieve Sample #1 *	Sieve Sample #2 **	Sieve Sample #3 **	Sieve Sample #4 **
3/8-in	9.500	100.0	100.0	100.0	100.0
4	4.750	100.0	100.0	99.8	100.0
8	2.360	100.0	100.0	99.7	99.8
16	1.180	99.7	99.9	99.6	99.8
30	0.600	99.3	99.6	99.4	99.6
50	0.300	83.3	82.3	85.9	84.8
100	0.150	69.0	67.6	71.8	71.1
200	0.075	44.6	43.4	44.0	45.9
Pan	0.000	0.0	0.0	0.0	0.0

* From 1st shipment

** From 2nd shipment

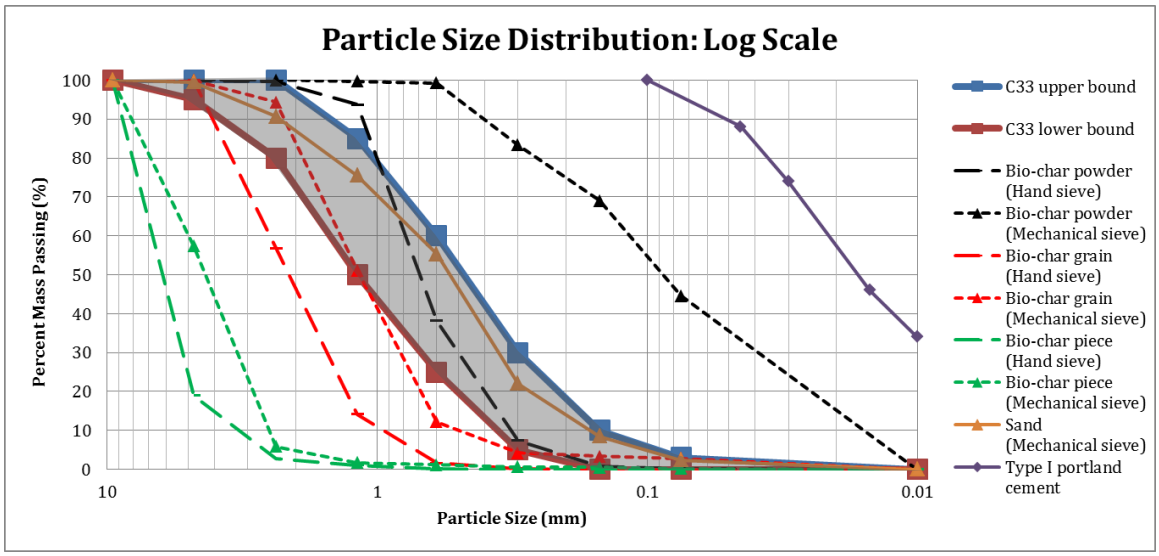

Figure 3.7 Particle Size Distribution of All Materials Considered

The particle size analyses indicate that, first, mechanical sieving has an effect on all three bio-char products, but the magnitude of the effect increases from the medium to the small, and from the

small to the dust. Observations of the individual sieves showed that elongated small and medium particles could pass through an opening only if the elongated axis was perpendicular to the screen. Otherwise long, narrow particles were retained. Observation of the dust, on the other hand, suggested that fine particles tended to agglomerate or clump together. Continued, vigorous shaking by the mechanical shaker could break these agglomerations, producing an apparently finer size distribution in comparison to results obtained by hand-shaking. (Whether the subsequent mixing of the bio-char, sand, cement, and water effectively de-flocculated the dust particles in the actual mortar mixtures is not known.) Thus it appears that the impact of mechanical shaking may not be so much the fracturing of particles during sieving, but in the efficiency with which the mechanical shaker breaks agglomerations of dust particles and rotates elongated particles until they pass through the openings of larger sieves.

Secondly, even after mechanical sieving, bio-char "medium" is coarser than sand meeting the requirements of ASTM C33. Because of this, bio-char "medium" was not considered as a sand-replacement in this study.

After mechanical sieving, the grading curve (red dot curve) of bio-char "small" fell inside the profile of standard concrete fine aggregate specified in ASTM C33, showing the closest resemblance to fine aggregate particle size. This made the bio-char "small" a candidate as a sand-replacement in the mortar study.

Bio-char "dust" is finer than the standard concrete fine aggregate specified in ASTM C33, but coarser than typical Type I portland cement as used in this study. Although finer than standard

concrete sand, bio-char "dust" remained a candidate for sand-replacement, pending the results of pilot tests.

3.5 Specific Gravity and Density

The specific gravity, density, and water absorption of bio-char "dust" and bio-char "small" was first tested using ASTM C128-12 'Standard Test Method for Density, Relative Density, and Absorption of Fine Aggregate'. The test was inconclusive because ASTM C128-12 requires that fine aggregate be soaked in water for 24±4 hours before measurement of density and absorption. Larger particle of the bio-char floated on the water, and finer particles appeared to almost dissolve, producing a black, thick liquid (resembling soup). It appeared, therefore, that the pre-soaking phase of the test was inapplicable.

After pre-soaking, C128 requires that the presumably saturated particles be dried to achieve saturated surface dry condition (SSD) by applying a gently moving current of warm air. (A small hair-dryer is typically used.) This did not work for the bio-char "dust" or finer end of the spectrum for the small bio-char because the lightweight particles were easily blown away by the slightest air current. Furthermore, arrival at the SSD state is identified by when the particles lose their surface water film and hence lose mutual attraction. This critical end-point was difficult to reliably and repeatably identify with bio-char.

As a further complication, it was observed that when mixed with water, some portion of the bio-char settled to the bottom while other portions floated. This simple observation clearly shows that density of individual particles varies from somewhere below to somewhere above the density of

water. For all of these reasons it was therefore concluded that the ASTM C128 procedure was not useful for determining the density or absorption of bio-char.

Figure 3.8 Bio-char "Dust" Soaked in Water for 24 Hours

(a) (b)

Figure 3.9 Bio-char "Small" Soaked in Water for 24 Hours: (a) Side View, and (b) Top View

3.6 CT Scan Technology to Determine Bio-char Density

High resolution X-ray computed tomography (CT) was an alternative method for determining the particle density of bio-char. Bio-char "dust" was sent to Cornell Institute of Biotechnology[3] , where the average particle density of individual particles (total mass of particle divided by bulk volume of particle including all internal pore space) was reported to be 0.70 g/ml (43.7 lb/ft^3). This was determined by computed tomography (CT-Scan) using a GE eXplore CT-120 X-ray image-analysis machine. First, a series of X-ray images were obtained of the bio-char "dust". The color value assigned to each pixel in the image in grey-scale picture is considered to be linearly proportional to its density value. (X-ray penetration is generally inversely proportional to density [Najjar, Aderhold, & Hover, 1986].) The value of bio-char density was thus obtained with the aid of visualization software (ImageJ) to filter the background noise. The method of interpreting particle density through CT scans is described in more detail in Appendix A.

3.7 Absorption

Absorption is defined as the relative change in the mass of oven dry aggregate due to water absorbed in the pore spaces within the constituent particle. This is important because the value of absorption of bio-char will influence the water content in the following experiment. If the bio-char readily absorbs water from the mortar, that will in turn not only reduce the workability or "flow" of the mortar, but will also reduce the water available to hydrate the portland cement, and reduce the volume occupied by free-water between cement, sand, and bio-char particles, the ASTM C128 was not feasible for determining absorption of bio-char.

[3] Cornell Nanobiotechnology Center and Cornell Institute of Biotechnology Imaging Facility, B46, Biotech Building, Cornell University, Ithaca

In the absence of a readily available means to precisely determine the absorption of the bio-char, an approximate method was developed that combined numerical and experimental method, in which successive upper- and lower-bound values were determined until a result was obtained with sufficient accuracy to support the experimental work. The average value of absorption of bio-char thus obtained was 125%. This method, including the derivation of the mass/volume relationships upon which it is based, is described in Appendix B. The derivation assumes a model of a typical particle, and accounts for key variables including the density of the solid structure of the bio-char, internal porosity of bio-char and the fraction of that porosity that is accessible by water. Overall measured density of the fresh and hardened mortar is considered, as is the measured air content.

3.8 Sequestration Potential

This section introduces the term and concept of "Carbon Sequestration Potential" defined as the estimated capacity of the hardened bio-char mortar to prevent subsequent oxidation of the carbon in to CO2, variously expressed relative to a number of compositional values (see Table 3.4). This index assumes that cement and bio-char are the only two ingredients in the bio-char-mortar mixture that have impact on carbon sequestration based on material consideration only. (Other factors such as CO_2 emission by transportation or energy harvest from manufacture of bio-char or etc. are therefore not accounted for this index). It is further assumed that all carbon in the bio-char has the capacity to react upon exposure to O_2 to form CO_2. Finally this index also requires the assumption that there is negligible diffusion of O_2 into the hardened mortar, which effectively and permanently seals the bio-char from oxygen. Discussion of the validity of these assumptions is continued in Chapter 7.

As is reported in Section 3.3, the analysis from Control Laboratory indicated that products from "Bio-char Now" were comprised of 80% carbon. Under the simplifying assumptions just described, there is therefore 0.8 gram carbon in every 1 gram of bio-char.

According to the reaction $C+O_2 = CO_2$, every 1 gram of carbon converts into 44/12= 3.7 gram of CO_2. So, every 1 gram of bio-char could convert into 80%×3.7 = 3.0 gram of CO_2. Such conversion to 3.0 gram of CO_2 is therefore prevented or sequestered for each gram of bio-char incorporated into the bio-char mortar mixtures. In contrast, and as reported in Chapter 2, for every 1 gram of cement manufactured, approximately 1 gram of CO_2 is released. Based on these premises, carbon sequestration potential of any mixture is therefore quantified by defining the following terms listed in Table 3.4.

Table 3.4 Carbon Sequestration Potential in Compositional Values

Term	Definition
Net CO_2 sequestered per unit mass cement used	$\frac{\text{Mass of } CO_2 \text{ sequestered}^* - \text{Mass of } CO_2 \text{ output}^{**}}{\text{Mass of cement used}}$
Net CO_2 sequestered per unit volume mortar used	$\frac{\text{Mass of } CO_2 \text{ sequestered}^* - \text{Mass of } CO_2 \text{ output}^{**}}{\text{Volume of mortar mixture}}$

Gross CO_2 sequestered per unit mass cement used	$\frac{\text{Mass of } CO_2 \text{ sequestered}^*}{\text{Mass of cement used}}$
Gross CO2 sequestered per unit volume mortar used	$\frac{\text{Mass of } CO_2 \text{ sequestered}^*}{\text{Volume of mortar mixture}}$

* By bio-char addition
** By cement production

Figure 3.10 demonstrates one example CO2 sequestration potential for one group of mixture proportions in which 1 part of cement is to 2.75 parts of fine aggregate, and bio-char replacement rate for sand varies from 0% to 100%.

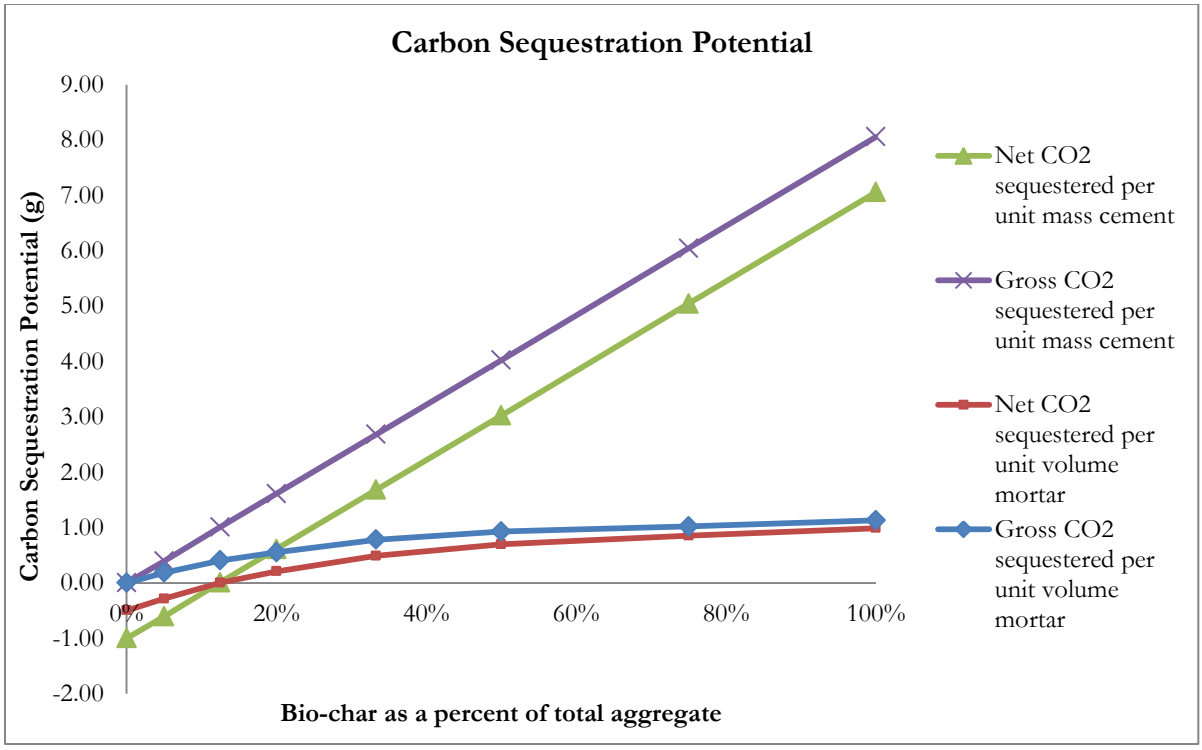

Figure 3.10 Example of Carbon Sequestration Potential

Note that in the Figure 3.10, the both lines of Net CO_2 sequestered per unit mass of cement and per volume mortar used intersect X-axis (at 12.5% in this case). The intersect point indicates that all the CO_2 output (by cement) is offset by all the CO_2 sequestered (by bio-char). The mortar mixture with zero Carbon Sequestration Potential is defined as "Carbon Neutral". All mortar mixtures of carbon positive and carbon negative are accordingly defined as less than or greater than zero Carbon Sequestration Potential.

3.9 Pilot Bio-char Mortar Mixture

Prior to the large-scale bio-char-mortar mixture experiment, pilot bio-char-mortar mixtures were prepared for the purpose of exploring the behavior of bio-char-mortar mixtures and to refine plans and procedures for the more numerous tests to come. Measured behavior included the change of flow (workability) and compressive strength as influenced by bio-char addition.

The pilot bio-char-mortar mixture was mixed with a Hobart N50 tabletop mechanical mixer with a bowl capacity of 4.7-liter (5-quart). (See Figure 3.11.)

Figure 3.11 Hobart N50 Tabletop Mechanical Mixer

The design, mixing and testing procedure of pilot bio-char mortar was consistent with the experimental method described in Chapter 4. All the mortar cylinders for the pilot test were cast and sealed (as described in Chapter 4) and cured for 7-days at an ambient temperature of 20 to 23 °C (68 to 73 °F). One interesting option explored in the pilot tests was the idea of pre-soaking the bio-char dust in water (generating the black soup noted earlier), and then introducing that water-bio-char slurry into the mixer along with cement and sand. As summarized below, this resulted in a slight strength increase compared to addition of bio-char as dry powder, but this result may be misleading. It proved to be so difficult to scrape all of the bio-char slurry out of the pre-soaking container that considerable bio-char remained in that container. The apparent strength increase may be the result of an actual decrease in bio-char addition. 5 sets of pilot bio-char-mortar mixture were studied. The results are shown in the Table 3.5.

Table 3.5 Pilot Bio-char-mortar Mixtures Test Summary

Pilot bio-char mortar mix	Cement (g)	Sand (g)	Bio-char (g)	Initial batch water (g)	Additional water (g)	Flow (%)	7-days compressive strength (MPa)
0% bio-char "dust"	740	2035	0	359	0	85	41.6
5% bio-char "dust"	740	1935	100	359	100	82.5	38.1
5% bio-char "dust" (pre-soak)*	740	1935	100	359	100	85	41.5
5% bio-char "small"	740	1935	100	359	100	82.5	26.8
100% bio-char "dust"	182	0	500	88	625	80	0.6

* pre-soak indicated that 100 gram bio-char was in contact with 359 gram water 24 hours in advance to the mix. The 359 gram water was intended for the initial batch water.

The pilot test results revealed that, first, pilot bio-char-mortar mixture indicated that in order to keep the flow constant with or without bio-char, for every gram of bio-char "dust"/ "small" added in the mixture, additional 1 to 1.25 gram of water required for target flow value of 100%, which suggested the absorption of bio-char "dust"/ "small" was in the neighborhood of 100% to 125%.

Secondly, it was feasible to produce 100% bio-char-mortar mixture while maintaining the target flow value of 100%.

At the 5% bio-char replacement level, use of bio-char "dust" increased the 7-days compressive strength by 42% as compared to the same mass of bio-char "small".

By pre-soaking bio-char "dust", an 8.3% increase in 7-days compressive strength was observed in 5% bio-char "dust" mixture. (See fuller discussion above.)

The soaking experiment also showed that bio-char was able to absorb 125% of its own mass within in course of 7-days.

3.10 Summary

Based on the findings in this chapter, bio-char "dust" is considered to be the optimal choice for use in the experimental program, for the reason that it provides the potential to create bio-char mortar with higher strength compared to bio-char "small".

It is also determined that the experimental program would not consider pre-soaking for the inconvenience to collect all the bio-char "dust" on the wall of pre-soaking container. In future experiments it may be useful to consider alternative methods for batching with pre-soaked bio-char.

CHAPTER 4

EXPERIMENTAL PLAN AND METHODS

4.1 Experimental Plan

4.1.1 Overall Purpose

The experimental program was designed to produce workable bio-char mortars and to observe the compressive and splitting tensile strengths as a function of a variable bio-char replacement of natural sand. The program was also designed to track the strength development of bio-char mortar beyond the conventional 28 days to observe longer-term properties as the rate of strength-gain diminished.

4.1.2 Overall Plan

Mortar mixtures were batched with a fixed mass of aggregate composed of a blend of natural sand and bio-char "dust", and variable water content so as to maintain a constant flow (workability) of all mixtures. The mass ratio of (bio-char) to (total sand plus bio-char) was varied in seven increments from 0 to 100%. Cylindrical specimens were cast with and cured in a sealed condition at a constant temperature. Mortar specimens were tested for compression strength and splitting tensile strength at ages-after-casting of 1, 7, 28 and 56 days.

8 sets of bio-char-mortar mixture proportion were cast: 0%, 5%, 12.5%, 20%, 33.3%, 50%, 75% and 100% bio-char as a fraction of the total aggregate mass. Samples were cured for 1, 7, 28 and 56 days prior to compressive and splitting tensile strength testing. Six replicate specimens were produced for each desired data point. The overall plan is summarized in the Table 4.1(a) and (b).

Table 4.1(a) Overall Plan of Full-scale Cylinder Production for Test Age of 1- and 7-days

Bio-char as a percentage of total aggregate	Number of specimen			
	Curing duration			
	1-day		7-days	
	Compressive strength test	Splitting tensile strength test	Compressive strength test	Splitting tensile strength test
0%	6	6	6	6
5%	6	6	6	6
12.5%	6	6	6	6
20%	6	6	6	6
33.3%	6	6	6	6
50%	6	6	6	6
75%	6	6	6	6
100%	6	6	6	6

Table 4.1(b) Overall Plan of Full-scale Cylinder Production for Test Age of 28- and 56-days

Bio-char as a percentage of total aggregate	Number of specimen			
	Curing duration			
	28-days		56-days	
	Compressive strength test	Splitting tensile strength test	Compressive strength test	Splitting tensile strength test
0%	6	6	6	6
5%	6	6	6	6
12.5%	6	6	6	6
20%	6	6	6	6
33.3%	6	6	6	6
50%	6	6	6	6
75%	6	6	6	6
100%	6	6	6	6

In total, 384 specimens were cast; 48 specimens for each batch. Ingredients for all 384 specimens were from the same shipment to minimize source variation. All specimens were cast over a 4-day

period to minimize the variability of materials and laboratory environmental conditions. The sequence of casting was: 0% and 5%, then 12.5% and 20%, then 33.3% and 50%, and 75% and 100% on the fourth day.

4.2 Materials

4.2.1 Bio-char

Material characterization of bio-char is covered in Chapter 3.

4.2.2 Cement

4.2.2.1 Source

ESSROC (LaFarge) Type I portland cement used in this research project. The material complies with ASTM C150 'Standard Specification for Portland Cement'. In total, four 43-kg (94-lb) bags of cement were purchased. All cement was purchased and delivered on 14th August, 2015, to minimize the source variation.

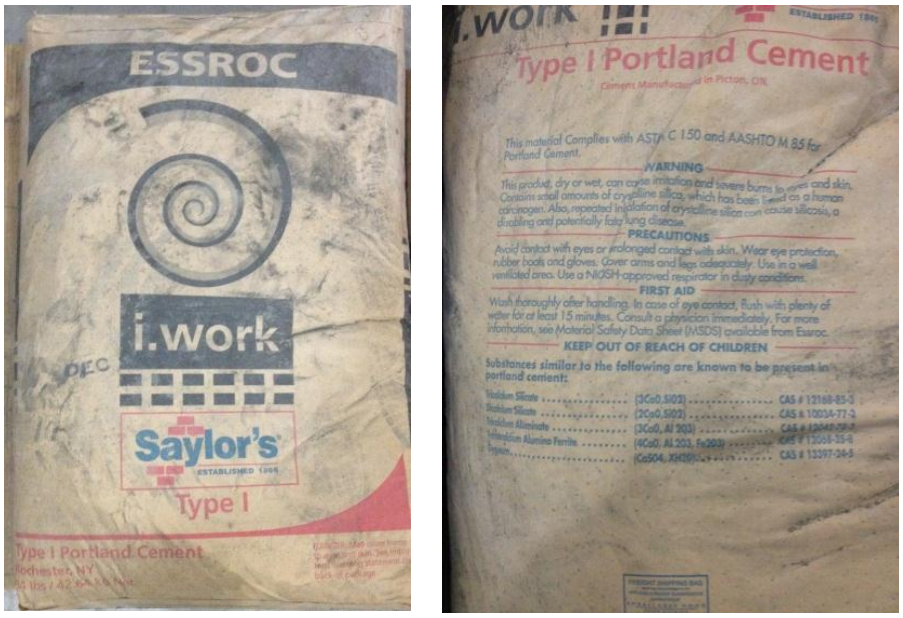

(a) (b)

Figure 4.1 Cement Packaging (a) Front and (b) Back

4.2.2.2 Storage

Cement was stored in the Winter Laboratory at Cornell University. When a bag of cement was opened, the bag of cement was emptied into a 114-liter (30-gallon) plastic trashcan kept covered with a snap-on plastic lid except when mortar was being batched. The cement that was not being used at the time was kept unopened in the bag stacked on a pallet. This minimized exposure to moisture, and therefore maintained the quality of cement over the duration of the project. The project consumed no more than 3 bags of cement over the four days of mixing and casting.

Figure 4.2 One Hundred and Fourteen Liter (30-Gallon) Plastic Trashcan

4.2.2.3 Characterization

The cement used in this research project was assumed to have a density of 3.15-g/ml (197-lb/ft^3).

4.2.3 Sand

4.2.3.1 Source

The sand use for this project was ASTMC33 standard concrete sand, and obtained locally from Saunders Concrete. On 14th August, 2015, 408-kg (900-lb) sand was ordered and delivered to the Winter Laboratory at Cornell University

4.2.3.2 Storage

The sand was stored in the Winter Laboratory at Cornell University. The sand was contained in four 114-liter (30-gallon) plastic trashcan since it was batched from Saunders Concrete. The containers were always covered with plastic lids except when mortar was being batched. The project consumed no more than 2 bins of sand.

4.2.3.3 Characterization

4.2.3.3.1 Particle Size Distribution

The particle size distribution was determined using ASTM C136-06 'Standard Test Method for Sieve Analysis of Fine and Coarse Aggregates'. In the process, a mechanical sieve shaker was used. Photo of mechanical sieve shaker are shown in Figure 4.3.

Figure 4.3 Sieve Stack and Mechanical Sieve Shaker

The particle size distribution test was performed 3 times on 2 samples from 2 different storage bins.

Table 4.2 Sieve Analysis Result for the Sand

Sieve #	Particle Diameter (mm)	Sieve Analysis Percent Mass Passing for Sand (%)
3/8-in	9.500	100.0
4	4.750	99.5
8	2.360	90.7
16	1.180	75.5
30	0.600	55.4
50	0.300	22.0
100	0.150	8.5
200	0.075	2.3
Pan	0.000	0.0

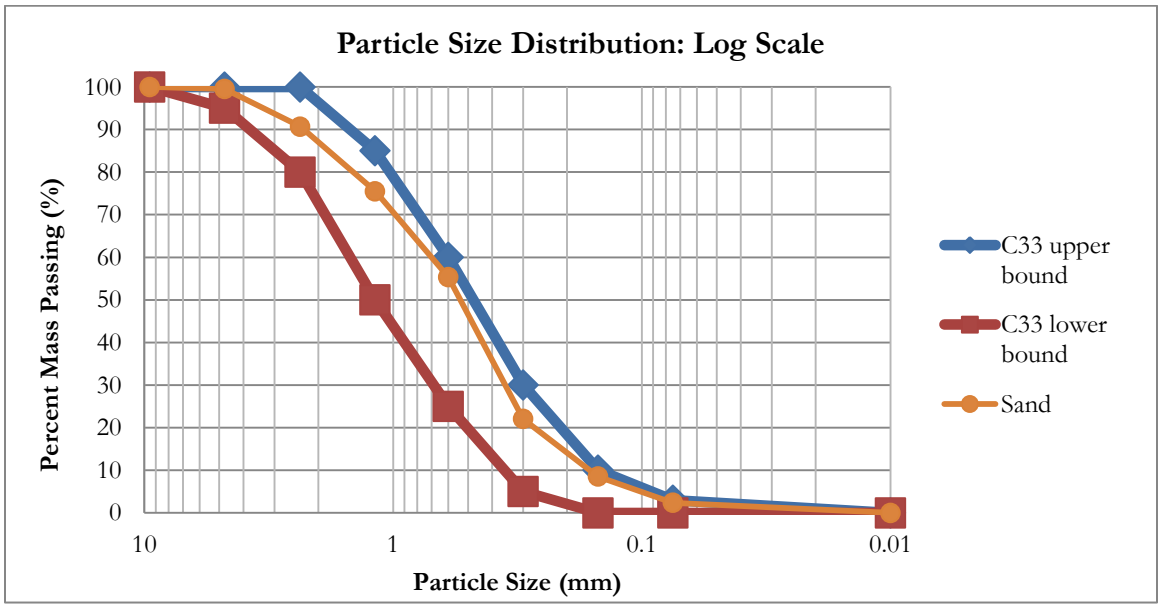

Figure 4.4 Particle Size Distribution for the Sand

4.2.3.3.2 Specific Gravity, Density and Absorption

The specific gravity, density and absorption were determined using ASTM C128-12 'Standard Test Method for Density, Relative Density (Specific Gravity), and Absorption of Fine Aggregate'.

Table 4.3 Specific Gravity, Density and Absorption Result

Sand characterization		Test 1		Test 2	
Mass of oven dry (OD) specimen	=	484.2	g	486.5	g
Mass of pycnomemter filled with water, to calibration mark	=	1135.8	g	1132.8	g
Mass of pycnometer filled with specimen and water to calibration mark	=	1448.0	g	1443.2	g
Mass of saturated surface-dry (SSD) specimen	=	500.0	g	500.0	g
Relative density (specific gravity) (OD)	=	2.58	g/ml	2.57	g/ml
Relative density (specific gravity) (SSD)	=	2.66	g/ml	2.64	g/ml
Apparent relative density (apparent specific gravity)	=	2.82	g/ml	2.76	g/ml
Density (OD)	=	2.58	g/ml	2.57	g/ml
Density (SSD)	=	2.66	g/ml	2.64	g/ml
Apparent density (SSD)	=	2.82	g/ml	2.76	g/ml
Absorption,%	=	3.26	%	2.77	%
Average OD density	=	2.58	g/ml		
Average SSD density	=	2.66	g/ml		
Average absorption	=	3.02	%		

4.2.4 Water

4.2.4.1 Source

The water used in the project was tap water in the Winter Laboratory at Cornell University.

4.2.4.2 Characterization

The water used in this research project was assumed to have a density of 1-g/ml (62.4-lb/ft3).

4.3 Mixture proportion formulation

The base mixture was intentionally chosen to match that prescribed in ASTM C109 'Standard Test Method for Compressive Strength of Hydraulic Cement Mortars' for the purpose of determining the compressive strength of hydraulic cement when all other variables including sand, water content and flow (workability) are constrained. The description of mixture proportion for base mixture was quoted as follow:

'…The proportions of materials for the standard mortar shall be one part of cement to 2.75 parts of graded standard sand by weight. Use a water-cement ratio of 0.485 for all portland cement…'[4]

For this work, the same ratio of 1 part of cement to 2.75 parts of fine aggregate was adopted as a baseline design parameter for all mortar mixture proportions. The mass ratio between cement and fine aggregate (W_{cement}: $W_{fine\ aggregate}$) for all mortar mixtures was maintained at the value of 1/2.75 = 0.36.

The same water cement ratio of 0.485 (in ASTM C109) was applied on 0% bio-char mortar mixture with the aforementioned mass ratio of 0.36 between cement and fine aggregate (W_{cement}: $W_{fine\ aggregate}$). In the pilot mortar mix reported in Chapter 3, using a 4.7-liter (5 quart) Hobart N50 Planetary (tabletop) Mixer, water cement ratio of 0.485 and cement aggregate ratio of 0.36 produced mortar

[4] Quote from ASTM C109

with the flow value of 100% (diameter of settled mortar cone= 203-mm (8-in)). (ASTM C109 suggests a target flow value of 110±5%.) The methodology of measuring flow is described in Section 4.10

Figure 4.5 Resulting Flow Value of 100% in Bio-char Mortar Pilot Experiment

Figure 4.6 Flow Table and Flow Mold

The mass ratio of bio-char to total sand plus bio-char varied in seven increments from 0 to 100%. Eight groups of bio-char-mortar mixture proportion were cast: 0% (base mixture), 5%, 12.5%, 20%, 33.3%, 50%, 75% and 100% of sand (fine aggregate) substitution by bio-char "dust" by mass.

In Chapter 3 'Material Characterization of Bio-char', it was reported that this bio-char "dust" had an estimated water absorption of 125%. This is critical since maintaining a near-constant flow (workability) required that additional mix-water be provided to satisfy the large absorption of the bio-char in addition to that needed to satisfy the small yet normal absorption of the natural sand.

Due to the absorption of bio-char, the additional water content of all 7 groups of mixtures with bio-char was adjusted at the time of mixing to obtain the target flow value. As is stated in Chapter 3, the pilot bio-char-mortar mixture indicated that to keep flow constant at about 100%, for every gram of bio-char "dust" in the mixture, an additional 1 to 1.25 gram of water was needed to compensate for the loss of workability (due to absorption by bio-char). Therefore in the full-scale experiment, 1 gram of additional mix-water per gram of bio-char was added to the initial mixture. More water was incrementally added as needed to reach the target flow. For the full-scale mixtures with the larger mixer (to be described), the target flow was in the range of the 110 ± 5 as recommended by ASTM C109.

The formulated mixture proportions based on the above mentioned ratios and constraints for all 8 sets of bio-char-mortar are listed in Table 4.4.

Table 4.4 Proposed Mixture Proportions

Bio-char as a percentage of total aggregate	Cement (kg)	Sand (kg)	Bio-char (kg)	Initial batch water (kg)	Estimated additional water (kg)	Estimated mixture volume (liter)	Target flow (%)
0%	1	2.75	0	0.485	0	2.04	110±5
5%	1	2.61	0.14	0.485	0.14	2.20	110±5
12.5%	1	2.41	0.34	0.485	0.34	2.44	110±5
20%	1	2.20	0.55	0.485	0.55	2.68	110±5
33.3%	1	1.83	0.92	0.485	0.92	3.11	110±5
50%	1	1.38	1.38	0.485	1.38	3.65	110±5
75%	1	0.69	2.06	0.485	2.06	4.45	110±5
100%	1	0	2.75	0.485	2.75	5.26	110±5

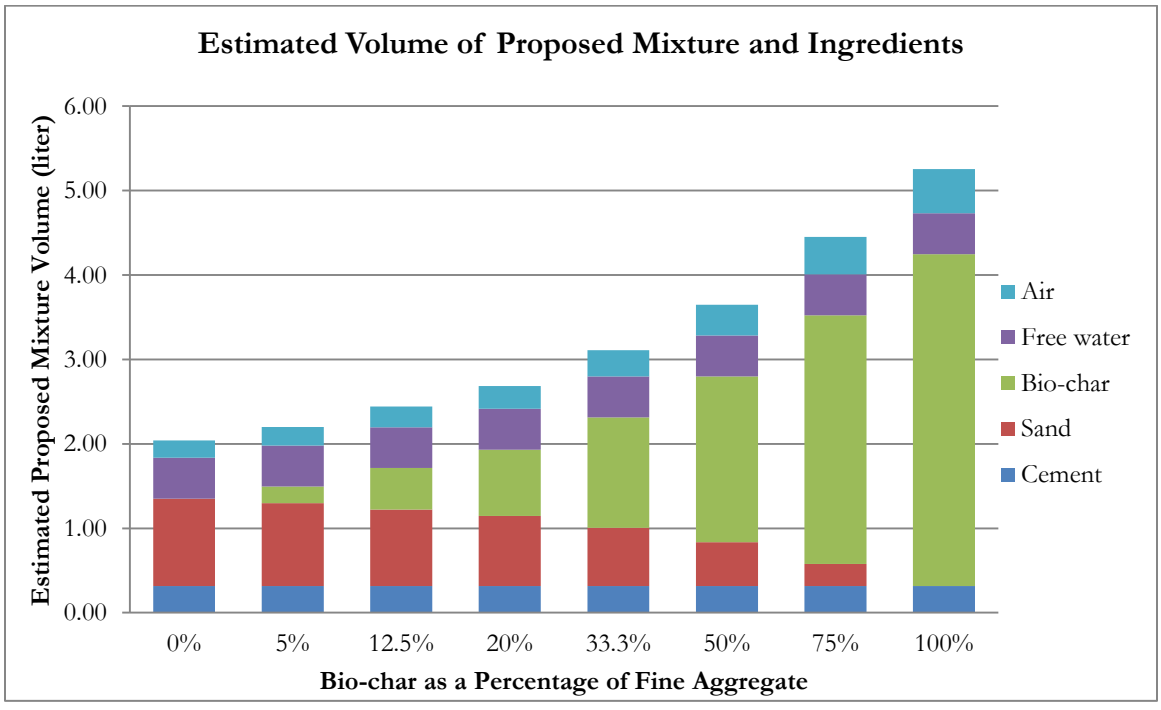

Figure 4.7 Estimated Volume of Proposed Mixture and Ingredients

The estimated volumes in Table 4.4 were determined prior to mixing the full-scale batches by assuming that all additional water is absorbed by bio-char instantly, and that the air content of the mortar is 10%. (This latter value is supported by the requirements of ASTM C150. As will be reported in Chapter 5, the average air content for all mixtures was 7%.) Estimated mixture volume was therefore approximated by the following equation:

$$V_{est.mix} = \frac{\frac{W_{cement}}{\rho_{cement}} + \frac{W_{SSD\ sand}}{\rho_{SSD\ sand}} + \frac{W_{bio-char}}{\rho_{bio-char}} + \frac{W_{initial\ batch\ water}}{\rho_{water}}}{(1 - \text{air content})}$$

For each mixture, a minimum of 48 cylinders were required. Each 2" by 4" cylinder had a volume of 206 ml. Assuming 1/3 wastage, the required minimum volume of mortar mixture was therefore:

$$206\ \text{ml} \times 50\ \times (1 + 50\%) = 15450\ \text{ml} = 15.5\ \text{liter}$$

As is observed in the Table 4.4, due to the low density of bio-char (0.7 g/ml), the volume of mortar mixture increases when fine aggregate substitution (by bio-char) ratio increases. To reduce waste, the mass of each ingredient was then scaled by a multiplier for producing estimated required volume of mortar. The scaled formulated mixture proportions for all 8 groups of bio-char-mortar mixture proportion are listed in the Table 4.5. Slight adjustments were made in actual batching as described in Chapter 5.

Table 4.5 Proposed Mixture Proportions Adjusted for Target Volume of 15.5 Liter

Bio-char as a percentage of total aggregate	Cement (kg)	Sand (kg)	Bio-char (kg)	Initial batch water (kg)	Estimated additional water (kg)	Estimated mixture volume (liter)	Target flow (%)
0%	7600	20900	0	3680	0	15.5	110±5
5%	7050	18400	970	3410	970	15.5	110±5
12.5%	6350	15270	2180	3080	2180	15.5	110±5
20%	5780	12700	3180	2800	3180	15.5	110±5
33.3%	4980	9140	4560	2410	4560	15.5	110±5
50%	4250	5840	5840	2060	5840	15.5	110±5
75%	3480	2400	7180	1690	7180	15.5	110±5
100%	2950	0	8110	1430	8110	15.5	110±5

4.4 Equipment Used

4.4.1 Mortar Mixer

A 0.17-m^3 (6-ft^3) capacity mortar mixer (Stone 655PM) manufactured by Stone, Inc. was used for the final mortar mixture in this research project. The mortar mixer consisted of a series of paddles that were connected to a rotating shaft, which ran through the center of the mixing drum. The shaft and blades of the mortar mixer are shown in the following figures. The mortar mixer operates at ~45rpm.

(a) (b)

Figure 4.8: (a) Stone 655PM Mortar Mixer with (b) Rotating Paddles

4.5 Weighing and Preparing Materials

Step 1	Twenty-four hours prior to batching, collect sand sample, weigh, and place in oven for determination of moisture content.
Step 2	Weigh bio-char, cement, and sand to a precision of 0.5% of the target batch mass, using a digital scale with a precision of 0.1 gram. Temporarily place the dry ingredients in separate containers before mixing.
Step 3	Weigh initial batch water (based on target w/c of 0.485) to a precision of 0.3% of the target batch mass, using a digital scale with a precision of 0.1 gram on a digital scale with the precision to 0.1 gram. Place the initial batch water in a container temporarily before mixing.
Step 4	Weigh estimated additional water (to satisfy absorption of sand and bio-char) and reach the target flow of 110±5) to a precision of 0.3% of the target batch mass, using a digital scale with a precision of 0.1 gram. Hold the estimated additional water in a container temporarily before mixing.

4.6 Mixing

The mixing procedure was based on ASTMC305-14 "Standard Practice for Mechanical Mixing of Hydraulic Cement Pastes and Mortars of Plastic Consistency" and ASTMC192 "Making and Curing Concrete Test Specimens in the Laboratory", with slight modifications due to the introduction of bio-char.

Step 5	Prior to the mixing, first put all dry cement, then initial batch water into the bottom of the mixer.  Figure 4.9 Placing Cement into Mixer
Step 6	Run the mixer with cement and initial batch water for 90s (about 70 revolutions).
Step 7	Stop the mixer; and simultaneously place all sand and bio-char into the mixer, taking care to introduce these materials as close as possible to the pre-mixed paste. This was done to minimize the dispersal of the fine bio-char "dust" into the air. (Pilot experiments demonstrated that a "cloud" of bio-char can otherwise be formed.) Then pour the estimated additional water on top of sand and bio-char.
Step 8	Run the mixer for 180s (about 140 revolutions).
Step 9	Stop the mixer; sample about 0.4-liter (0.015-cubic foot) bio-char mortar from the

	mixer; perform the flow test. If the is approximately on the range of 110±5, then move to Step 11. If less than this range, return the sample to the mixer and move to Step 10. (The estimated additional water had been calculated and controlled such that the first flow value never exceeded the target range.) (The procedure followed ASTM C1437-13 'Standard Test Method for Flow of Hydraulic Cement Mortar'. The flow test and apparatus are further described in Section 10 ,Chapter 4)
Step 10	When more water was required to achieve the target flow, that increment was determined by operator experience, typically in increment of about 5% of the originally estimated additional water content. That amount was then weighed to a precision of less than 0.1% of the total water content in the batch. Incremental water was then added by distributing over the surface of the mixed material. Then move to Step 6. (Note that the goal of this step is to adjust the flow of the batch slowly. It usually takes more than one trial to reach the target flow value. For some mixtures more than 1.25 gram of additional water was required per gram of bio-char to maintain flow.)
Step 11	Stop the mixer; pour all the mortar mixture (~17000-ml, 4.5 gallon) from the rotating drum to a 38-liter (10-gallon) plastic mixing container.
Step 12	Using a small steel trowel, collect one sample of mortar from the mixing container.

Step 13	Perform air indicator test. (See Section 11, Chapter 4)
Step 14	Quickly spray inside of mixer with water from a hose, partially fill mixer with water with mixer running for a few minutes, stop mixer and let stand until later cleaning while following next steps in batching, casting, and consolidation process.
Step 15	Clean the mixer before the residual mortar hardens.

4.7 Placing and Consolidation

The vibration system was designed and tailor-made for this research. The system consisted of a vibration table and a vibration box. The development of vibration system and vibration protocol was described in Appendix C.

Figure 4.10 Vibration Table and Vibration Box

There were 16 slots in the vibration box, and therefore the vibration procedure was performed repeatedly for 3 times for each batch.

The procedure of placing and consolidation is described as follow.

Step 16	Prior to placing mortar, mark all cylinder molds from 1-48
Step 17	Ensure that vibration box is already clamped to the vibration table
Step 18	With gloved hands, place uncompacted mortar in cylinder mold approximately form 1/2 to 2/3, and fill cylinder mold (starting from cylinder #1) (At this stage do not tamp or compact mortar into mold.)
Step 19	Leaving the mold uncapped; place each partially-filled cylinder mold into its slot in the vibration box until all 16 slots are loaded. The sequence of loading cylinder molds follows. 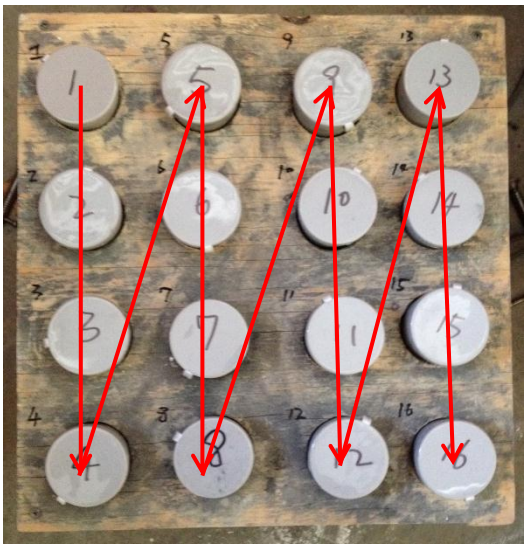 Figure 4.11 Sequence of Loading Cylinder Molds
Step 20	Turn on vibration table with power switch at medium level for 15 seconds.

	 Figure 4.12 Power Level of Vibration Table
Step 21	Leaving the molds in-place in the vibration box, fill each cylinder mold to over-full, with an approximate 10 mm mound at the top of each cylinder.
Step 22	Start second vibration period with power switch at medium level for 15 seconds. During vibration add mortar if consolidation is creating a depression at the top of the molded cylinder.
Step 23	Pull all 16 cylinder molds out of the vibration box without spilling mortar.
Step 24	Using a small steel trowel, collect one sample of mortar from the top of a consolidated cylinder.
Step 25	Perform air indicator test. (See Section 11, Chapter 4)
Step 26	Scrape off the excessive mortar from the top of cylinder mold with a steel trowel by placing the trowel at the edge of the cylinder mold and moving it parallel to the top of the cylinder mold.
Step 27	Cap cylinder mold with its plastic lid, ensuring a flat surface and a tight seal.
Step 28	Clean the exterior of cylinder mold with paper towel. Remove all mortar and other debris from the mold surface.
Step 29	Weigh cylinder mold filled with bio-char mortar to the nearest 0.1 gram. Record the

	mass.
Step 30	Seal cylinder mold with duct tape around the gap between cylinder mold and lid.
Step 31	Clean the vibration box with pressurized air from an air nozzle.

4.8 Curing

Filled cylinder molds had been sealed to prevent drying or absorption of moisture from the environment. After consolidation, all sealed mortar cylinders were moved to a temperature-controlled storage space inside Winter Laboratory, at Cornell University, maintained at 22 degree Celsius as continuously monitored by a temperature sensor (AD590, Analog device/Temperature transducer) for the duration of the curing period.

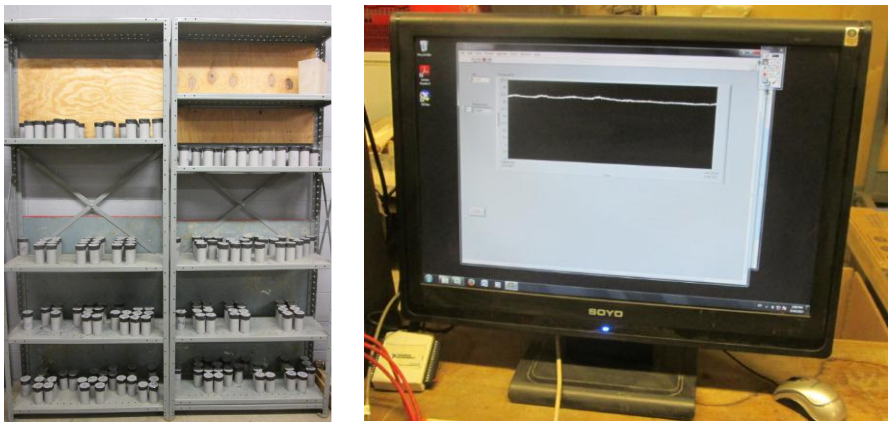

(a) (b)

Figure 4.13: (a) Curing Space with (b) Continuously Recording Temperature

4.9 Testing Hardened Mortar

Step 1	Assign a random number for testing sequence to all 48 cylinder specimens from the same batch prior to testing (this is to minimize any bias due to order of casting and consolidation) 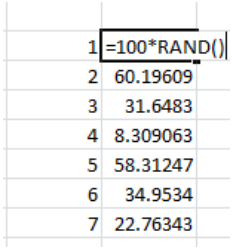 Figure 4.14(a) Demonstration of Sequencing Test Specimen (Step 1)
Step 2	Rank the assigned random numbers from smallest to largest. Specimens are tested in ascending order of the assigned random numbers 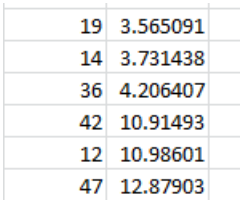 Figure 4.14(b) Demonstration of Sequencing Test Specimen (Step 2)
Step 3	For any given mixture at any given age, specimens with lowest 6 assigned random numbers became the test subjects for splitting tensile strength The 6 specimens with next 6 assigned random numbers are the test subjects for compressive strength

	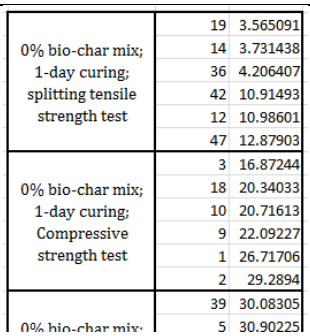 Figure 4.14(c) Demonstration of Sequencing Test Specimen (Step 3)
	Recalling that 2 mixtures were cast each day for four consecutive days, two mixtures were therefore tested on the day immediately following casting, then again one week later, then 4 weeks later, and finally 8 weeks later. To expedite testing, specimens from both mixtures to be tested on a given day were removed from their molds and prepared for testing, such that immediately prior to initiation of the tests, 6 specimens for each test from each of two mixtures were in the queue, for a total of 24 cylinders.
Step 4	Perform Step 1 to 3 for each mixture at 1, 7, 28 and 56 days after casting
Step 5	For any given day's testing, unseal all 24 randomly designated cylinder molds in the order of testing. Use a box-cutter knife, slit one side of each cylinder mold. De-mold cylinders were placed on a table in the concrete testing laboratory. 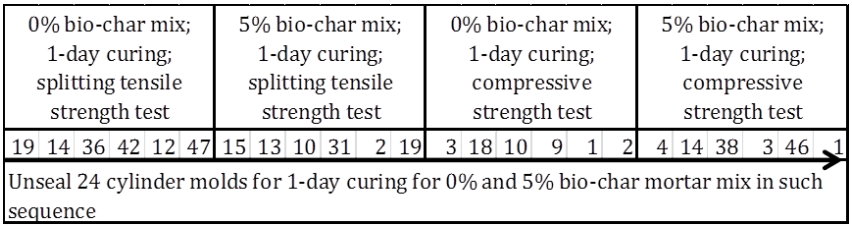 Figure 4.14(d) Demonstration of Sequencing Test Specimen (Step 4)
Step 6	After all 24 cylinders have been removed from their molds, photograph each unsealed, untested mortar cylinders with its specimen number, in the designated order of testing.

	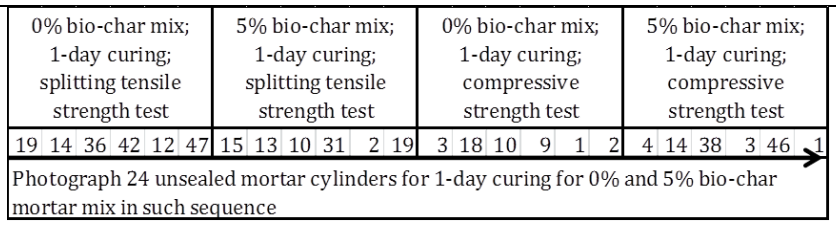 Figure 4.14(e) Demonstration of Sequencing Test Specimen (Step 5)
Step 7	After all 24 cylinders have been removed from their molds and photographed, measure diameter, height and mass of all 24 unsealed mortar cylinders in the designated order of testing. 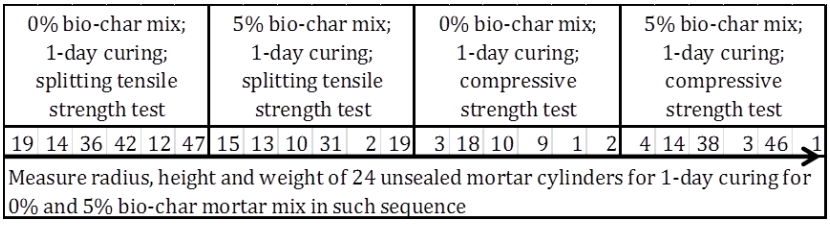 Figure 4.14(f) Demonstration of Sequencing Test Specimen (Step 6)
Step 8	Perform splitting tensile and compression strength tests in the designated order of testing, in accordance with ASTM C496 "Standard Test Method for Splitting Tensile Strength of Cylindrical Concrete Specimens" and ASTM C39 "Standard Test Method for Compressive Strength of Cylindrical Concrete Specimens," using a Wiedemann Baldwin 26.7-kN (60,000-lb force) universal (tension/compression) hydraulic testing machine. For splitting tensile specimens, metal backer-plates with wooden strips were used to develop the required concentrated lineload, as shown in Figure 4.15. Compression specimens used neoprene caps meeting the requirements of ASTM C1231

	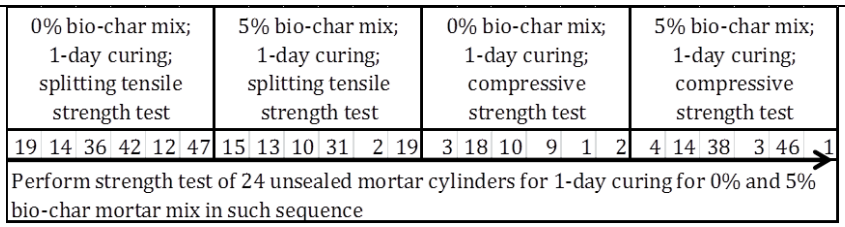 Figure 4.14(g) Demonstration of Sequencing Test Specimen (Step 7) 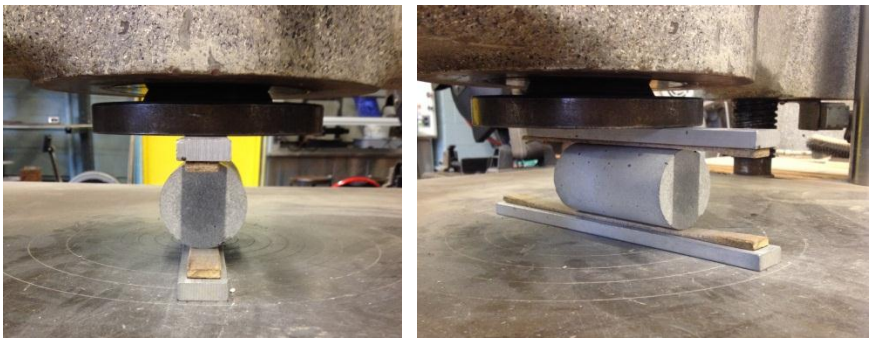 (a) (b) Figure 4.15 Demonstration of Splitting Tensile Strength Test (a)Front View and (b)Side View  Figure 4.16 Demonstration of Compressive Strength Test
Step 9	Retain the fragments from each tested specimens, identified by specimen number
Step 10	Photograph all tested mortar cylinders with its specimen number

<table>
<tr><td></td><td> 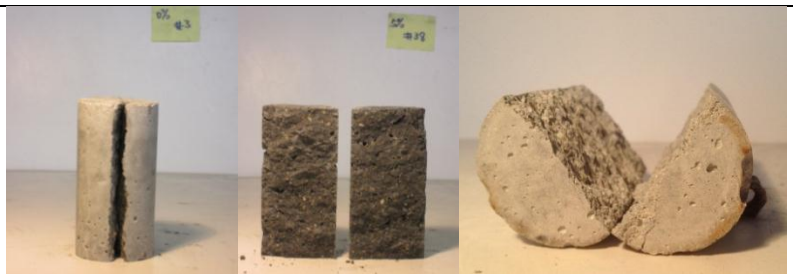
(a) (b) (c)
 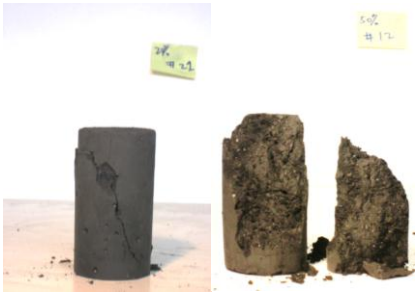
(d) (e)
Figure 4.17 Specimen Photograph of (a) Split Cylinder, (b) Splitting Surface Front View, (c) Splitting Surface Longitudinal View, (d) Compressed Cylinder and (e) Fracture Surface</td></tr>
<tr><td>Step 11</td><td>Store all tested mortar cylinders for future reference
 
Figure 4.18 Broken Cylinder Storage</td></tr>
<tr><td>Step 12</td><td>Repeat Step 5-11 for all remaining mixtures and test-ages</td></tr>
</table>

4.10 Flow Test

The flow of mortar was used to characterize the workability of mortar. ASTM C1437-13 "Standard Test Method for Flow of Hydraulic Cement Mortar" stated that:

"…It (flow) is commonly used in standard tests that require the mortar to have a water content that provides a specified flow level……The flow is the resulting increase (from the procedure required in ASTMC1437-13) in average base diameter of the mortar mass, expressed as a percentage of the original base diameter…"[5]

$$\text{Flow (\%)} = \frac{\text{Final diameter } (D_2) - \text{Initial diameter } (D_1)}{\text{Initial diameter } (D_1)}$$

As is provided in ASTM C1437-13, the basic procedure for flow test is quoted as follow:

"… (Before performing flow test), carefully wipe the flow table clean and dry. Place the flow mold at the center. Place a layer of mortar about 25-mm (1-in) in thickness in the mold and tamp 20 times with the tamper. The tamping pressure shall be just sufficient to ensure uniform filling of the mold. Tamping should be uniformly distributed over the cross section of each layer. For bottom layer this will necessitate inkling the tamper when tamping near the perimeter. Then fill the mold with mortar and tamp as specified for first layer. Cut off the mortar to a plane surface flush with the top of the mold by drawing the straightedge or the edge of the trowel with a sawing motion across the top of the mold. Wipe the table top clean and dry, being especially careful to remove any water from

[5] Quote from ASTM C1437

around the edge of the flow mold. Lift the mold away from the mortar 1 min after completing the mixing operation. Immediately drop the table 25 times in 15s…"[6]

Figures 4.19 and 4.20 present the apparatus for flow test and the demonstration of measuring a flow.

Figure 4.19 Flow Table and Flow Mold

Figure 4.20 Measuring Flow

[6] Quote from ASTM C1437

4.11 Measure Air Content Using Air Indicator

The air indicator is an AASHTO standard method described in AASHTO T-199-00 (2004) 'Air Content of Freshly Mixed Concrete by the Chace Indicator'. It is a toolset that enables approximate indication of air content of mortar. The picture of indicator is shown as follow.

(a) (b) (c)

Figure 4.21: (a) Air Indicator, (b) Glass Tube and Stem; (c) Cup

The basic procedure of measuring air content using air indicator is summarized as follow: Mortar was sampled after mixing and consolidating. Then the cup was filled with mortar (with no tamping or compacting). The cup was inserted assembly in glass tube. A rubber syringe was used to squeeze isopropyl alcohol into tube through stem until liquid was at the top line. A finger was placed over stem opening to prevent loss of liquid and roll indicator from side to side gently to dissolve all mortar from cup into alcohol. Then the indicator was placed in an upright position on a level surface and the number of spaces the liquid dropped in the stem was counted and recorded. The conversion

table indicated that for mortar (without coarse aggregate), every one stem reading implied 1.78% air content. All parts were washed and cleaned promptly with water and brush.

The discussion on the validity of air indicator conversion table is continued in Appendix D.

CHAPTER 5

EXPERIMENTAL RESULTS

This chapter presents the actual mixture proportions as adjusted for total batch volume, and the results of tests on freshly-mixed mortar as well as compressive and splitting tensile strength tests for all proportions of bio-char and at all test ages.

5.1 Freshly Mixed Mortar Properties

5.1.1 Batching and Material Condition

As is reported in Section 3, Chapter 4, it was necessary to adjust the batch mass of each mixture to accommodate the increasing volume of bio-char, and to adjust water content to maintain the target flow of 110±5%. The masses of all ingredients as-batched are reported in Table 5.1.

Table 5.1 Actual Mass of Each Ingredient Batched

Bio-char as a percent of total aggregate	Cement (g)	Sand (g)	Dry bio-char powder (g)	Initial batch water (g)	Additional water (g)	Total water (g)
0%	7700	21140	0	3730	0	3730
5%	7700	20120	1040	3730	1570	5300
12.5%	6100	14690	2100	2950	3460	6410
20%	6250	13760	3440	3030	5820	8850
33.3%	4880	8960	4470	2360	7290	9650
50%	4000	5500	5500	1940	9260	11200
75%	2590	1780	5340	1250	10250	11500
100%	2220	0	6100	1070	12110	13180

The mass of total water shown in the table is the sum of initial batch water (to create cement paste) and additional water (to bring the final flow to target value of 110±5%).

The mass ratio between initial batch water and cement in all 8 mixtures was kept constant to create the cement paste in the first step of mixing procedure. The intention was to maintain the ratio at a constant of 0.485 based on ASTM C109. In all mixtures, the mass ratio between cement and total aggregate (sum of sand and bio-char) was kept constant at 0.36. Variations in batching quantities resulted from the precision of the batching process. All ingredients were weighed to the nearest 10 grams.

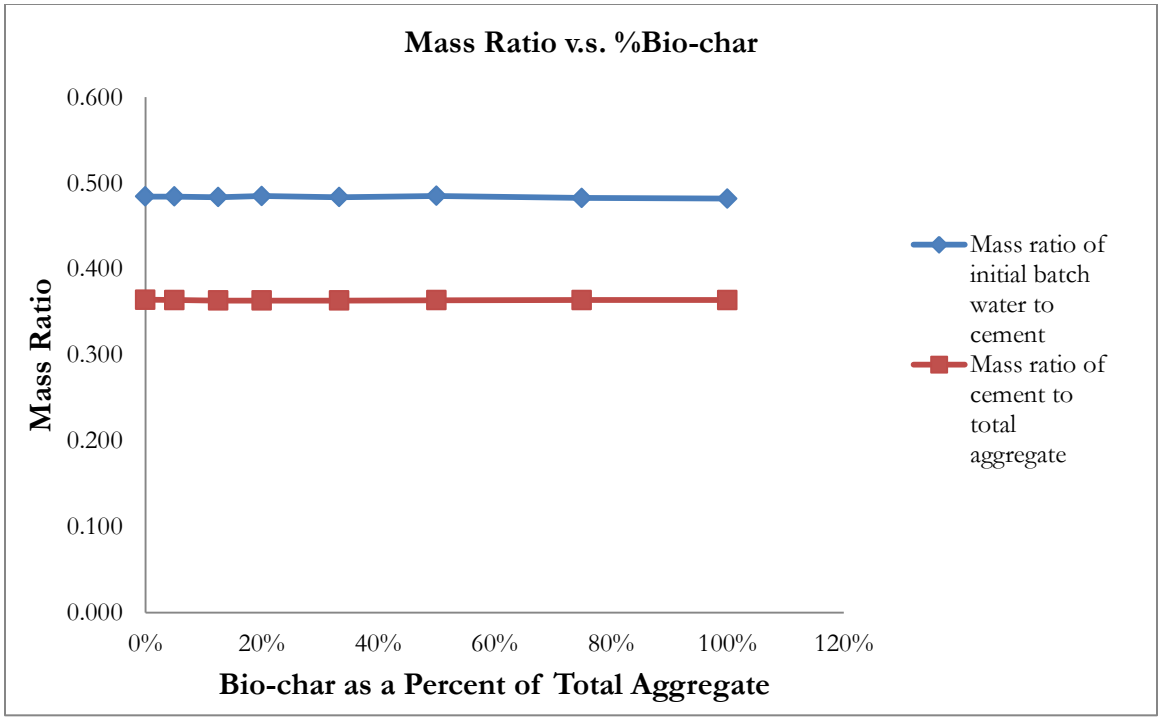

Figure 5.1 Initial Batch Water Cement Ratio and Cement to Sand Plus Bio-char Ratio

For all mixtures, sand was sampled 24-h in advance of mixing for determination of moisture content. This value was used to account for the mass of batch water absorbed into sand, or contributed by

wet sand. Note that any water adjustment due to the sand was on the order of 3% of the water adjustment required by the bio-char. Sand moisture content is reported in Table 5.2.

Table 5.2 Moisture Content of Sand

Bio-char as a percent of total aggregate	Sand Moisture Content
0%	3.20%
5%	3.20%
12.5%	4.30%
20%	4.30%
33.3%	6.97%
50%	6.97%
75%	2.18%
100%	2.18%

The continuous increase in moisture content of sand over the first six batches was due to the non-uniformity of sand moisture in the storage bin. Sand at the top of the bin was relatively dry, trending to relatively moist at the bottom. Sand for the last two batches came from the top of a second bin. Sand in both bins had been acquired from the same source at the same time, and varied only in moisture content.

5.1.2 Mortar Flow

The value of the ASTM C230 flow measured for all mixtures is presented in Table 5.3. The target value of flow as obtained for mortar of 0.485 water cement ratio with 0% bio-char was 100% when

mixed in the Hobart table-top mortar mixer. The target value of flow for the proposed mixture proportions was 110±5 when mixed in the Stone mortar mixer.

Table 5.3 ASTMC230 Flow of Each Mixture Proportion

Bio-char as a percent of total aggregate	Diameter (m)		Flow (D2-D1)/D1 (%)
	Initial (D1)	Final (D2)	
0%	0.10	0.21	106
5%	0.10	0.21	103
12.5%	0.10	0.21	103
20%	0.10	0.21	106
33.3%	0.10	0.21	106
50%	0.10	0.21	106
75%	0.10	0.21	103
100%	0.10	0.21	103

5.1.3 Air Content

As described in Chapter 4, air content was measured for all mixtures using the Chace air indicator (AASHTO T-199). The conversion factor for the air indicator is 1.78% air per increment read on the indicator.

Table 5.4 Air Content of Each Mixture Proportion

Bio-char as a percent of total aggregate	Air indicator reading	Air volume as a percent of mortar volume (%)
0%	5.0	8.90
5%	3.0	5.34
12.5%	3.0	5.34
20%	4.5	8.01
33.3%	4.0	7.12
50%	3.0	5.34
75%	5.0	8.90
100%	3.0	5.34

The plot of air content against bio-char as a percent of total aggregate is presented in Figure 5.2.

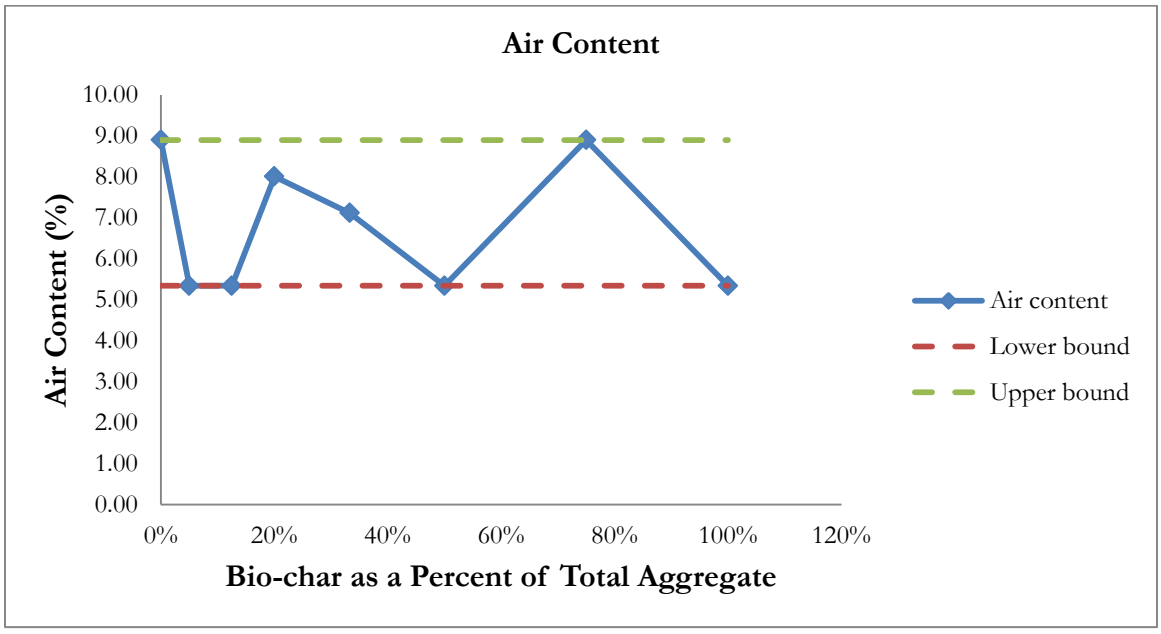

Figure 5.2 Air Volume as a Percent of Mortar Volume

The plot suggests no obvious trend in air content as the percentage of fine aggregate substitution by bio-char increases, other than lower and upper bound value values of about 5.5% to 9% air. Given the approximate nature of the Chace air indicator, one might consider an average air content of about 7% for all mixtures. Interestingly, 9% air in the mortar is a reasonable value for air entrained concrete proportioned in accordance with ACI 211.1, while 5.5% air in mortar is more characteristic of non-air-entrained concrete. Note that while no air entraining admixtures were used in these experiments, the carbon in the bio-char would normally be considered to be considered to be an air-de-trainer or anti-foamer (just as grease collapses the detergent foam when washing dished). It is likely, therefore, that the air bubbles trapped in these mortars are not the fine or so-called "entrained" air bubbles, which are more prevalent in the presence of a detergent-like air-entraining admixture.

5.1.4 Fresh Mortar Density

The mass of filled cylinders was determined after placing, consolidation, and capping as reported in Table 5.5 (mass of molds and caps had been subtracted). The average volume of empty cylinder molds was determined by water-displacement to be 207-ml (12.6-cubic inch). The fresh mortar density of all mixtures was then calculated as reported in the table.

Table 5.5 Average Mass and Density of Mortar Cylinder of Each Mixture Proportion

Bio-char as a percent of total aggregate	Number of specimens	Mortar cylinder mass			Density (g/ml)
		Mean (g)	Standard deviation	Coefficient of variation	
0%	48	483.3	1.54	0.003	2.35
5%	48	460.1	3.00	0.007	2.23
12.5%	48	408.5	2.25	0.006	1.98
20%	48	376.4	2.06	0.005	1.83
33.3%	48	344.0	1.44	0.004	1.67
50%	48	306.6	1.24	0.004	1.49
75%	48	273.0	1.00	0.004	1.33
100%	48	255.9	0.94	0.004	1.24

The plot of mortar density against percentage of fine aggregate substitution by bio-char is presented in Figure 5.3. It is clear that as the percentage of bio-char in aggregate increases, the value of mortar density decreases. Figure 5.3 also shows predicted density based on two key assumptions. Second, it is assumed that the bio-char "immediately" absorbs water upon contact in the amount of 125% of the dry mass of the bio-char. The implications of this assumption are discussed in detail in Chapter 6. These comparative values are also reported in Table 5.6

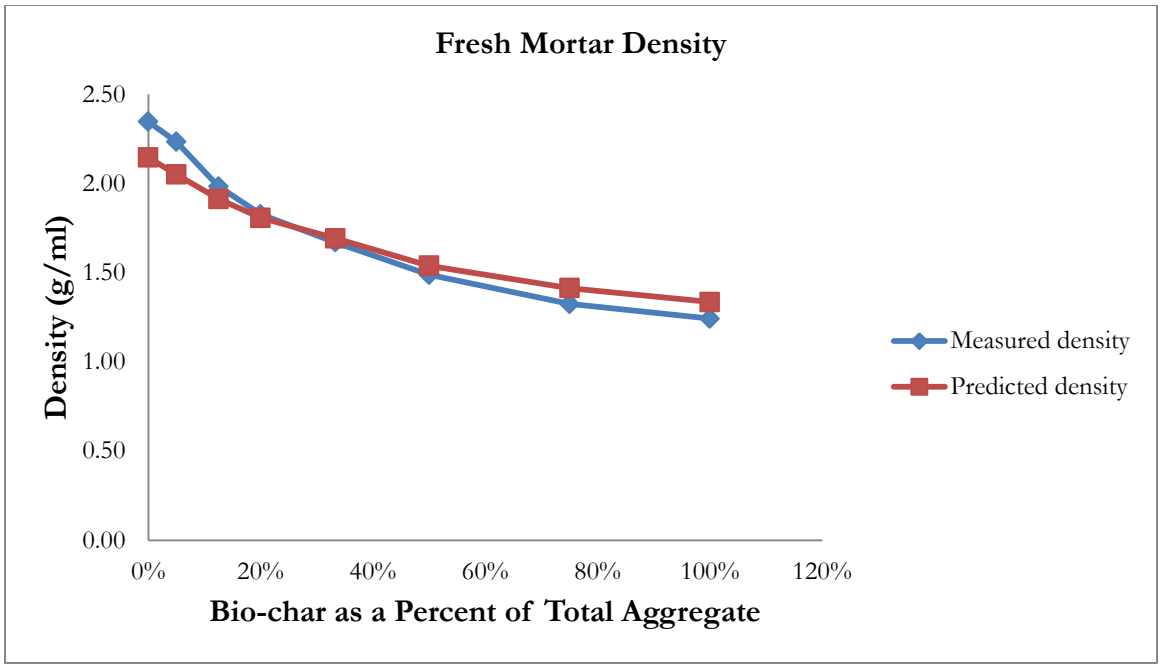

Figure 5.3 Measured Density and Predicted Density of Each Mixture Proportion

Table 5.6 Measured Density and Predicted Density

Bio-char as a percent of total aggregate	Measured density (g/ml)	Predicted density (g/ml)
0%	2.35	2.15
5%	2.23	2.05
12.5%	1.98	1.91
20%	1.83	1.81
33.3%	1.67	1.69
50%	1.49	1.54
75%	1.33	1.41
100%	1.24	1.34

5.1.5 Water Cement Ratio

Water cement ratio (w/c) is the ratio between the mass of free water (i.e., the water that occupies volume between and among the solid particles) and the mass of cement used in a mortar mixture. To compute the mass or volume of free water one must subtract from the total water any water that is absorbed by the sand and bio-char.

In Section 5.1.1, the actual quantities of batched ingredients are reported. The mass of free water (accounting for absorption into sand and bio-char, and contribution of water from wet sand) is plotted against the mass of bio-char in Figure 5.4.

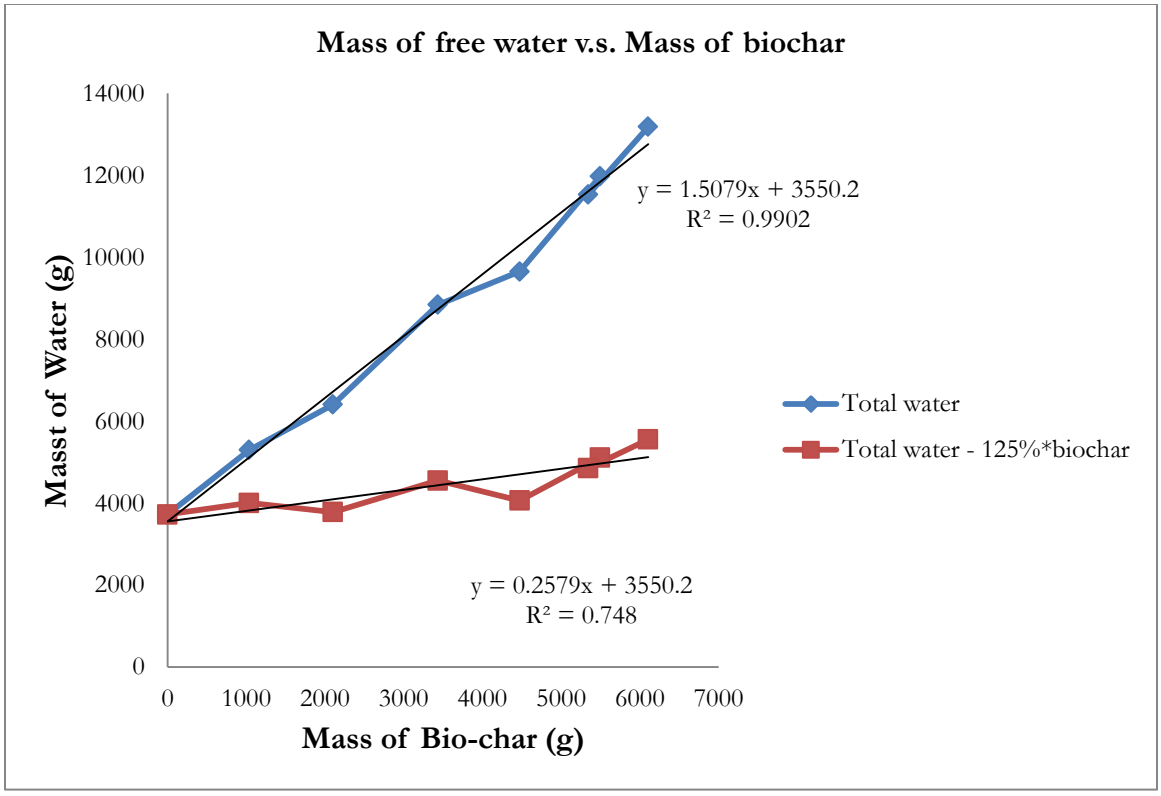

Figure 5.4 Mass of Free Water vs. Mass of Bio-char

Assuming bio-char absorption is 0% (or that absorption is sufficiently slow that zero water is absorbed over the time period required to mix and cast the cylinders), linear regression on the upper curve in Figure 5.4 indicates that for every 1 gram of bio-char used in the mixture proportion, 1.5 gram of additional free water was required to maintain flow. Assuming bio-char absorption is 125% (and that water is immediately absorbed upon contact), linear regression on the lower curve in Figure 5.4 indicates that for every 1 gram of bio-char used in the mixture proportion, 0.25 gram of additional free water was required to maintain flow.

Since the actual absorption of bio-char (or its rate) is unknown, and the estimated value from derivation is 125% (Section 7, Chapter 3), the water cement ratio is calculated under four different absorption values (0%, 100%, 125% and 150%) of bio-char to gain insight to the influence of bio-char on water cement ratio of all mixtures. These values are termed "Effective Absorption", reflecting the combined effect of the available pore space inside bio-char particles, the tendency of water to enter those pores (hydrophobic or hydrophilic, and the time required for such absorption to occur. The calculated values of w/c are reported in Table 5.7 and plotted in Figure 5.4. The implication of "Effective (Bio-char) Absorption" is continued in Section 6.2.

Table 5.7 Water Cement Ratio with E.A Varies

Bio-char as a percent of total aggregate	w/c			
	Effective Absorption of Bio-char			
	0%	100%	125%	150%
0%	0.48	0.48	0.48	0.48
5%	0.69	0.55	0.52	0.49
12.5%	1.05	0.71	0.62	0.53
20%	1.42	0.87	0.73	0.59
33.3%	1.98	1.06	0.83	0.60
50%	2.80	1.43	1.08	0.74
75%	4.44	2.38	1.86	1.35
100%	5.94	3.19	2.50	1.82

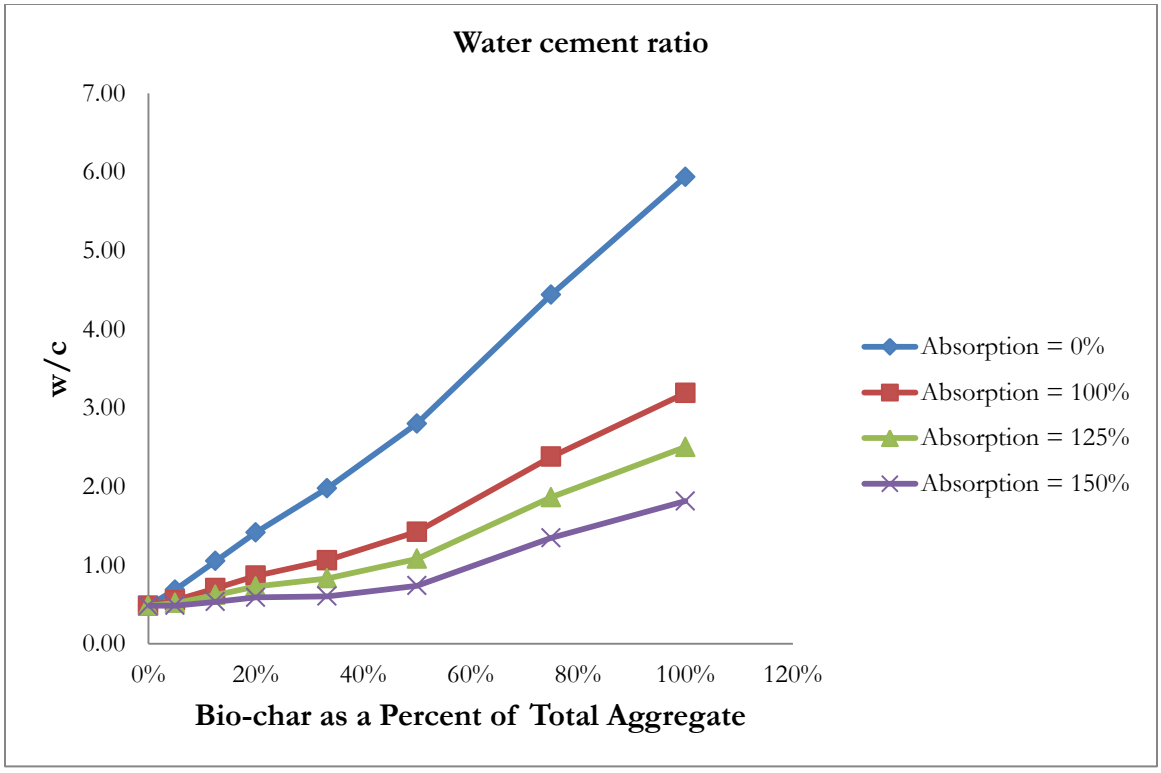

Figure 5.5 Apparent w/c as a Function of Effective Absorption of Bio-char

5.2 Hardened Mortar Properties

5.2.1 Compressive Strength

Compressive strength test results for all bio-char mortar are summarized in Table 5.8(a)-(d).

Table 5.8(a) Average Compressive Strength Summary for Each Mixture at Test Age of 1-day

Bio-char as a percent of total aggregate	Curing duration			
	1-day			
	Number of specimen	Average Compressive strength (MPa)	Standard deviation	Coefficient of variation
0%	6	19.24	1.04	0.05
5%	6	10.00	0.68	0.07
12.5%	6	3.29	0.16	0.05
20%	6	1.69	0.09	0.05
33.3%	6	1.11	0.07	0.07
50%	6	0.49	0.05	0.09
75%	6	0.25	0.03	0.11
100%	4	0.22	0.04	0.20

Table 5.8(b) Average Compressive Strength Summary for Each Mixture at Test Age of 7-days

Bio-char as a percent of total aggregate	Curing duration			
	7-days			
	Number of specimen	Average Compressive strength (MPa)	Standard deviation	Coefficient of variation
0%	6	35.85	0.90	0.02
5%	6	21.43	0.99	0.05
12.5%	6	6.84	0.23	0.03
20%	6	3.77	0.19	0.05
33.3%	6	2.19	0.09	0.04
50%	6	1.17	0.08	0.07
75%	1	0.40	n/a	n/a
100%	2	0.36	0.05	0.13

Table 5.8(c) Average Compressive Strength Summary for Each Mixture at Test Age of 28-days

Bio-char as a percent of total aggregate	Curing duration			
	28-days			
	Number of specimen	Average Compressive strength (MPa)	Standard deviation	Coefficient of variation
0%	6	43.33	2.06	0.05
5%	6	27.32	1.13	0.04
12.5%	6	9.67	0.77	0.08
20%	6	5.87	0.27	0.05
33.3%	6	3.26	0.12	0.04
50%	6	1.61	0.14	0.09
75%	5	0.55	0.07	0.13
100%	2	0.51	0.04	0.08

Table 5.8(d) Average Compressive Strength Summary for Each Mixture at Test Age of 56-days

Bio-char as a percent of total aggregate	Curing duration			
	56-days			
	Number of specimen	Average Compressive strength (MPa)	Standard deviation	Coefficient of variation
0%	6	46.89	1.85	0.04
5%	6	29.41	1.61	0.05
12.5%	6	11.55	0.68	0.06
20%	6	6.26	0.37	0.06
33.3%	6	3.72	0.24	0.06
50%	6	1.77	0.18	0.10
75%	5	0.66	0.06	0.09
100%	4	0.53	0.05	0.09

Fewer than 6 specimens were tested for 75% and 100% bio-char mixtures because of the fragility of these mixtures. Several specimens were damaged while extracting them from their cylinder molds.

Individual specimen strengths deviated from the average strength of any group by an average of 7%. In Figure 5.6, the compressive strength of each mixture is plotted against the fraction of bio-char to the total aggregate mass at 1, 7, 28 and 56 curing age. Close inspection of Figure 5.6 reveals 95% confidence-interval error bars, which are in general difficult to see due to the limited scatter in results.

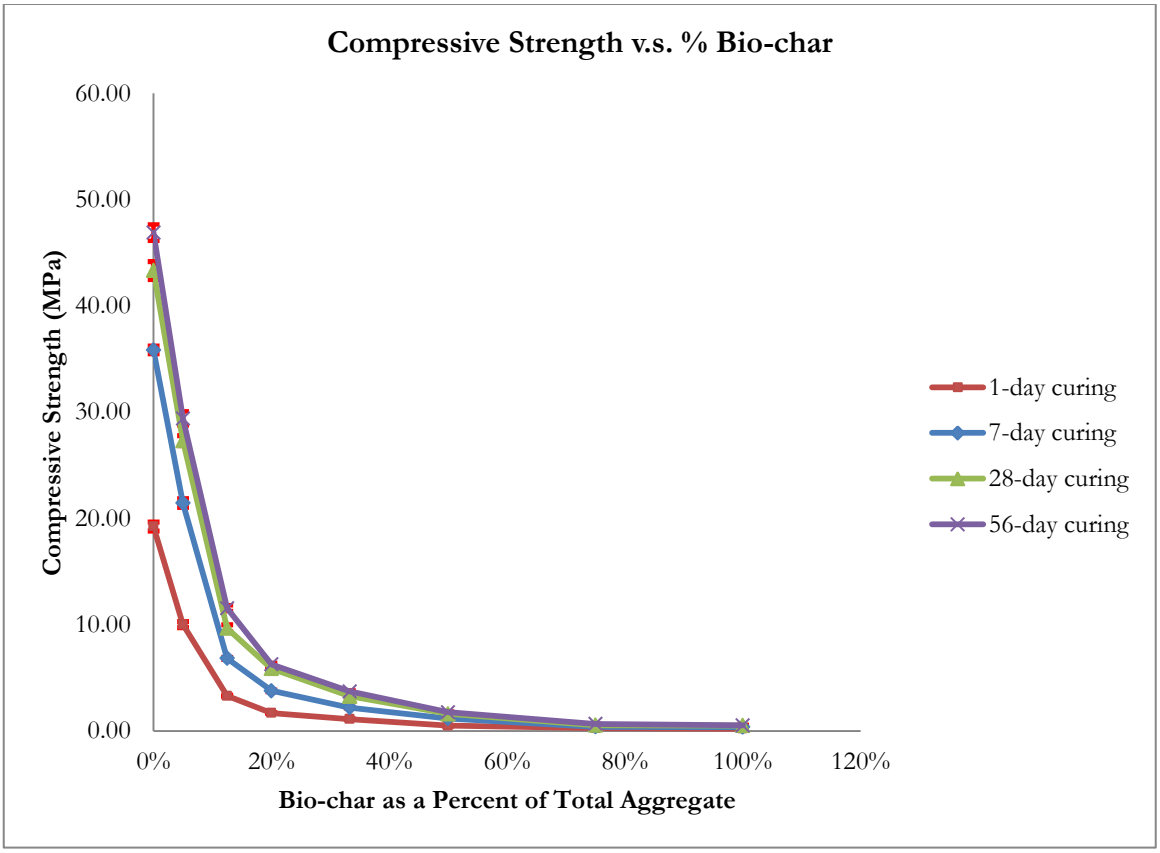

Figure 5.6 Compressive Strength vs. % Bio-char with 95% Confidence Error Bar

There is an obvious and continuous reduction in compressive strength with increasing bio-char content. Compressive strength normalized to zero bio-char mixture at 28-days curing age is listed in Table 5.9.

Table 5.9 Compressive Strength Normalized to 0% Bio-char at Test Age of 28-days

Bio-char as a percent of total aggregate	Compressive strength reduction			
	Curing duration			
	1-day	7-days	28-days	56-days
0%	44.4%	82.7%	100.0%	108.2%
5%	23.1%	49.5%	63.1%	67.9%
12.5%	7.6%	15.8%	22.3%	26.7%
20%	3.9%	8.7%	13.6%	14.5%
33.3%	2.6%	5.1%	7.5%	8.6%
50%	1.1%	2.7%	3.7%	4.1%
75%	0.6%	0.9%	1.3%	1.5%
100%	0.5%	0.8%	1.2%	1.2%

Compressive strength is plotted against curing duration to observe strength development of all mixtures in Figure 5.7.

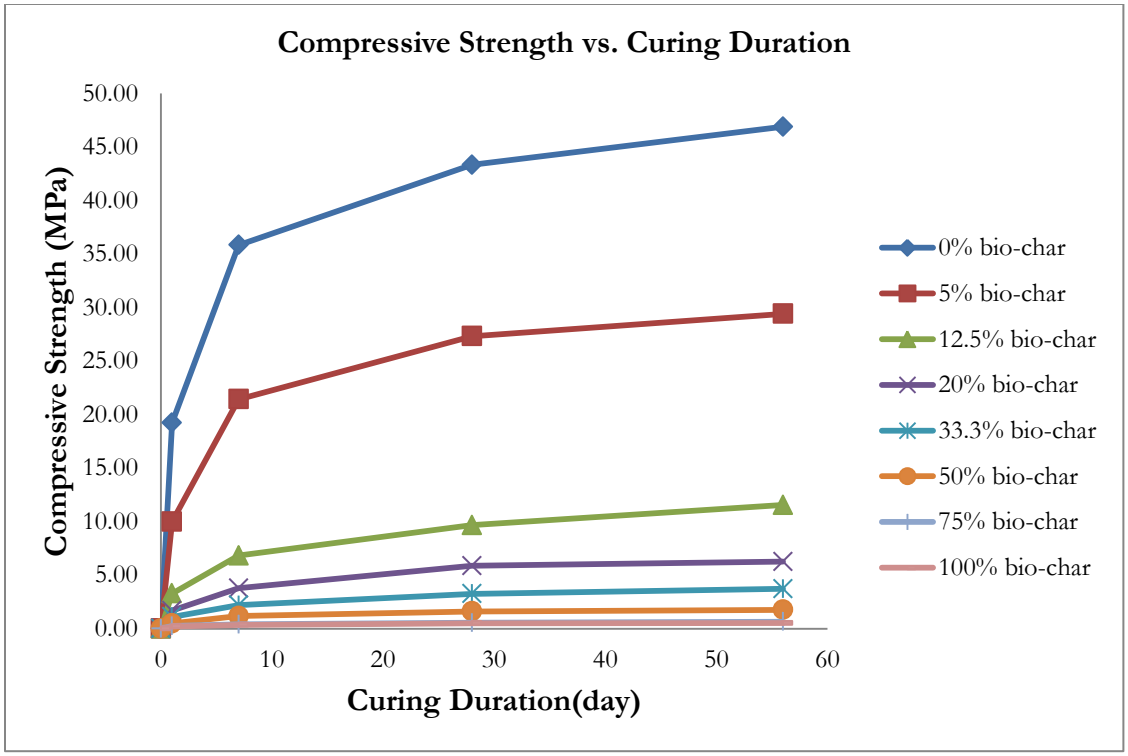

Figure 5.7 Compressive Strength vs. Curing Duration

To gain insight to whether bio-char addition influenced the rate of compressive strength development, to include the possibility of differences in early- vs. later-age effects, Figures 5.8(a), (b), (c) and (d) normalized compressive strength with respect to 1-, 7-, 28- and 56-days compressive strength, error bars are included for 95% confidence intervals, which indicate frequent overlap from one mixture to another.

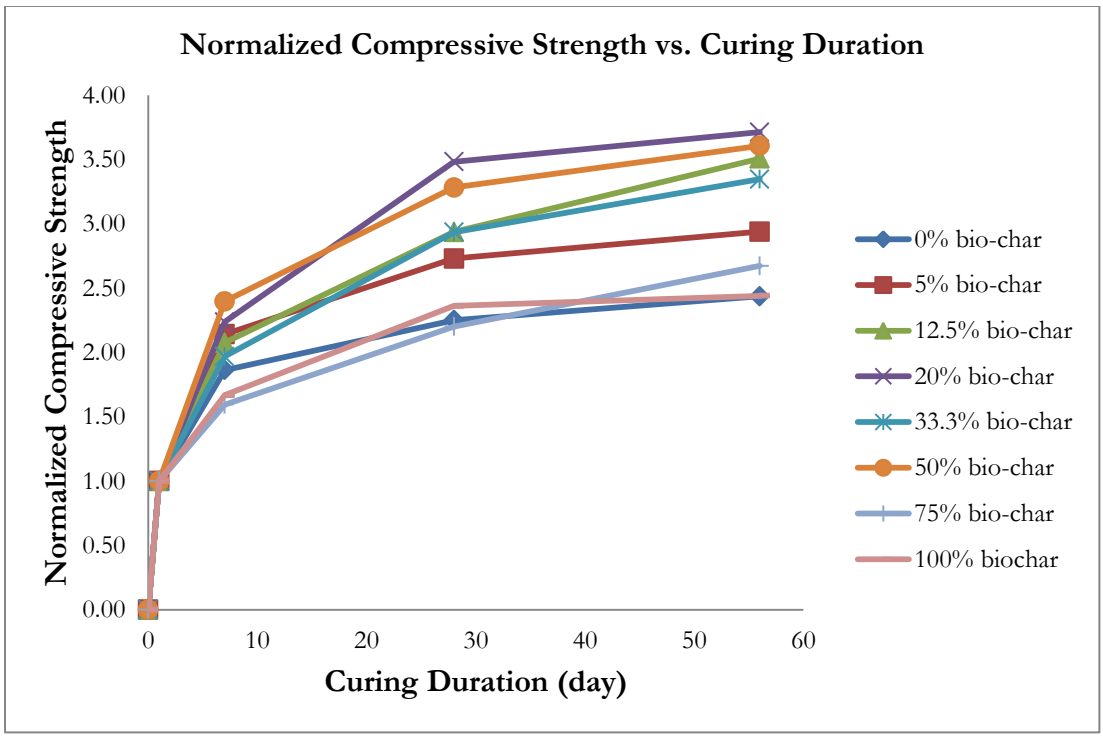

Figure 5.8(a) Normalized with respect to 1-day Compressive Strength

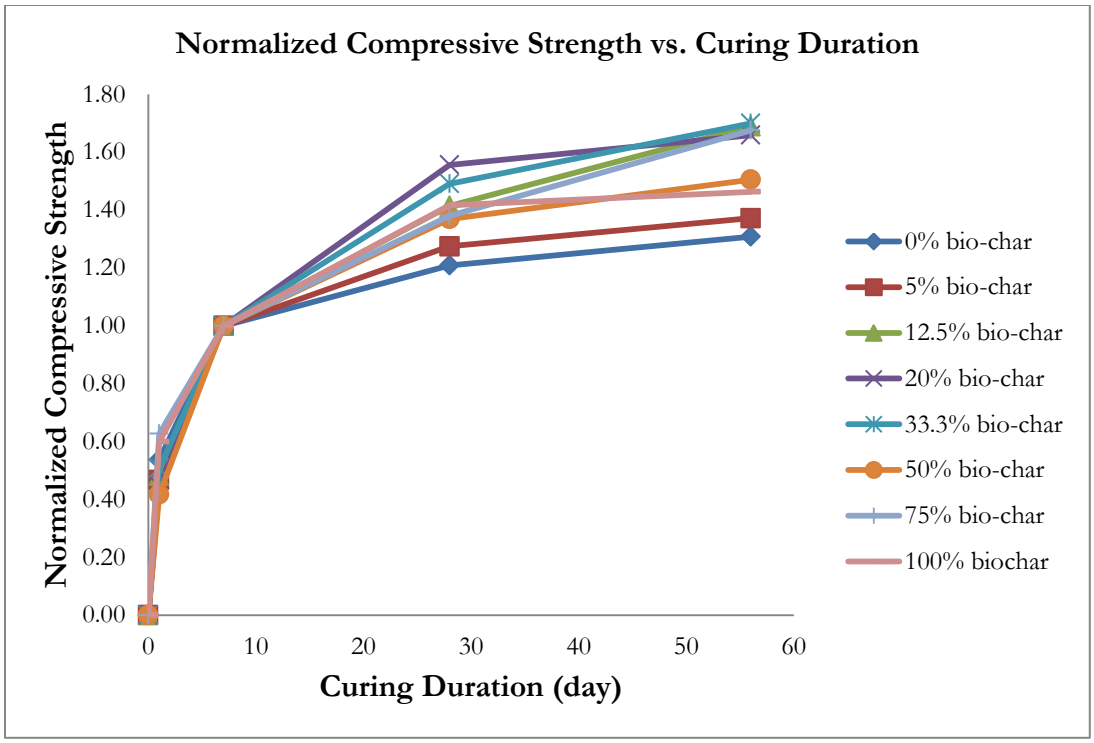

Figure 5.8(b) Normalized with respect to 7-days Compressive Strength

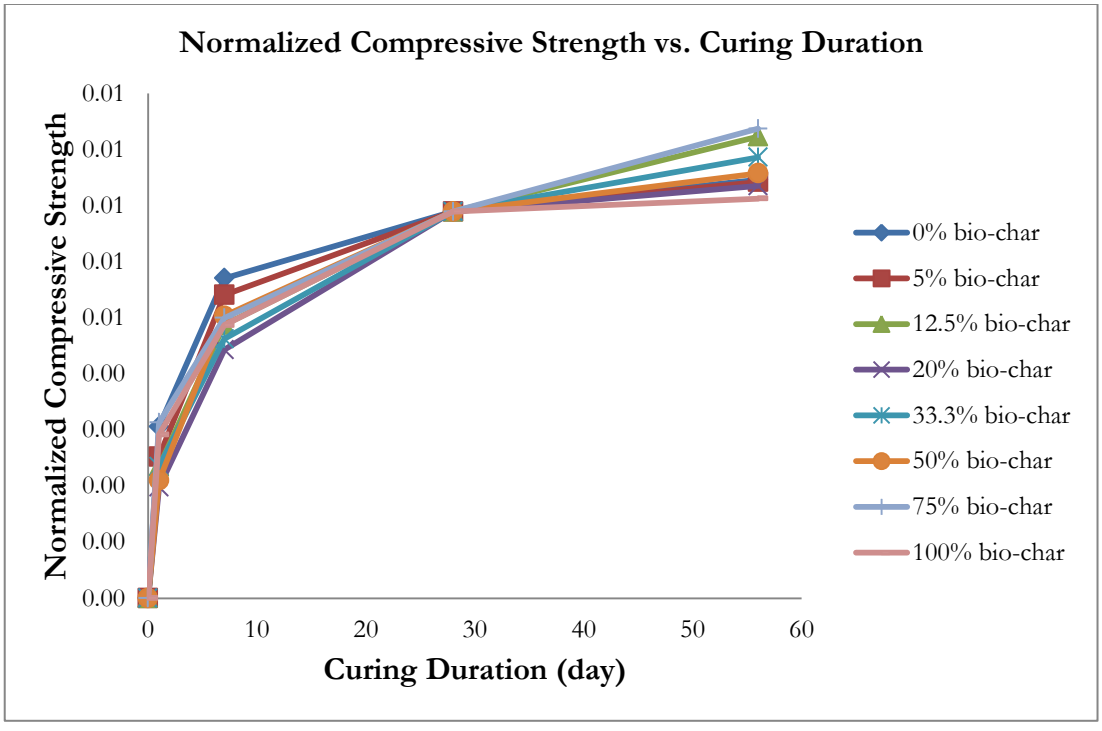

Figure 5.8(c) Normalized with respect to 28-days Compressive Strength

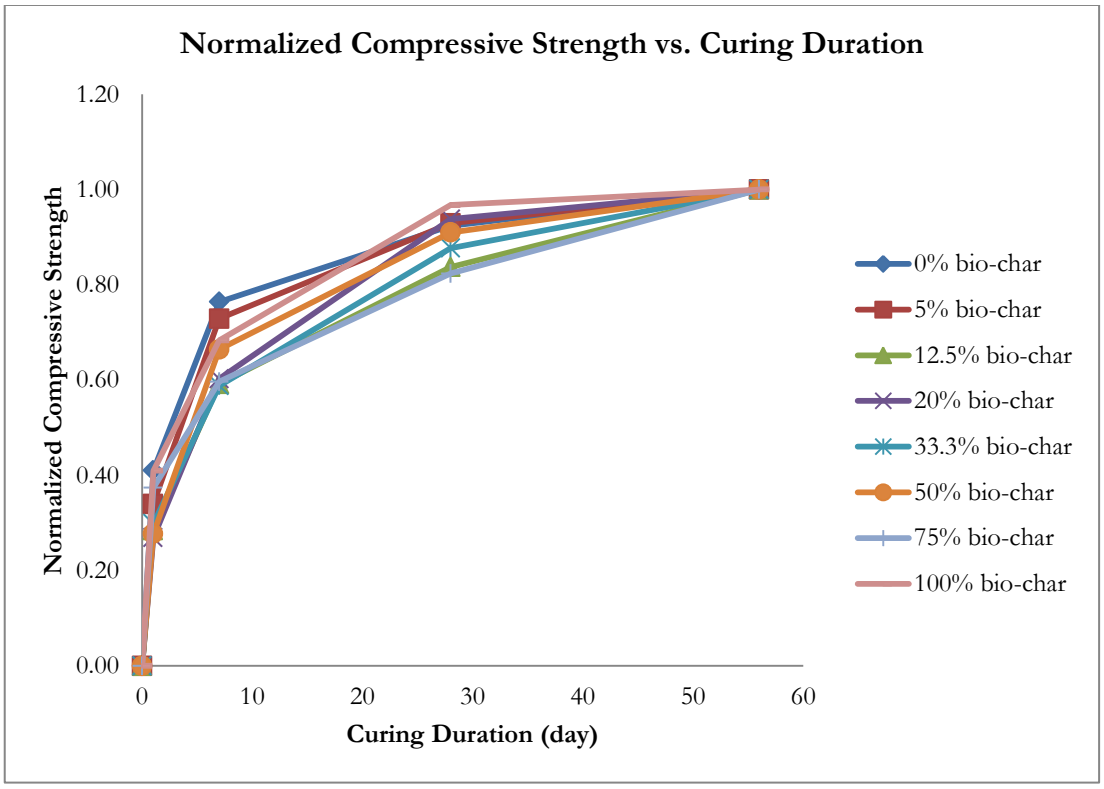

Figure 5.8(d) Normalized with respect to 56-days Compressive Strength

5.2.2 Splitting Tensile Strength

The splitting tensile strength test results for all 8 groups of bio-char-mortar mixture proportion are summarized in the Tables 5.10(a)-(d).

Table 5.10(a) Average Splitting Tensile Strength Summary for Each Mixture at Test Age of 1- day

Bio-char as a percent of total aggregate	Curing duration			
	1-day			
	Number of specimen	Average splitting tensile strength (MPa)	Standard deviation	Coefficient of variation
0%	6	2.27	0.55	0.24
5%	6	1.10	0.10	0.09
12.5%	6	0.39	0.04	0.09
20%	6	0.19	0.01	0.06
33.3%	6	0.12	0.02	0.21
50%	6	0.05	0.00	0.09
75%	4	0.02	0.00	0.18
100%	3	0.01	0.00	0.12

Table 5.10(b) Average Splitting Tensile Strength Summary for Each Mixture at Test Age of 7-days

Bio-char as a percent of total aggregate	Curing duration			
	7-days			
	Number of specimen	Average splitting tensile strength (MPa)	Standard deviation	Coefficient of variation
0%	6	4.45	0.91	0.20
5%	6	1.99	0.23	0.12
12.5%	6	0.70	0.07	0.09
20%	6	0.37	0.04	0.11
33.3%	6	0.25	0.02	0.08
50%	6	0.13	0.01	0.08
75%	1	0.04	n/a	n/a
100%	3	0.03	0.00	0.09

Table 5.10(c) Average Splitting Tensile Strength Summary for Each Mixture at Test Age of 28-days

Bio-char as a percent of total aggregate	Curing duration			
	28-days			
	Number of specimen	Average splitting tensile strength (MPa)	Standard deviation	Coefficient of variation
0%	6	4.22	0.75	0.18
5%	6	2.76	0.51	0.19
12.5%	6	1.14	0.11	0.10
20%	6	0.58	0.06	0.11
33.3%	6	0.42	0.03	0.07
50%	6	0.18	0.01	0.07
75%	3	0.05	0.00	0.09
100%	2	0.07	0.01	0.08

Table 5.10(d) Average Splitting Tensile Strength Summary for Each Mixture at Test Age of 56-days

Bio-char as a percent of total aggregate	Curing duration			
	56-days			
	Number of specimen	Average splitting tensile strength (MPa)	Standard deviation	Coefficient of variation
0%	6	5.12	0.19	0.04
5%	6	3.42	0.38	0.11
12.5%	6	1.40	0.20	0.14
20%	6	0.71	0.03	0.05
33.3%	6	0.44	0.03	0.07
50%	6	0.20	0.01	0.06
75%	6	0.07	0.01	0.10
100%	5	0.06	0.01	0.15

As remarked for the compression tests, fewer than 6 splitting-tensile specimens were tested for 75% and 100% mixtures due to damage while extracting these fragile mortars from their cylinder molds.

The variability of splitting tensile strength between specimens in a group was greater than that of compressive strength. The coefficient of variation ranged from 5% to 24%. The splitting tensile strength of each mixture proportion at 1, 7, 28 and 56 curing age is plotted against the fraction of bio-char to the total aggregate mass.

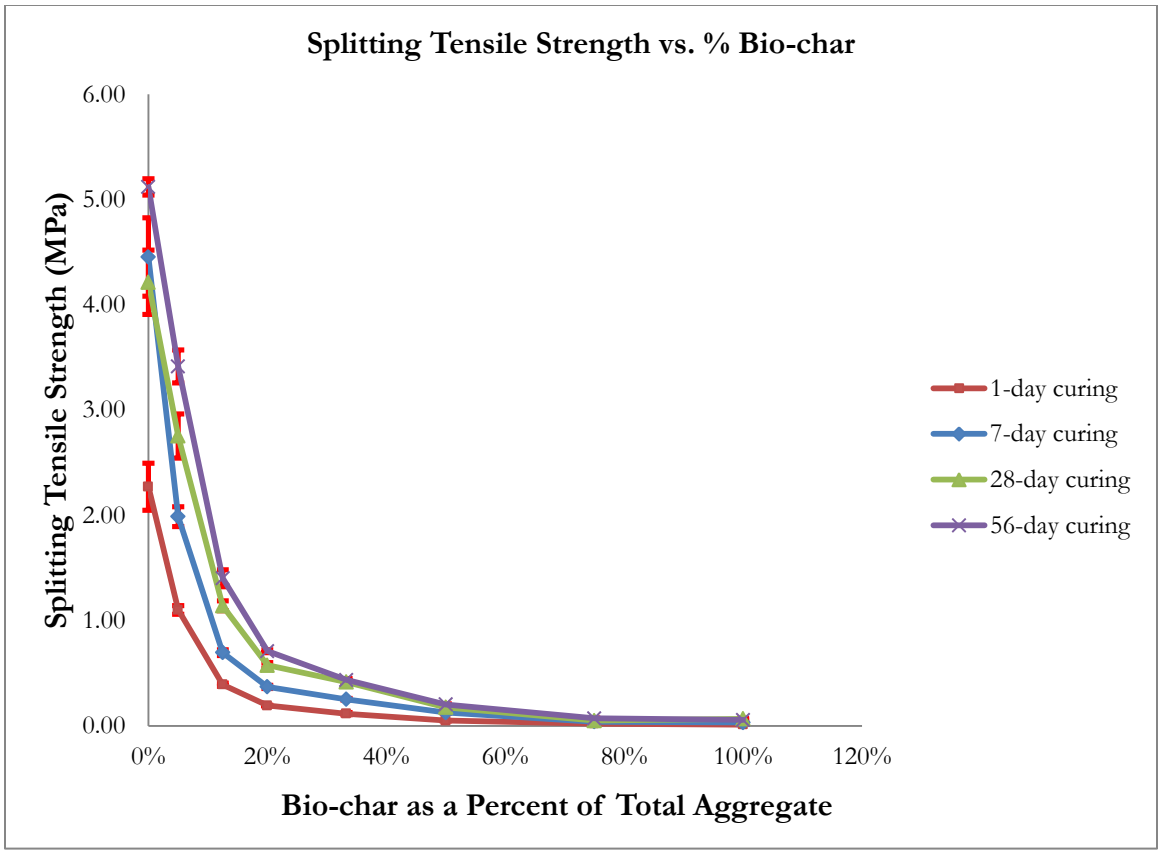

Figure 5.9 Splitting Tensile Strength vs. % Bio-char with 95% Confidence Error Bar

There is an obvious and continuous reduction in splitting tensile strength with an increase in bio-char content. The strength reduction compared to mixture of no bio-char content at the same curing age is listed in the Table 5.11.

Table 5.11 Splitting Tensile Strength Normalized to 0% Bio-char at Test Age of 28-days

Bio-char as a percent of total aggregate	Splitting tensile strength reduction			
	Curing duration			
	1-day	7-days	28-days	56-days
0%	53.9%	105.7%	100.0%	121.5%
5%	26.1%	47.2%	65.4%	81.0%
12.5%	9.3%	16.5%	27.1%	33.3%
20%	4.6%	8.8%	13.7%	16.9%
33.3%	2.8%	6.0%	9.9%	10.4%
50%	1.2%	3.0%	4.2%	4.9%
75%	0.5%	1.0%	1.2%	1.7%
100%	0.3%	0.8%	1.6%	1.3%

The splitting tensile strength is plotted against curing duration to observe strength development in Figure 5.10.

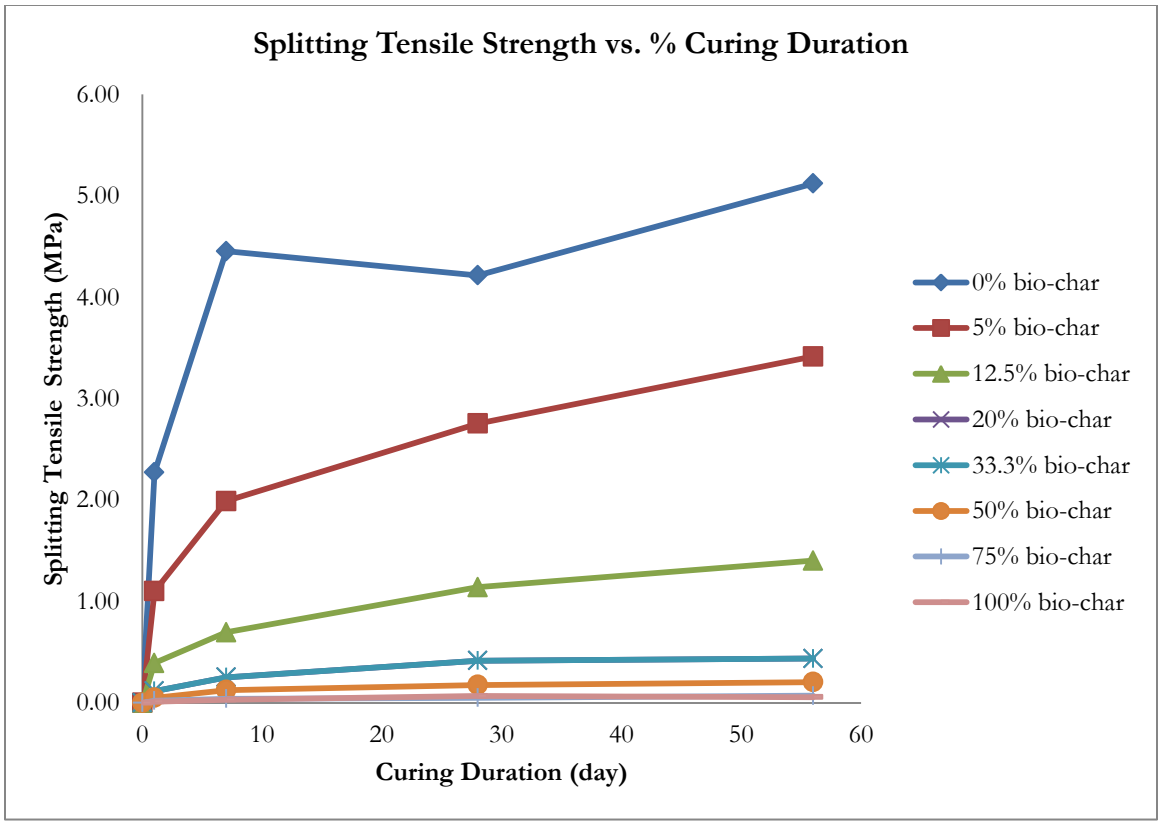

Figure 5.10 Splitting Tensile Strength vs. Curing Duration

5.2.3 Compressive strength vs. Splitting Tensile Strength

The splitting tensile strength of all mixtures is plotted against compressive strength within its mixture group across curing duration (Figure 5.12) and at the same curing age across groups (Figure 5.11). Using the 5% bio-char mixture as an example, linear regression on splitting tensile vs. compressive strength at 28-days validates the general rule-of-thumb that splitting tensile strength is about 1/10 of the compressive strength. The same pattern is repeated for all mixtures at all ages, with validation of the same general rule.

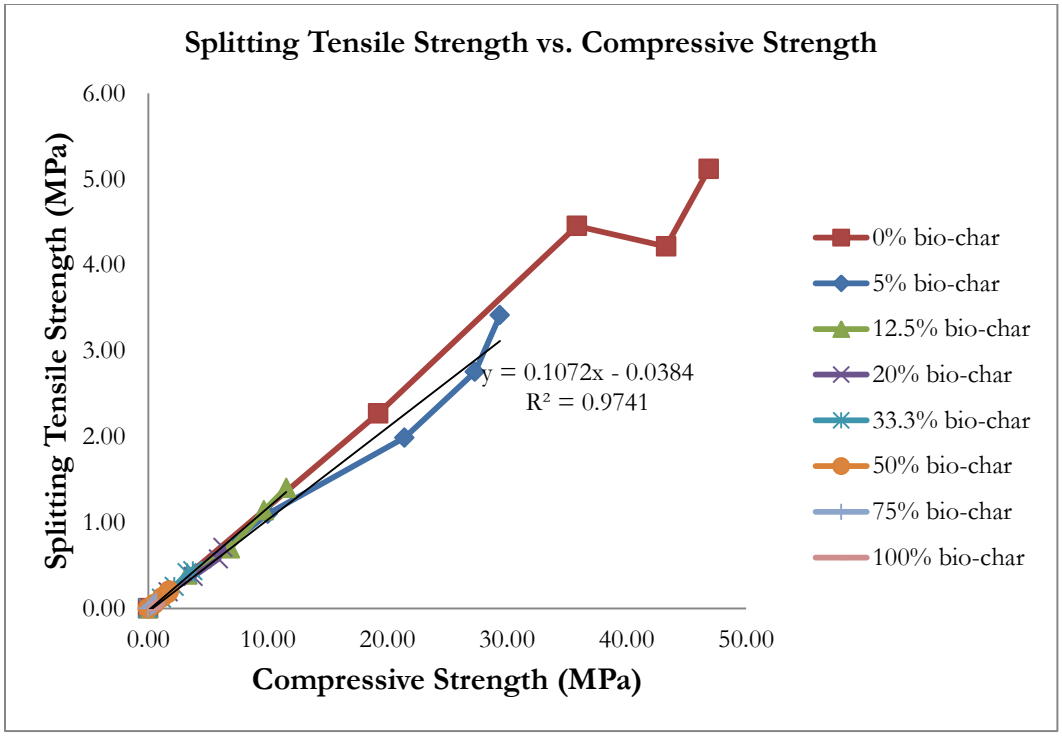

Figure 5.11 Compressive Strength vs. Splitting Tensile Strength at Test Age of 28-days

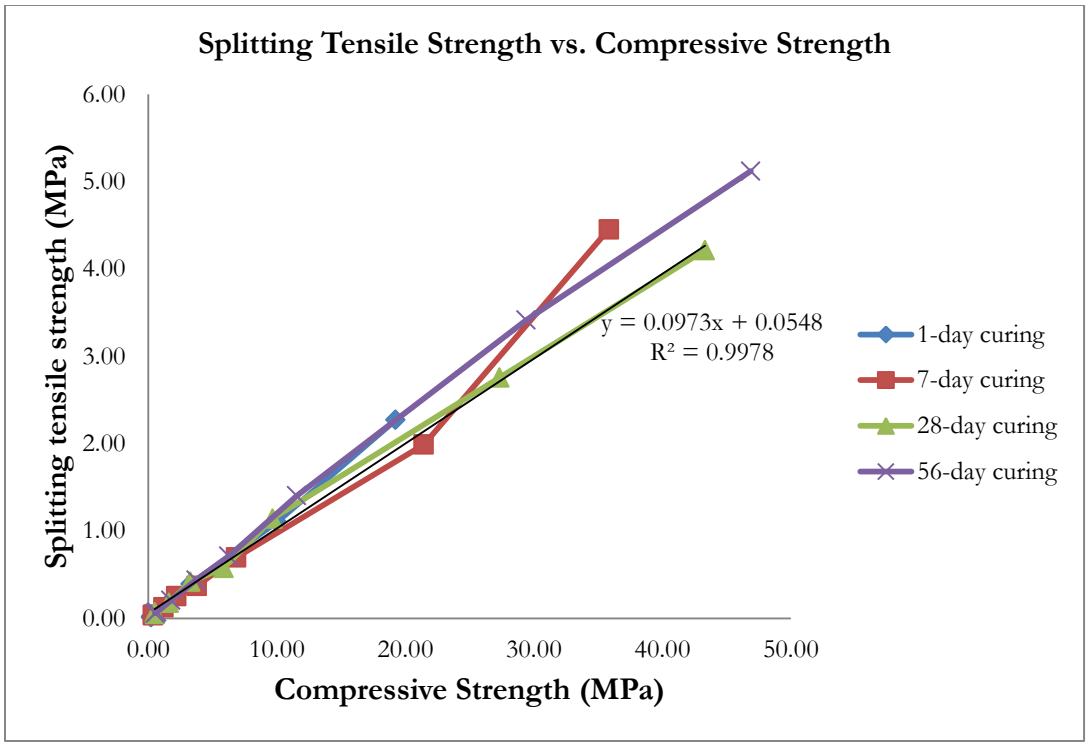

Figure 5.12 Compressive Strength vs. Splitting Tensile Strength for All Test Age

5.2.4 Three-dimensional Plot

Both the mass fraction of bio-char to total aggregate and curing duration influence compressive strength of the mortars tested mixture. Three-dimensional surface and column plots summarize the experiment data in Figures 5.13(a) and (b).

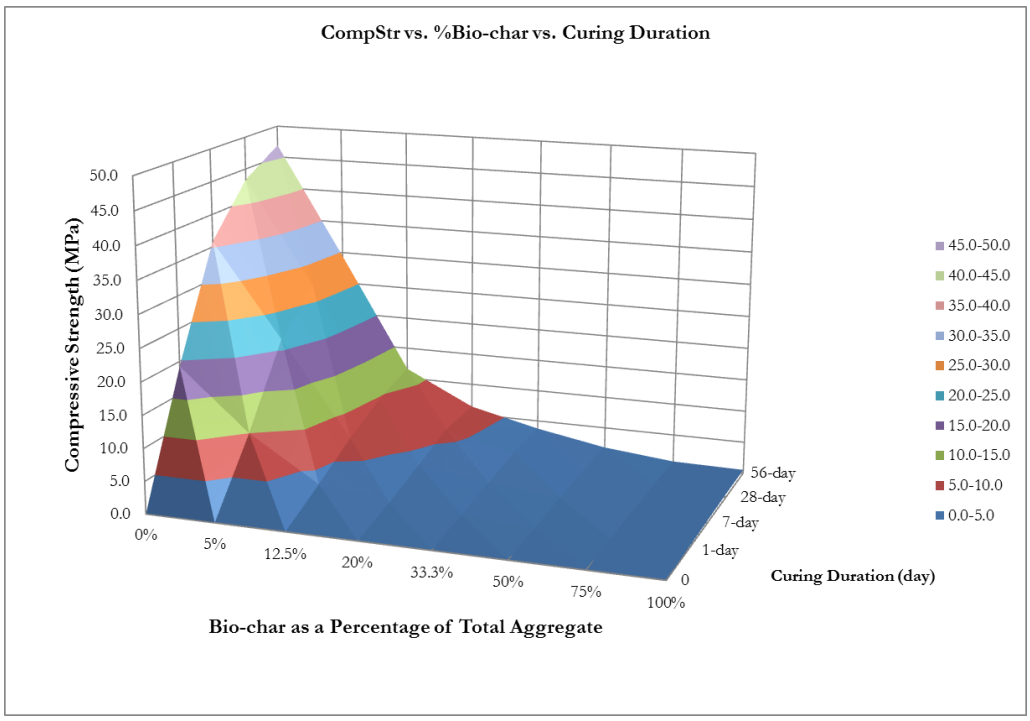

Figure 5.13(a) Compressive Strength vs. %Bio-char vs. Curing Duration (Surface Plot)

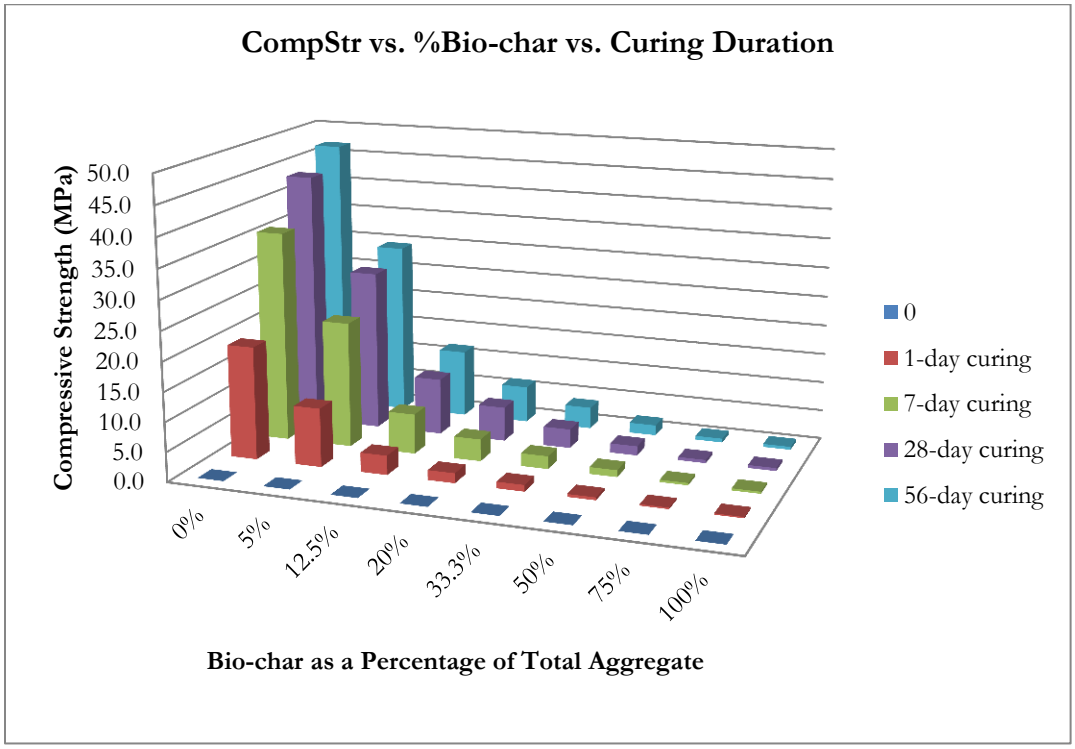

Figure 5.13(b) Compressive Strength vs. %Bio-char vs. Curing Duration (Column Plot)

5.2.5 Sequestration Potential

As mentioned in the chapter on material characterization of bio-char, the carbon sequestration potential of bio-char is quantified. And therefore the ability of carbon sequestration of each mixture in this research project is quantified and summarized in Table 5.12.

Table 5.12 Carbon Sequestration Potential

Bio-char as a percent of total aggregate	Net CO_2 seq. /unit weight cement (g)	Gross CO_2 seq. /unit weight cement (g)	Net CO_2 seq. /unit volume mortar (g)	Gross CO_2 seq. /unit volume mortar (g)
0%	-1.00	0.00	-0.50	0.00
5%	-0.61	0.39	-0.28	0.18
12.5%	0.01	1.01	0.00	0.41
20%	0.61	1.61	0.21	0.57
33.3%	1.68	2.68	0.51	0.81
50%	3.03	4.03	0.72	0.96
75%	5.04	6.04	0.89	1.06
100%	7.06	8.06	1.03	1.18

The sequestration potential is plotted against compressive strength for 28-days curing in Figure 5.14. According to these results, the maximum achievable compressive strength at 28-days for carbon neutral or negative mortar is around 13.7-MPa (2000-psi).

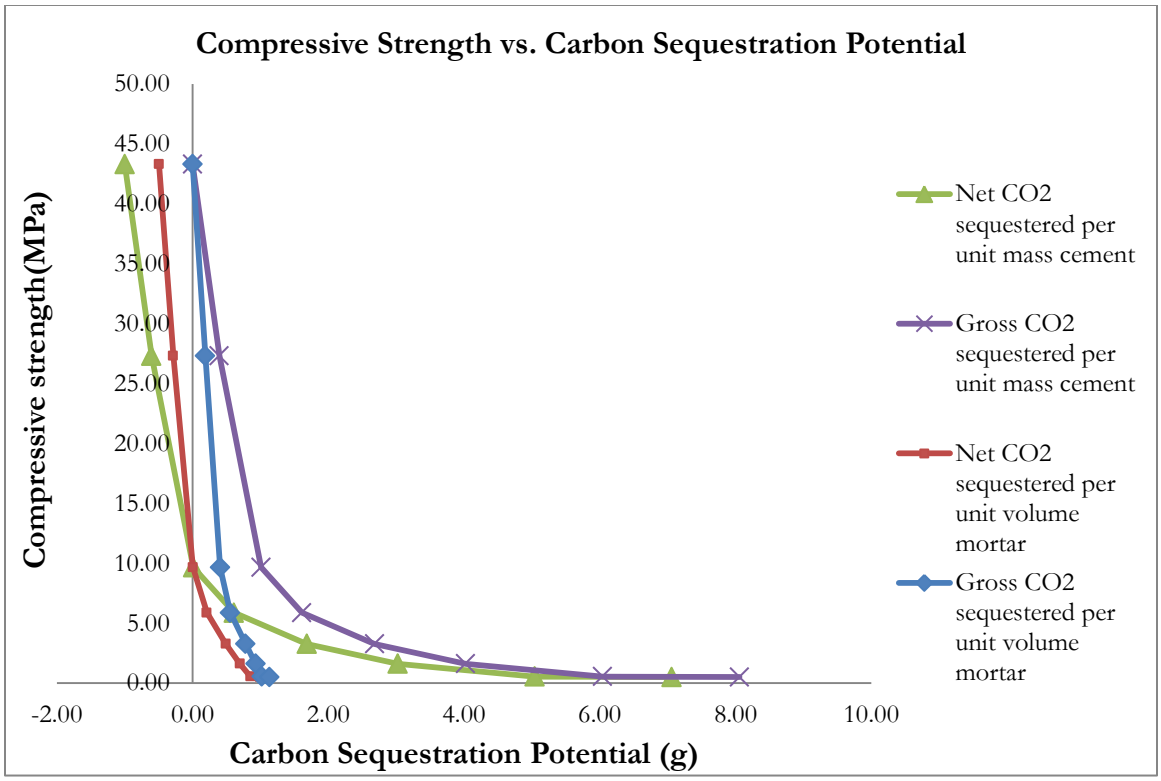

Figure 5.14 Compressive Strength vs. Carbon Sequestration Potential

5.2.6 Summary Plot

The summary plot (Figure 5.15) combines the information of mortar mixture, mortar strength and mortar carbon sequestration ability.

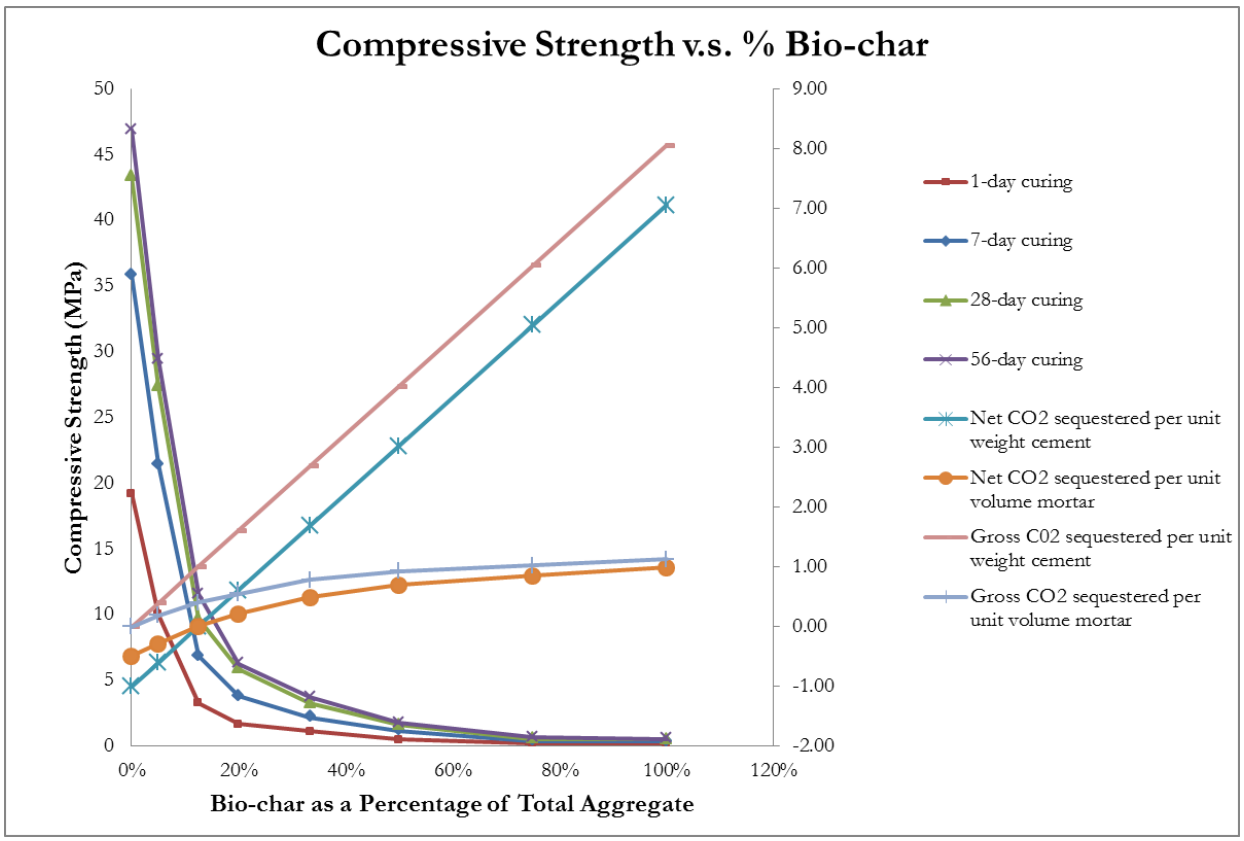

Figure 5.15 Summary Plot

CHAPTER 6

ANALYSIS AND INTERPRETATION OF RESULTS

6.1 General Introduction to the Analysis

This chapter presents an explanation of the behavior of fresh and hardened bio-char mortar based on the background knowledge on mortar mixture reported in Chapter 2, and the experiment results reported in Chapter 5. Models to predict strength of bio-char-mortar mixture are introduced, compared and evaluated.

6.2 Behavior of Fresh Mortar

Workability (flow), air content, and density of fresh mortar were measured at the time of batching and casting. The most critical aspect of the batching was the observation that maintaining flow as bio-char content increased required an additional 1.25 to 1.9 gram of water per gram of bio-char. Details of these phenomena are discussed below.

6.2.1 Interpretation of the Additional Water Required for Bio-char-mortar Mixture

As reported in Chapter 3, bio-char has an absorption of 125% as estimated by algebraic derivation combined with experimental data. Subsequent experimentation (Chapter 3) verified that over an approximate 7-days soaking period, the bio-char has the capacity to absorb at least 125% of its own oven-dry mass, and as pointed-out above, for some mixtures more than 1.25 gram of additional water was required per gram of bio-char to maintain flow.

This additional water is important because it influences workability, and any additional water that is not absorbed into the bio-char particle (free-water) affects the porosity of the paste. Water on the surface of the bio-char particles increases workability, occupies volume, generates porosity in the paste, separates the cement particles, and thus lowers strength. Water absorbed into the bio-char particles does not occupy volume in the paste, does not lower strength, but neither does it contribute to workability. Thus it is important to at least qualitatively separate the water absorbed into the bio-char from the water residing as a surface film, both of which increase with bio-char content. First, a film of cement and water paste must coat the surface of all particles and air bubbles in mortar mixtures [Mindess & Young, 1981]. This is true of all mortars and concretes. As particle surface area increases, additional water will be required to maintain workability, independently of any absorption effects. Examples of this effect include the need for higher water contents in mortar or concrete containing finer cement, fine sands, and especially silica fume [Mehta & Monteiro, 2006].

According to the results of sieve analyses reported in Chapter 3 and Chapter 5, the fineness modulus (FM) of the sand and bio-char "dust" is 2.48 and 0.48 respectively. (Fineness modulus is defined by ASTM C192 as a particle fineness index where the smaller the FM, the finer the particles.) If both sand and bio-char "dust" used in the experiment are assumed to consist of spherical particles, an average bio-char "dust" particle is in the range of about 30 to 40 times smaller than an average sand grain. Particle diameter is approximated by assuming an average of the sieve opening just above and the sieve opening upon which that particle is retained. The average diameter of particle is calculated by taking a weighted average to account for the particle size distribution. With these approximations it can be estimated that the surface area of bio-char "dust" is on the range of 100 times greater than that for an equivalent mass of sand.

For the surface-area effect, it appears reasonable that increasing bio-char content inflates its surface area in bio-char-mortar mixtures, thus requiring a significant amount of additional water to create the water film in between particles to lubricate the mortar, and maintain workability to reach the target flow of 110±5%.

Secondly, apart from the surface area effect, water is absorbed into bio-char particle as it is into sand or any other porous aggregate. The potentially accessible pore space inside bio-char particles is estimated to be about 125%, as reported in Chapter 3. Given that the rate of absorption into bio-char remains unknown, it is unclear whether all additional water was absorbed during the 2-hour mixing and casting period. In any case, neither the effect of surface area alone nor actual absorption of bio-char over time could be precisely and quantitatively accounted for in this study. For that reason the term "Effective Absorption" has been adopted.

As presented in Section 5.1.5, when the "Effective Absorption" varies from 0% to 150%, the upper- and lower- bound water-cement ratio are calculated for all 8 mixtures and shown in Table 5.7.

6.3 Behavior of Hardened Mortar

This section presents the interpretation of the factors that affect both compressive strength and splitting tensile strength of bio-char-mortar mixtures based on the upper- and lower- bounds assumption of "Effective Absorption" from Section 6.2.

6.3.1 General Age Impact on Strength

6.3.1.1 Strength vs. Age

As reported in Chapter 5, the age of mortar positively affects the strength of bio-char mixtures, which concurs with the behavior of traditional cementitious materials as reported in Chapter 2.

In Figure 6.1(a), strength is plotted against age, and examples of strength as a log function of age of 0% and 5% bio-char-mortar mixtures are provided. The regressions on the rest of bio-char-mortar mixtures are provided in Table 6.1.

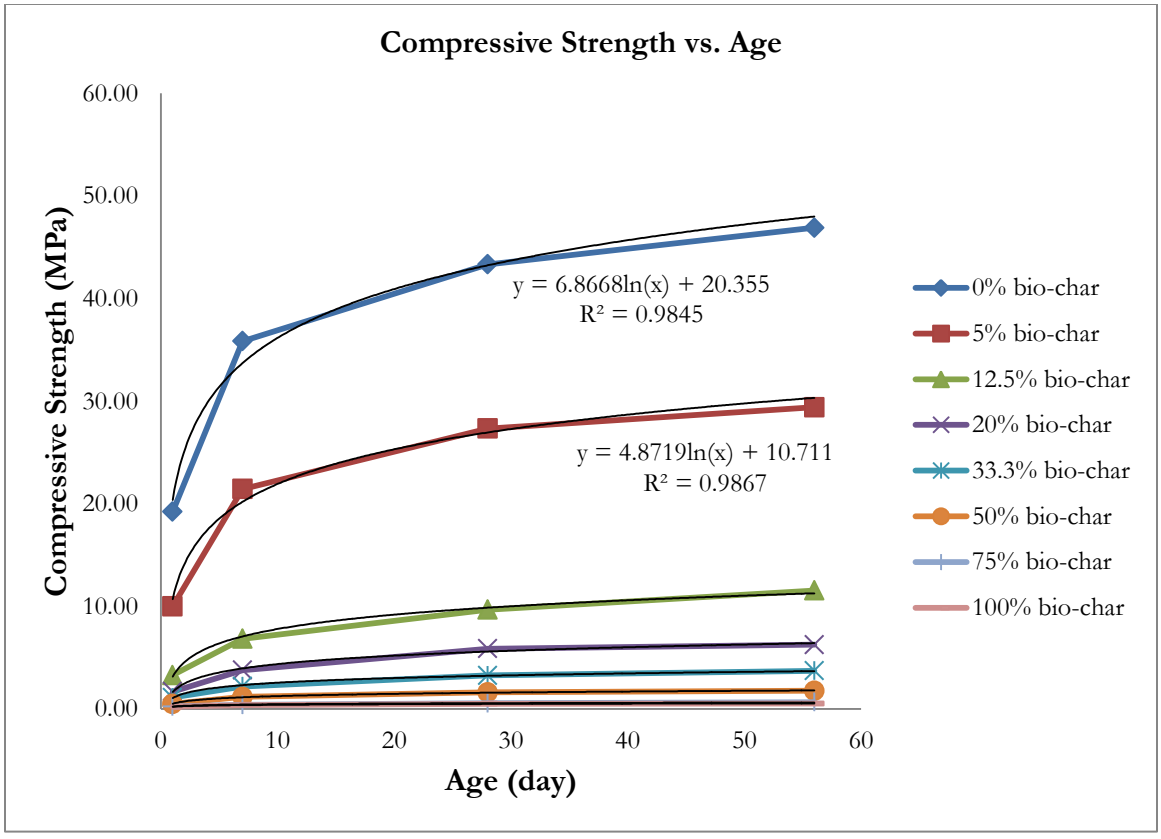

Figure 6.1(a) Compressive Strength vs. Age

Table 6.1 Regression for Compressive Strength as a Function of Age

Bio-char as a percent of total aggregate	Regression equation (Strength in unit of psi, age in unit of day)	Correlation coefficient (R^2)
0%	$\text{Compressive strength} = 6.87\ln(\text{Age}) + 20.36$	0.985
5%	$\text{Compressive strength} = 4.87\ln(\text{Age}) + 10.71$	0.987
12.5%	$\text{Compressive strength} = 2.02\ln(\text{Age}) + 3.14$	0.995
20%	$\text{Compressive strength} = 1.18\ln(\text{Age}) + 1.65$	0.990
33.3%	$\text{Compressive strength} = 0.65\ln(\text{Age}) + 1.05$	0.994
50%	$\text{Compressive strength} = 0.32\ln(\text{Age}) + 0.51$	0.996
75%	$\text{Compressive strength} = 0.10\ln(\text{Age}) + 0.23$	0.976
100%	$\text{Compressive strength} = 0.08\ln(\text{Age}) + 0.21$	0.985

In ACI 209, a study of concrete strength versus age indicates a general equation in the form:

$$(f'_c)_t = \frac{t}{\alpha + \beta t}(f'_c)_{28}$$

where α (in days) and β (unitless) are constants, $(f'_c)_{28}$ is 28-days strength and t is the age of concrete in days.

The values of α and β for each bio-char mixture are provided in regression equations in Table 6.2, and are compared in Figure 6.1(b).

Table 6.2 Regression for ACI209

Bio-char as a percent of total aggregate	Regression equation (Strength in unit of psi, age in unit of day)	Correlation coefficient (R^2)
0%	$(f'_c)_t = \frac{t}{1.467 + 0.934t}(f'_c)_{28}$	0.970
5%	$(f'_c)_t = \frac{t}{2.072 + 0.918t}(f'_c)_{28}$	0.989
12.5%	$(f'_c)_t = \frac{t}{3.275 + 0.832t}(f'_c)_{28}$	0.924
20%	$(f'_c)_t = \frac{t}{3.842 + 0.878t}(f'_c)_{28}$	0.963
33.3%	$(f'_c)_t = \frac{t}{3.363 + 0.857t}(f'_c)_{28}$	0.924
50%	$(f'_c)_t = \frac{t}{2.962 + 0.881t}(f'_c)_{28}$	0.983
75%	$(f'_c)_t = \frac{t}{2.067 + 0.875t}(f'_c)_{28}$	0.780
100%	$(f'_c)_t = \frac{t}{1.869 + 0.969t}(f'_c)_{28}$	0.891

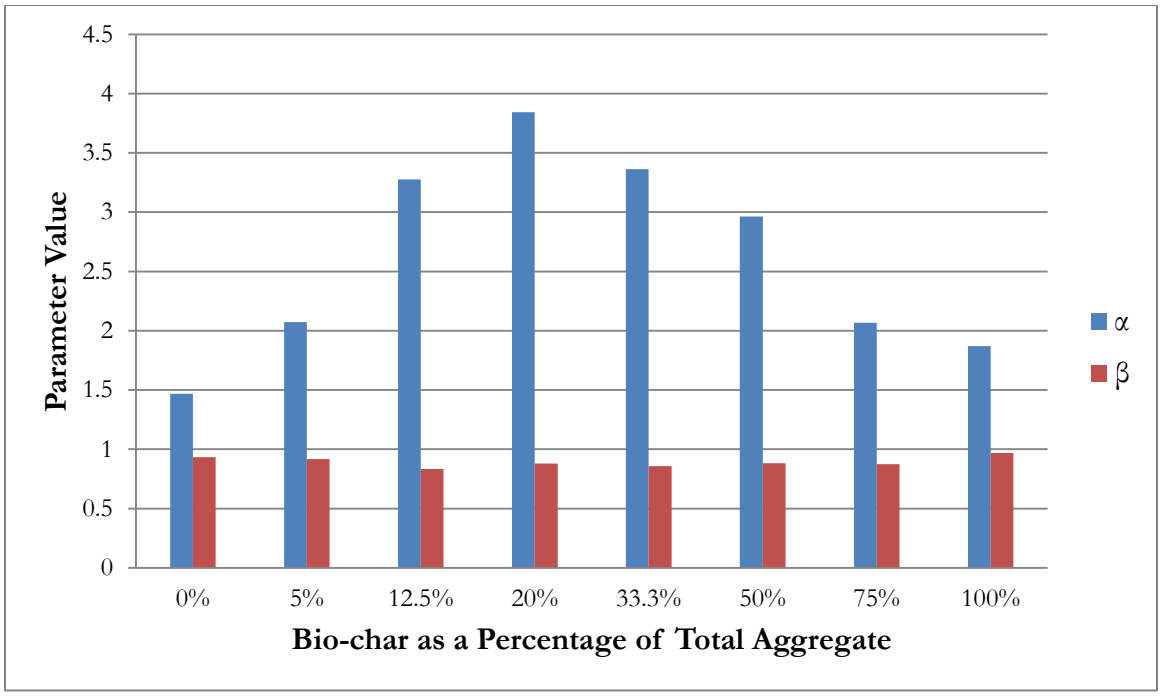

Figure 6.1(b) Parameters for ACI209

ACI209 further suggests the ranges of α and β for normal weight, sand lightweight or all-lightweight concrete are: α = 0.05 to 9.25, β = 0.67 to 0.98. In this study, the values of α are within the suggested range, and there is clear pattern observed that α increases with first with bio-char as a percentage of total aggregate, arrives peak value at 20% bio-char (as a percentage of total aggregate), and then decreases with bio-char content. The values of β are in the vicinity from 0.832 to 0.969, showing a pattern for all 8 sets of bio-char-mortar mixtures that is more consistent than observed for conventional concrete. All correlation coefficients (R^2) are greater than 0.89 except for 75% bio-char (as a percentage of total aggregate), indicating that the strength-age relationship suggested by ACI209 still strongly applies in the bio-char mortar.

Given the general trends just discussed, the balance of this chapter will focus only on behavior at an age of 28-days after casting.

6.3.1.2 Interpretation of Rate of Strength Development

As shown in Figures 5.8(a), (b), (c) and (d) in Section 5.2.1, the overlap of the variability of normalized strength suggests that on the basis of this experimental program, no conclusion on the rate of strength development among all mixtures can be drawn. The varying rates appear to be responding to factors other than mere bio-char content. Note, however, that even though variable temperature commonly affects rate of strength gain in cementitious materials, temperature was held constant in this experiment.

6.3.2 Overall Trends Observed for Strength at 28-days

In the following analyses, the abbreviation "28CS" is used for compressive strength at age of 28-days after casting for all bio-char-mortar mixtures; "28TS" is used for splitting tensile strength at age of 28-days after casting for all bio-char-mortar mixtures.

The individual factors that are considered to affect the strength of bio-char-mortar mixtures in this study are listed in Table 6.3.

Table 6.3 Individual Factors Affecting Mortar Strength

Symbol	Variable name	Equation
%bio-char	Mass percentage of total aggregate that has been replaced by bio-char	$\frac{M_{bio-char}}{M_{bio-char} + M_{sand}}$
ϱ_{mortar}	Density of bio-char-mortar	$\frac{M_{mortar\ in\ cylinder}}{V_{cylinder}}$

w/c	Water-cement ratio (based on "Effective Absorption") is the ratio between the mass of free water (i.e., the water that occupies volumes between and among the solid particles) and the mass of cement used in a mortar mixture. To compute the mass or volume of free water, one must subtract from the total water any water that is absorbed by the sand and bio-char.	$\frac{M_{free\ water}}{M_{cement}}$
$\%V_a$	Volume percentage of total mortar that has been occupied by air	$\frac{V_{air}}{V_{mortar}}$
$\%V_b$	Volume percentage of total mortar that has been occupied by bio-char	$\frac{V_{bio-char}}{V_{mortar}}$
$\%Vf_w$	Volume percentage of total mortar that has been occupied by free water	$\frac{V_{free\ water}}{V_{mortar}}$
$\%V_c$	Volume percentage of total mortar that has been occupied by cement	$\frac{V_{cement}}{V_{mortar}}$

6.3.2.1 Strength vs. %Bio-char

In this study, "%bio-char" was a defining variable around which the experimental program was designed.

As shown in Figures 6.2(a) and (b), both compressive strength (left hand axis) and splitting tensile strength (right hand axis) at the test age of 28-days are plotted against bio-char as a mass percentage of total aggregate.

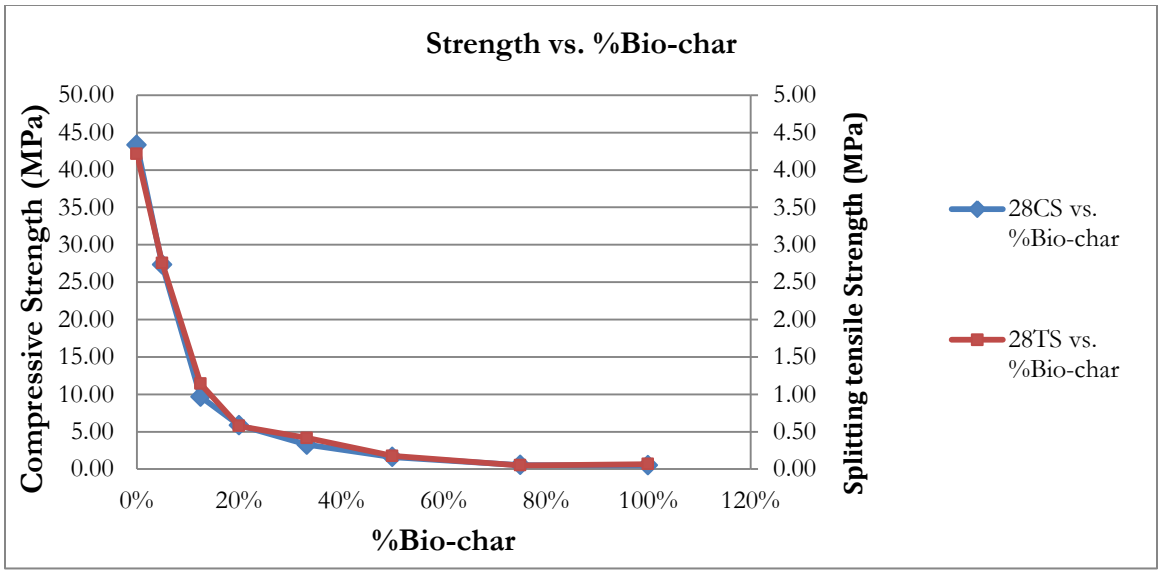

Figure 6.2(a) Strength vs. %Bio-char

In Figure 6.2(b), the experiment result of the 0% bio-char mixture is excluded, and then the regression is applied to seek the strength prediction model using "%bio-char" as predictor. When "%bio-char" is in range of 5% to 100%, the strength fits the power function of "%bio-char", with the coefficients of correlations (R^2) of 0.98 for compressive strength and 0.95 for splitting tensile strength.

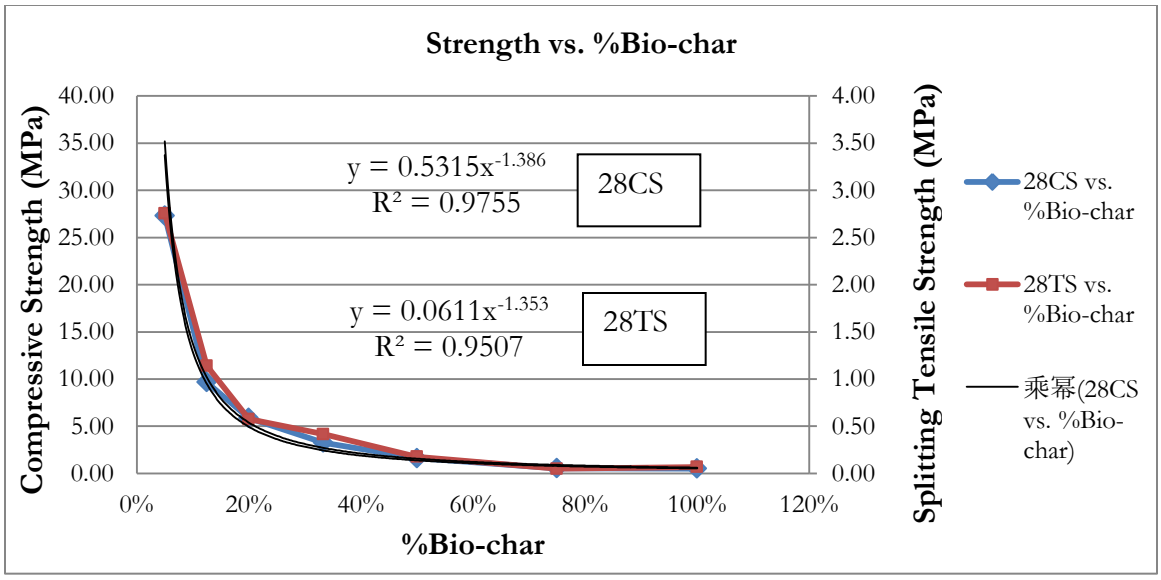

Figure 6.2(b) Strength vs. %Bio-char with Regression Equation

6.3.2.2 Strength vs. Density

The density of mortar represents the ratio between the mass contributed by solid ingredients and the volume of mortar mixtures. The solid in mortar includes cement paste and total aggregate bond by cement paste positively contributes to strength of mortar [Mindess & Young, 1981], as reported in Chapter 2.

As shown in Figures 6.3(a), (b) and (c), both compressive strength (left hand axis) and splitting tensile strength (right hand axis) at the test age of 28-days are plotted against mortar density.

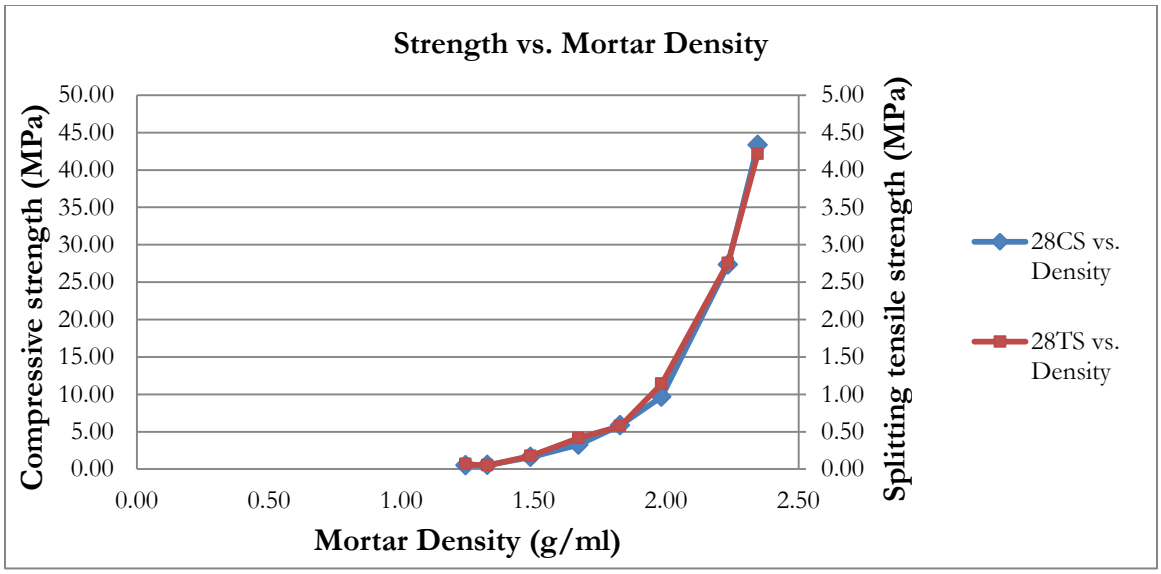

Figure 6.3(a) Strength vs. Mortar Density

The regression is applied to seek the strength prediction model using "ϱ_{mortar}" as predictor. The strength fits the power function of "ϱ_{mortar}", with the coefficients of correlations (R^2) of 0.99 for compressive strength and 0.98 for splitting tensile strength.

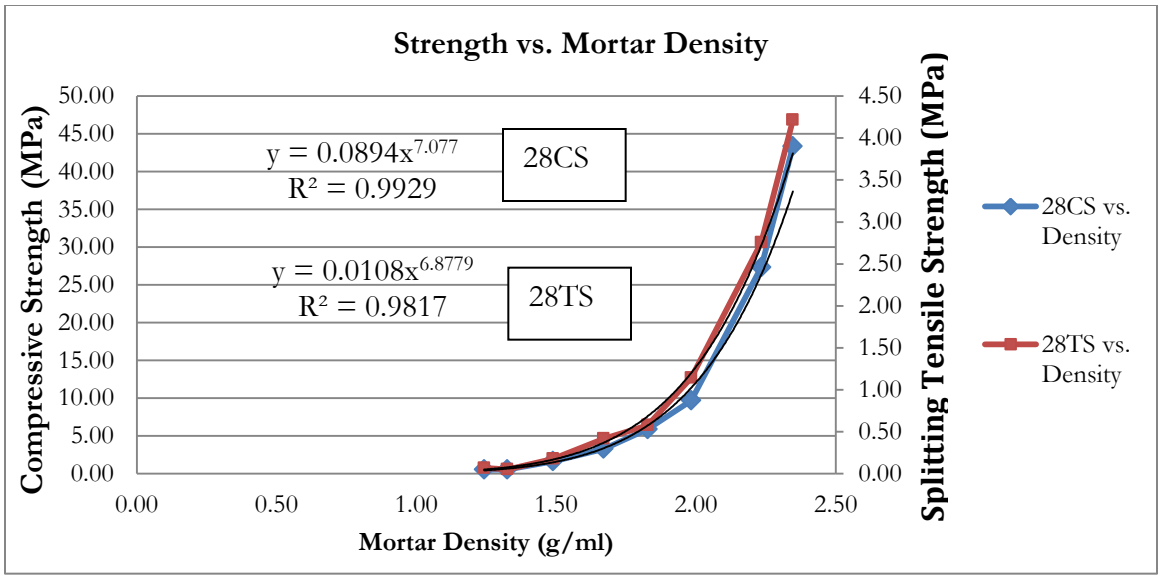

Figure 6.3(b) Strength vs. Mortar Density with Regression Equation

In Figure 6.3(c), the data are plotted on log-scale axes, showing the linear correlation between log of strength and log of "ϱ_{mortar}".

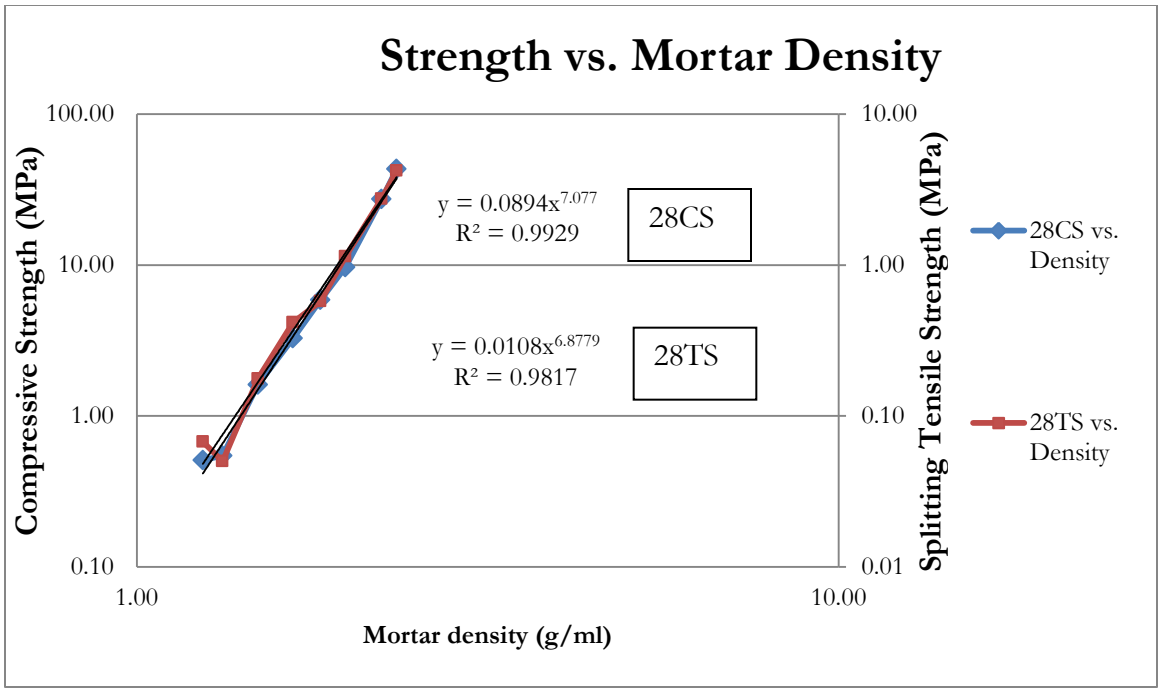

Figure 6.3(c) Strength vs. Mortar Density in Log Scale

6.3.3 Exploring Individual Factors Affecting Strength

6.3.3.1 Strength vs. w/c

As reported in Chapter 2, in traditional cementitious materials, the strength of properly compacted mortar or concrete at a given age is strongly correlated with the water-cement ratio [Mindess & Young, 1981], defined as the mass of free water relative to the mass of cement or other cement-like (cementitious) materials. Water-cement ratio is therefore an often-used indicator to predict strength. As is also mentioned in Section 6.2, the introduction of bio-char content led to the introduction of additional water, which in turn affected water-cement ratio of all bio-char-mortar mixtures for combined impact from the surface area and the absorption of bio-char "dust".

In Figures 6.4(a) and (b), compressive and splitting tensile strength at the test age of 28-days are plotted against water-cement ratio calculated using 4 different values of "Effective Absorption" (Abbreviated as "E.A" in Figures and Tables). Values of E.A. indicate the mass of water that is assumed to have been absorbed into the bio-char as of the time of casting the mortar cylinders, expressed as a percentage of the oven-dry mass of the bio-char in that same mixture. Under such assumptions, that portion of the additional water that has not been absorbed is likewise assumed to be "free water" that occupies volume between the cement particles, and contributes to the water counted in the w/c.

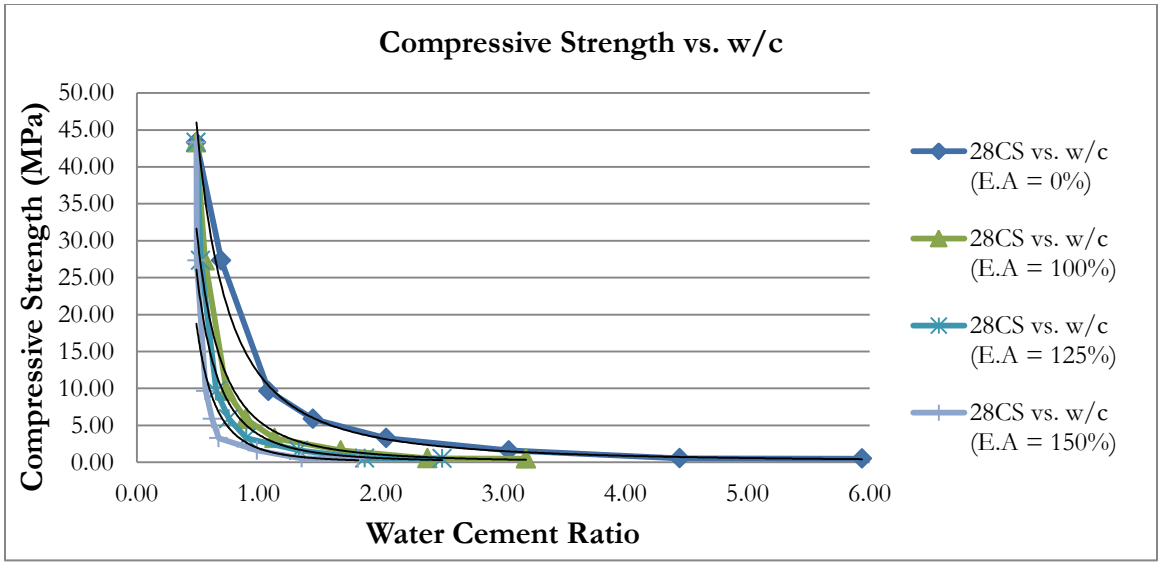

Figure 6.4(a) Compressive Strength vs. w/c

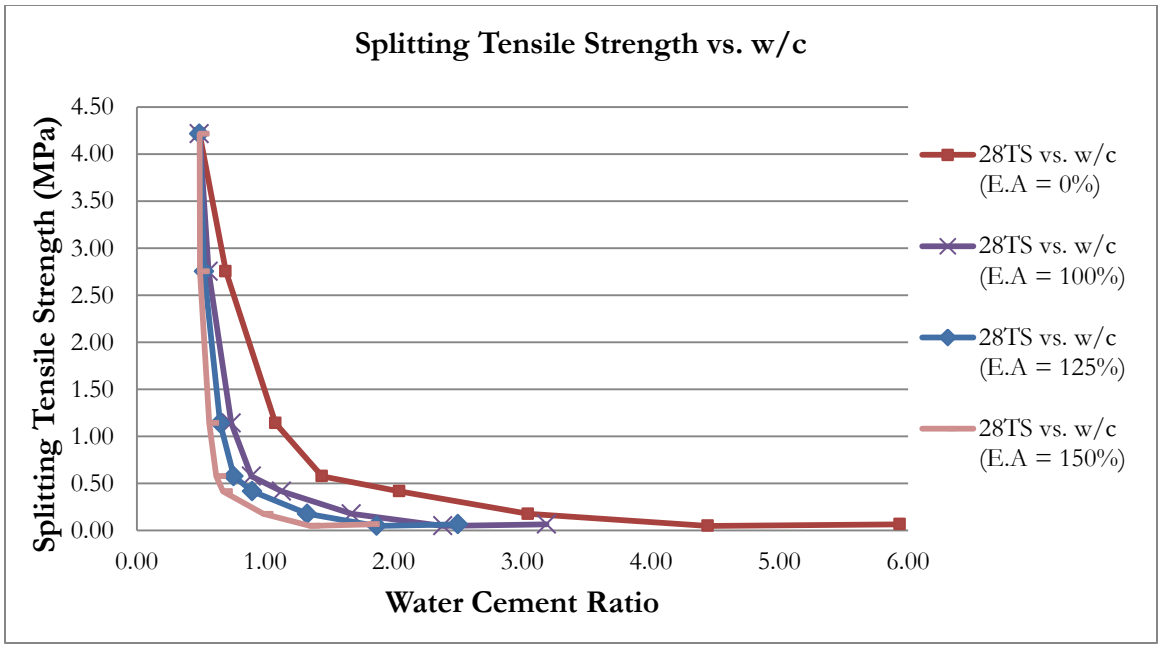

Figure 6.4(b) Splitting Tensile Strength vs. w/c

In Figures 6.4(c) and (d), the data are plotted on log-scale axes, where the linear correlation between log of strength and log of "w/c" is shown. In both figures, the first regression equation at the top presents the compressive and splitting tensile strength as a power function of water-cement ratio when "Effective Absorption" is taken as 0%. The second, third and fourth equation are for mortar strength when "Effective Absorption" is taken as 100%, 125% and 150%.

The coefficients of correlations (R^2) of these regression lines ranged from 0.89 to 0.99. The highest value of R^2 (0.9921) is obtained with "Effective Absorption" is taken as 0% and lowest (0.893) when "Effective Absorption" is taken as 150%.

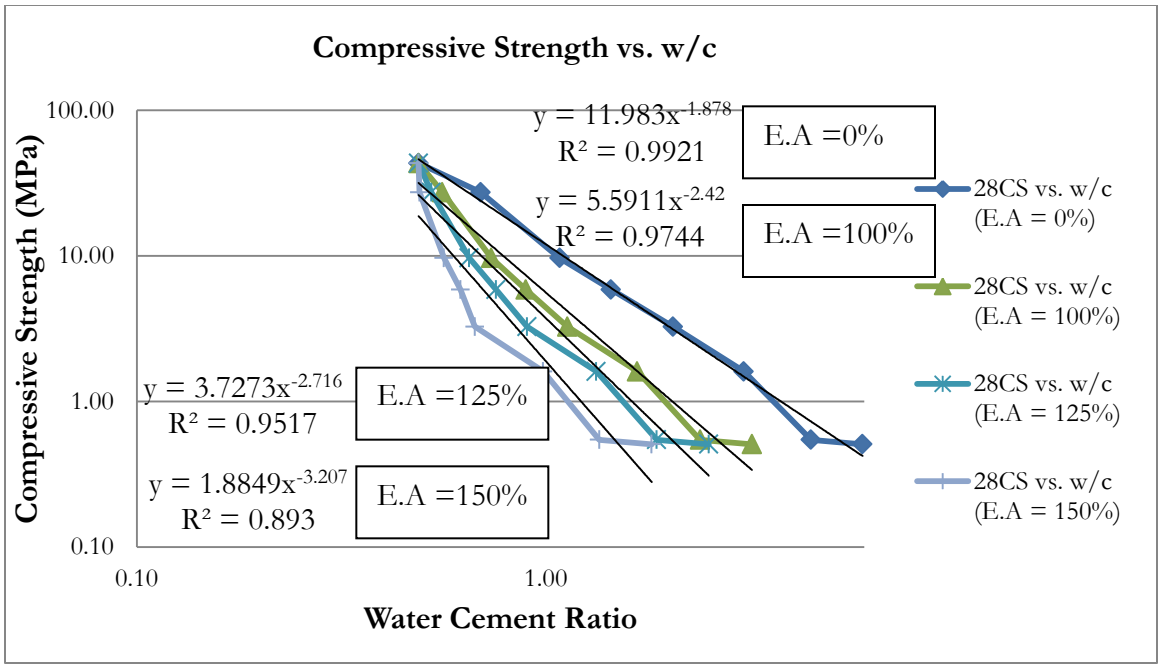

Figure 6.4(c) Compressive Strength vs. w/c with Regression Equation in Log Scale

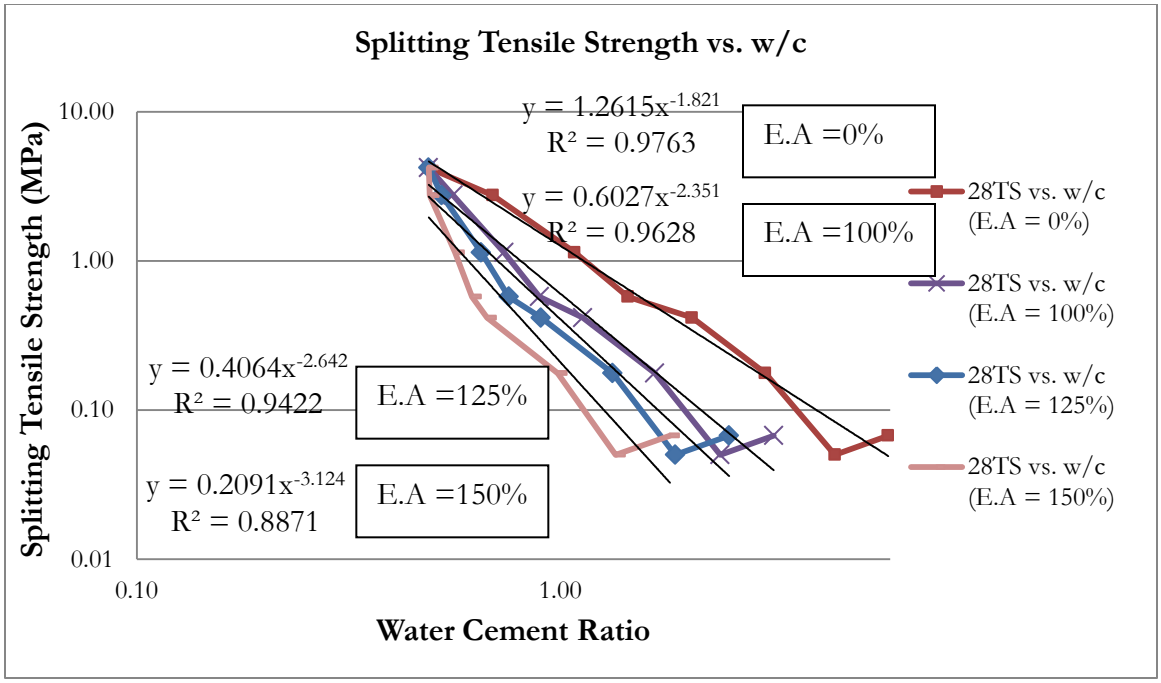

Figure 6.4(d) Splitting Tensile Strength vs. w/c with Regression Equation in Log Scale

Abrams' "Law" [Neville, 1981] established a formula that strength is taken to be inversely proportional to a constant raised to a power equivalent to the water-cement ratio in the following equation:

$$f_c = \frac{K_1}{K_2^{w/c}}$$

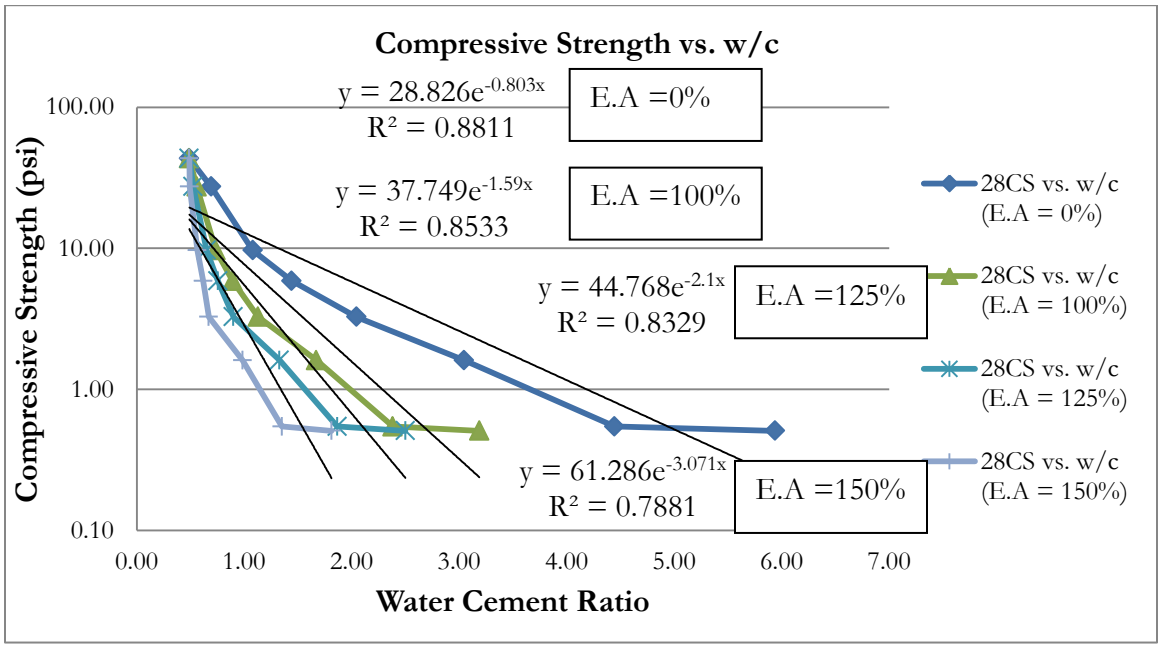

Figure 6.4(e) Abrams Law

Table 6.4 Coefficient for Abrams Law

E.A	0%	100%	125%	150%
K_1	4181	5475	6493	8889
K_2	0.448	0.204	0.122	0.046
R^2	0.88	0.85	0.83	0.79

Although there is a general conformance to Abram's relationship, it would appear that strength of the bio-char mortar is governed by additional factors besides w/c. On the other hand, since the

experiment did not include a range of values of w/c for fixed values of %bio-char, more detailed conclusions about the effect of w/c as an independent variable cannot be drawn.

6.3.3.2 Strength vs. $\%V_a$

As reported in Chapter 2, an increase in air content results in a strength loss for concrete and mortar mixtures at any given water-cement ratio [Mindess & Young, 1981]. In Figure 6.5, compressive strength (left hand axis) and splitting tensile strength (right hand axis) at the test age of 28-days are plotted against measured air content (as a volume percentage of mortar) as was estimated by the Chace air indicator during mixing and consolidation.

As reported in Section 5.1.3, the air content of all 8 mixtures was scattered randomly in as shown in Figure 5.2 with no apparently consistent trend. And therefore, when strength is compared to the air content, there is also no apparent trend to suggest a correlation between air and strength of bio-char-mortar mixtures. Further experiments with more control on actual air content and its more precise measurement would be required to resolve this issue.

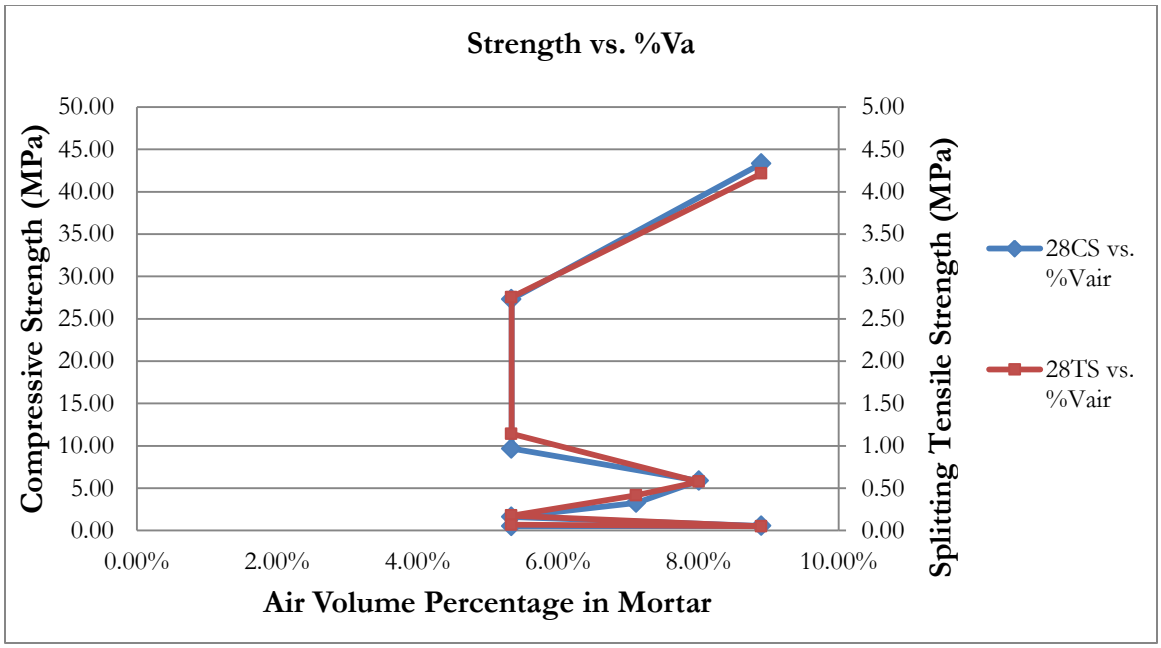

Figure 6.5 Strength vs. $\%V_a$

6.3.3.3 Strength vs. $\%V_b$

As reported in 6.3.1.1, bio-char content in all mortar mixtures in this study was the defining variable around which the mixture proportion was designed. And the volume of bio-char content influences strength of hardened mortar as shown in Figures 6.6(a) and (b), where compressive strength and splitting tensile strength at the test age of 28-days are plotted against bio-char content (as a volume percentage of mortar). Since the value variation of "Effective Absorption" changes the volume of free water content in the mortar, this also affects the bio-char volume percentage along with volume percentages of all ingredients in the mortar mixtures.

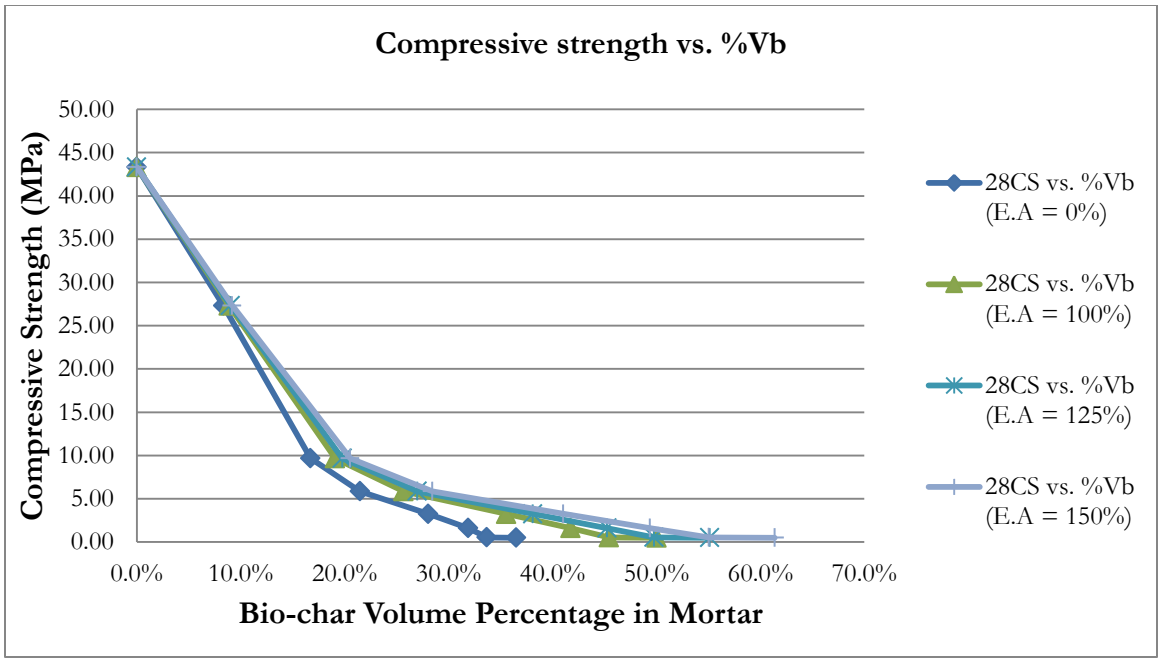

Figure 6.6(a) Compressive Strength vs. $\%V_b$

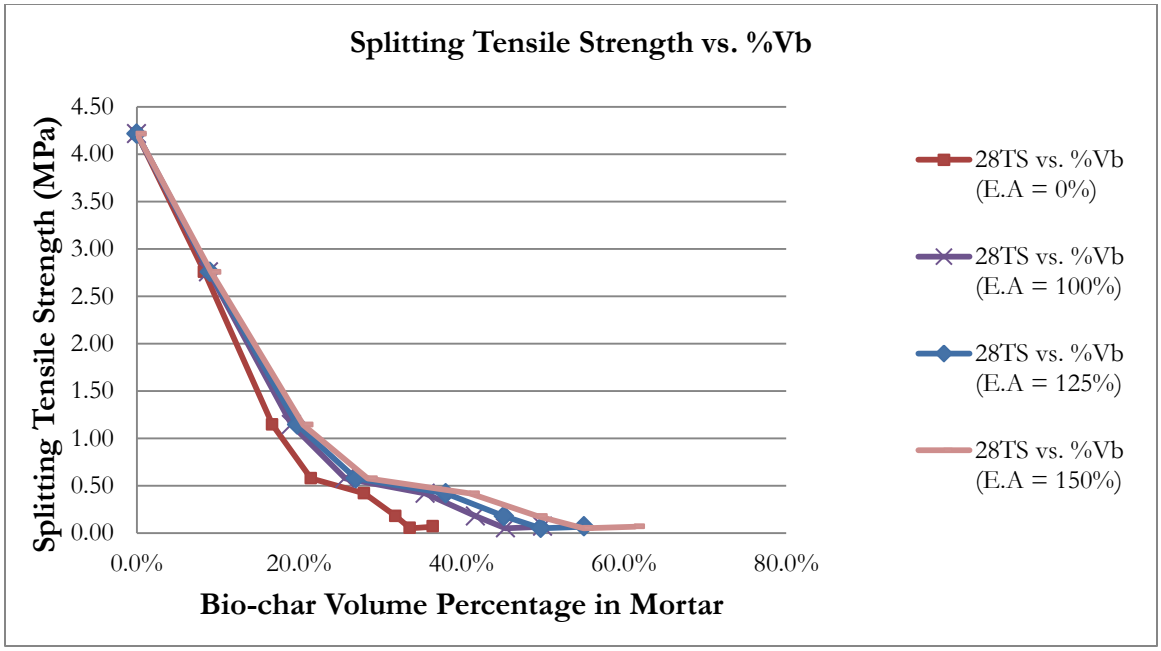

Figure 6.6(b) Splitting Tensile Strength vs. $\%V_b$

In Figures 6.6(c) and (d,) the data are plotted on log-scale axes, where the linear correlation between strength and log of "$\%V_b$" is shown. In both figures, the first regression equation at the top presents the compressive and splitting tensile strength as a log function of "$\%V_b$" when "Effective Absorption" is taken as 150%. The second, third and fourth equation are for mortar strength when "Effective Absorption" is taken as 125%, 100% and 0%.

In Figures 6.6(c) and (d), the experimental result of the 0% bio-char mixture is excluded, and then the regression analyses are applied to seek the strength prediction model using "$\%V_b$" as predictor. When "$\%V_b$" is greater than zero, the strength fits the log function of "$\%V_b$", with the correlation coefficient (R^2) in range of 0.93 to 0.96 for compressive strength and 0.95 to 0.97 for splitting tensile strength.

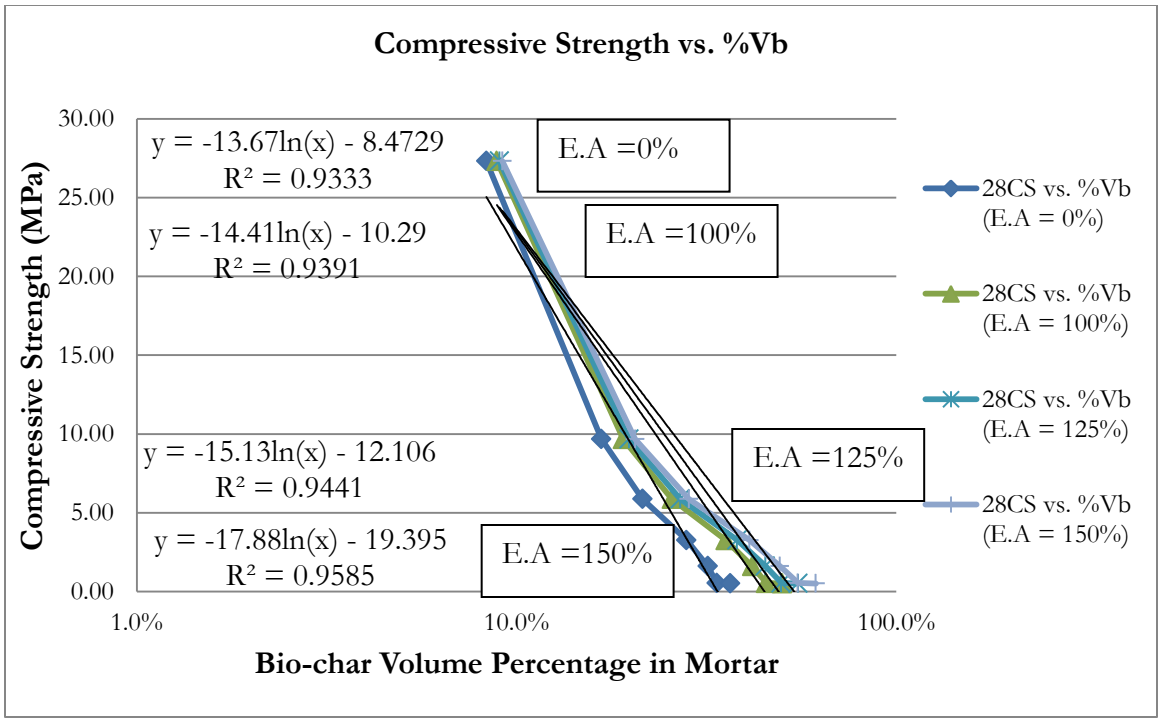

Figure 6.6(c) Compressive Strength vs. $\%V_b$ with Regression Equation in Log Scale

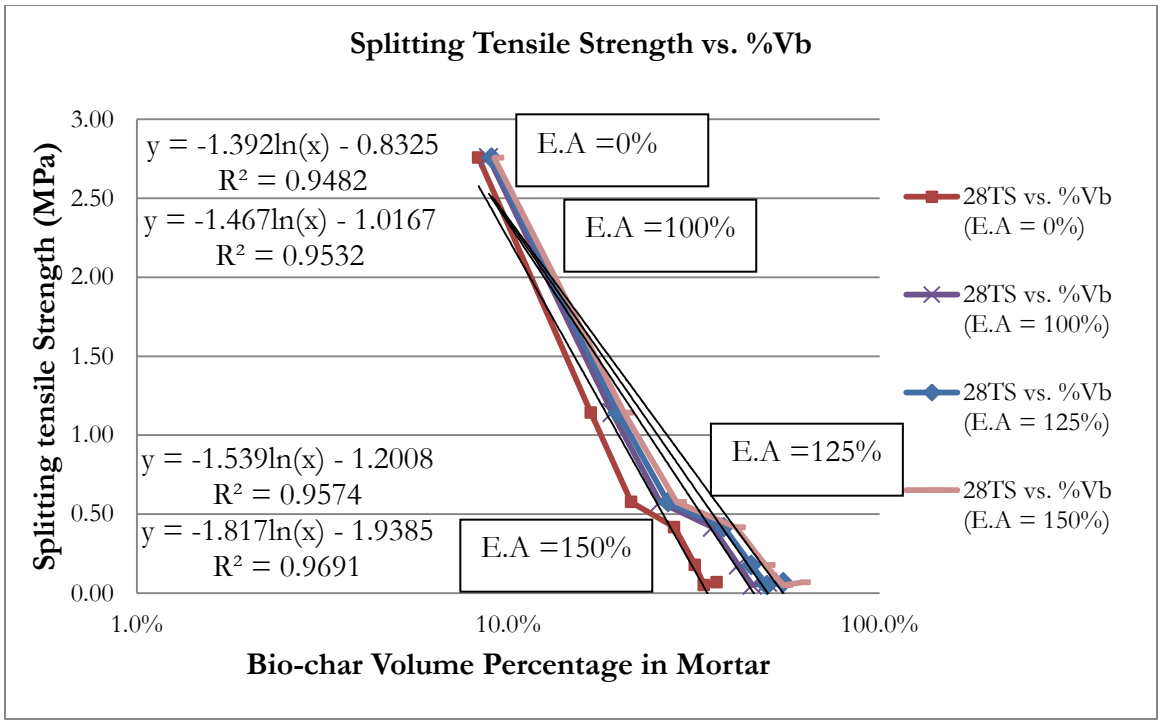

Figure 6.6(d) Splitting Tensile Strength vs. $\%V_b$ with Regression Equation in Log Scale

Although bio-char was originally perceived as "solid" aggregate particles and as a sand-replacement, the result clearly shows that increasing the amount of bio-char consistently and predictably reduces both compressive and tensile strength.

6.3.3.4 Strength vs. $\%V_{fw}$

As reported in Chapter 2, the free water in the mortar not only occupies volume, but is also available for hydration of the cement paste. The total volume of a typical cement-water mixture remains essentially unchanged during the hydration process, and therefore after hydration, the volume that had been initially occupied by the free water remains a contributor to void volume. All such void space adversely affects the strength [Mehta & Monteiro, 2006].

In Figures 6.7(a) and (b), compressive strength and splitting tensile strength at the test age of 28-days are plotted against free water content (as a volume percentage of mortar).

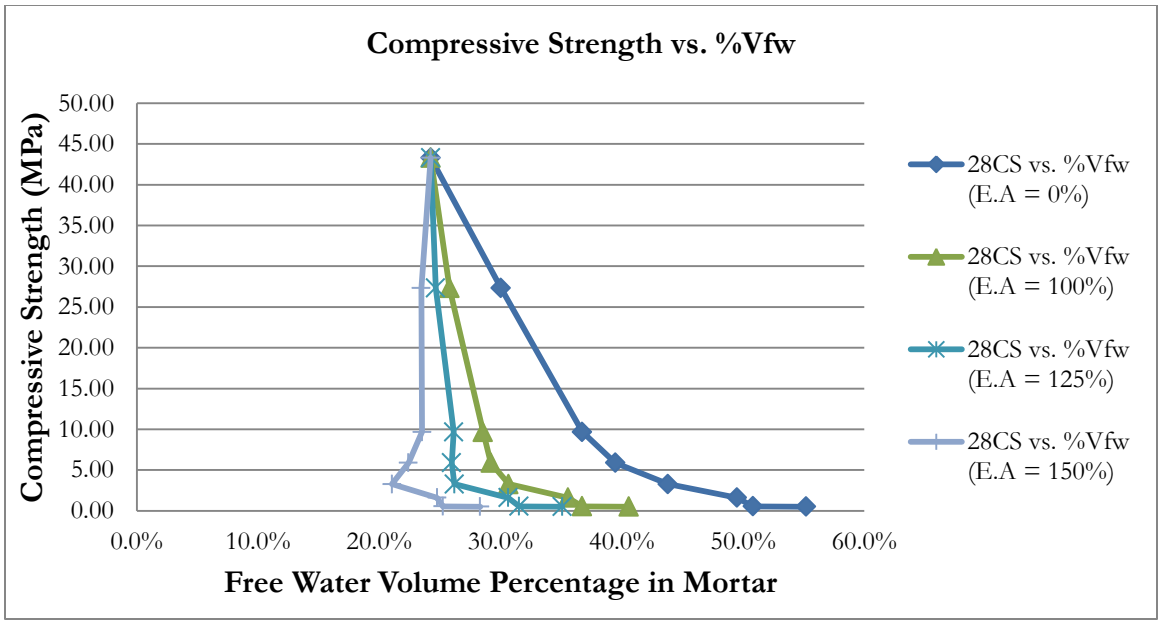

Figure 6.7(a) Compressive Strength vs. $\%V_{fw}$

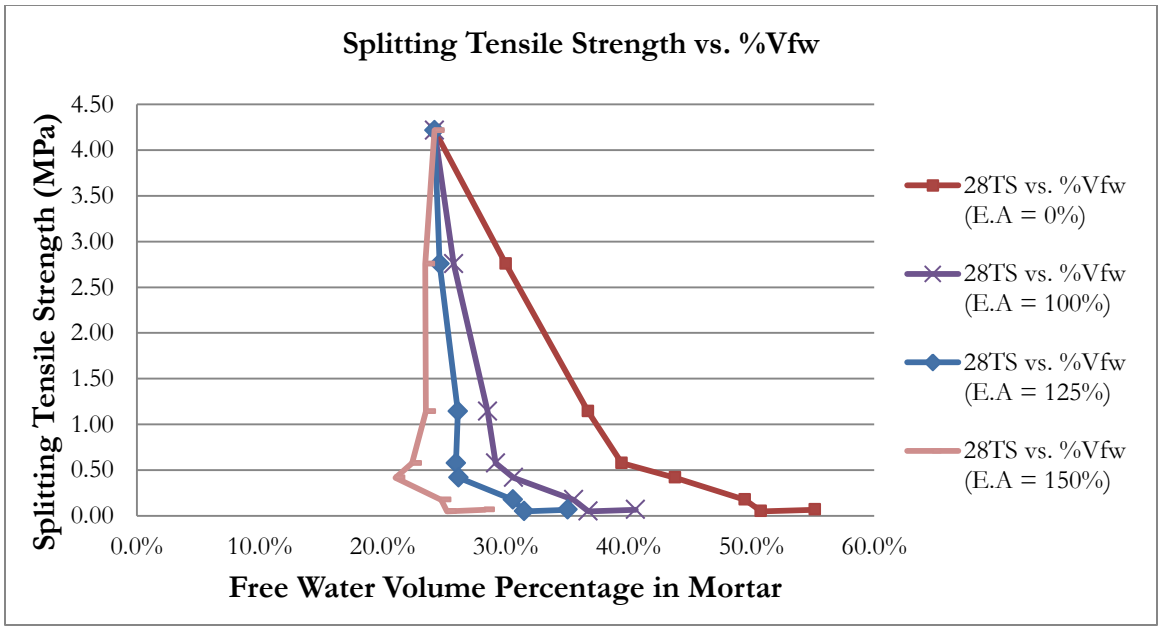

Figure 6.7(b) Splitting Tensile Strength vs. $\%V_{fw}$

It is noted that in Figures 6.7(a) and (b), the curves for EA = 125 and 150% exhibit a feature one might call a "heel." This is the interesting outcome of the fact that if one considered that all of the additional water required to maintain flow were immediately absorbed into the bio-char, and that this matched the value of assumed EA, the computed free water would be a constant value over the entire range. This is close to what actually occurred for EA = 125% for 0 to 33% bio-char. For an assumed EA = 150%, the values of computed free water are about constant for up to 75% bio-char. These near-constant values of free water content are plotted as almost vertical line segments in Figures 6.7(a) and (b). These trends are clearer in the bar-graphs of Figures 6.7(c)-(f).

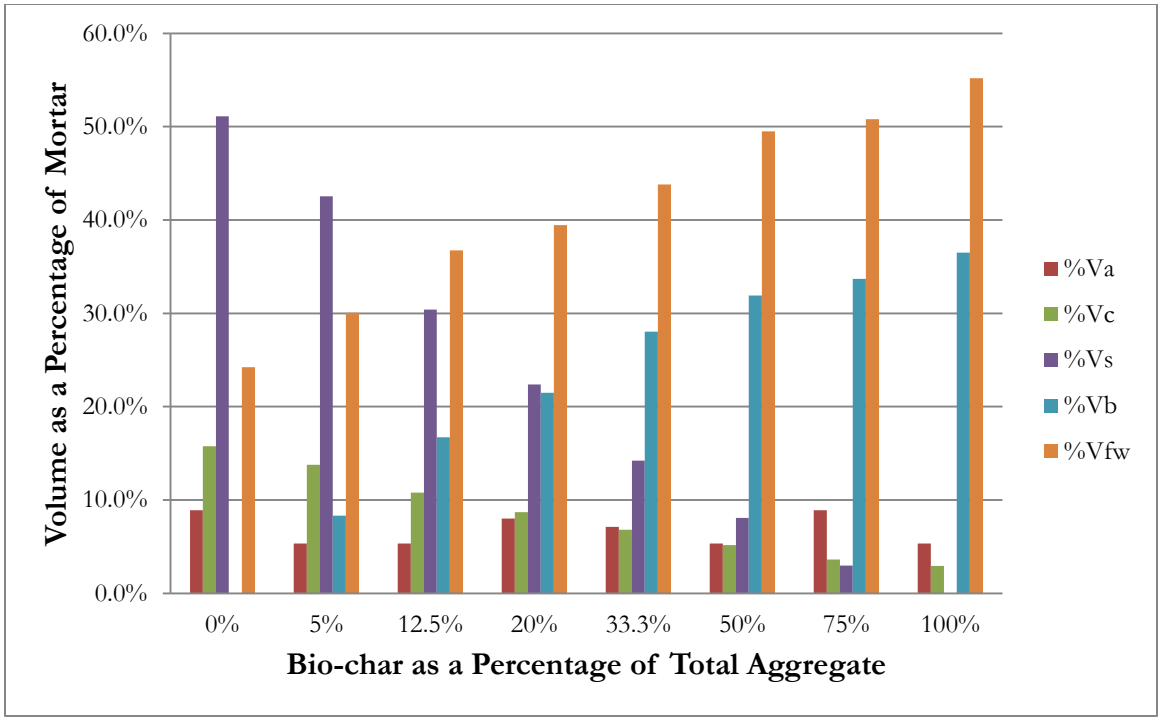

Figure 6.7(c) Volume Percentage of Each Ingredient When E.A = 0%

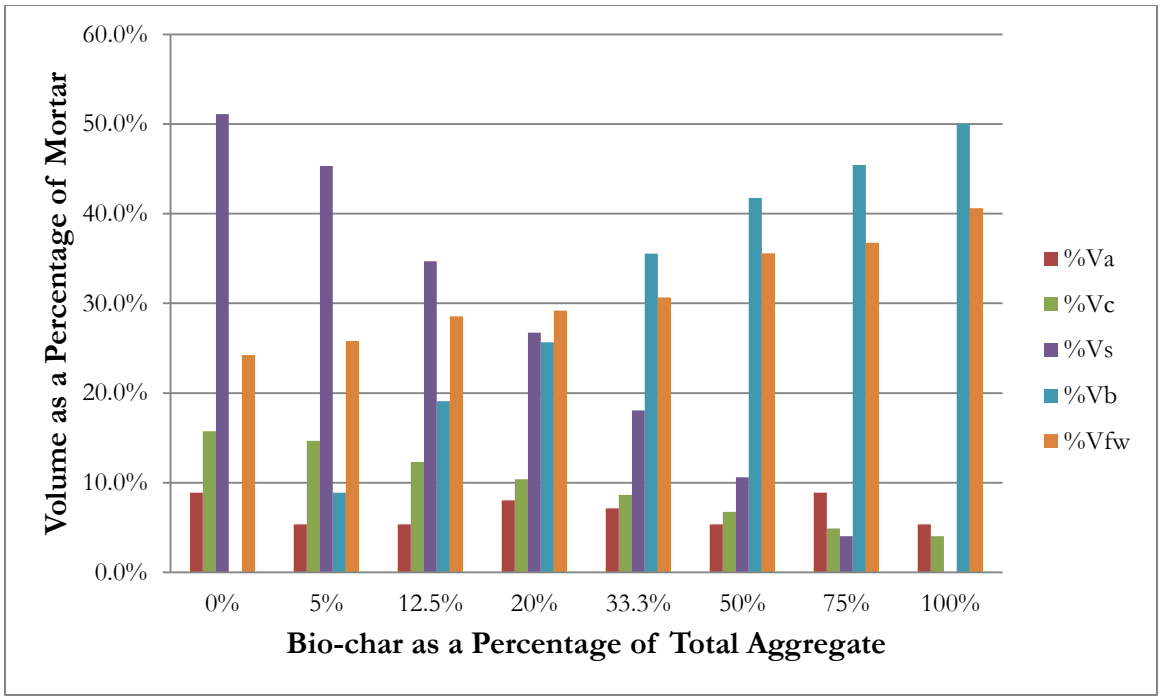

Figure 6.7(d) Volume Percentage of Each Ingredient When E.A = 100%

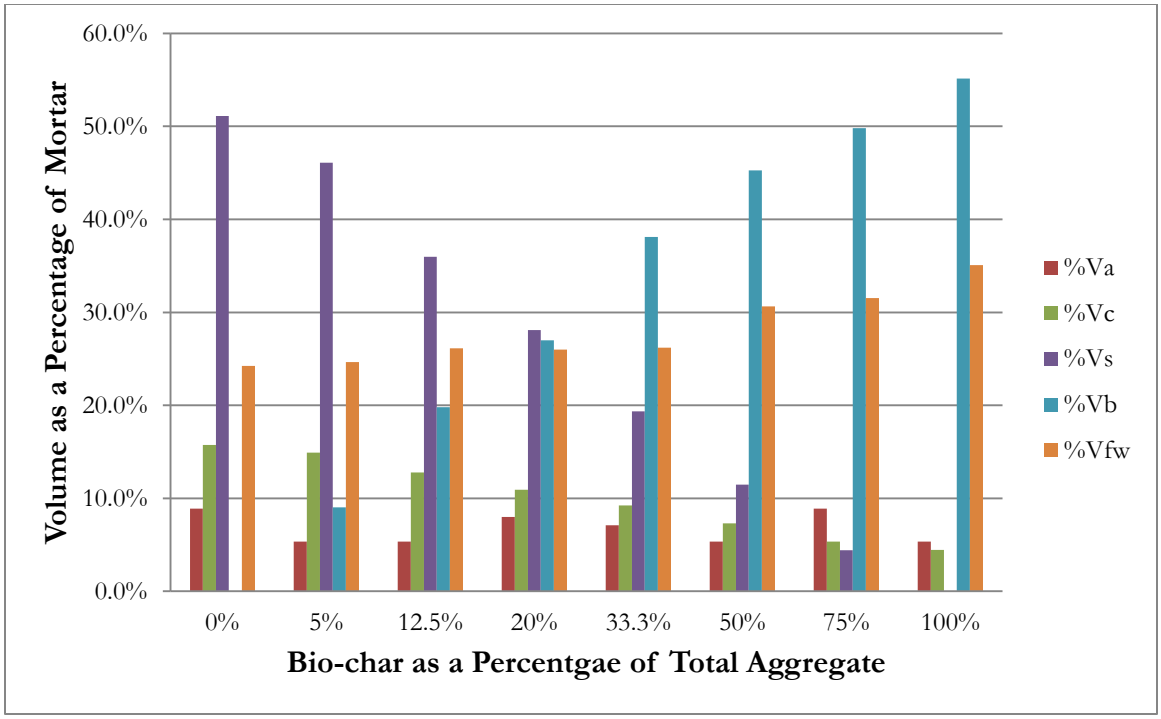

Figure 6.7(e) Volume Percentage of Each Ingredient When E.A = 125%

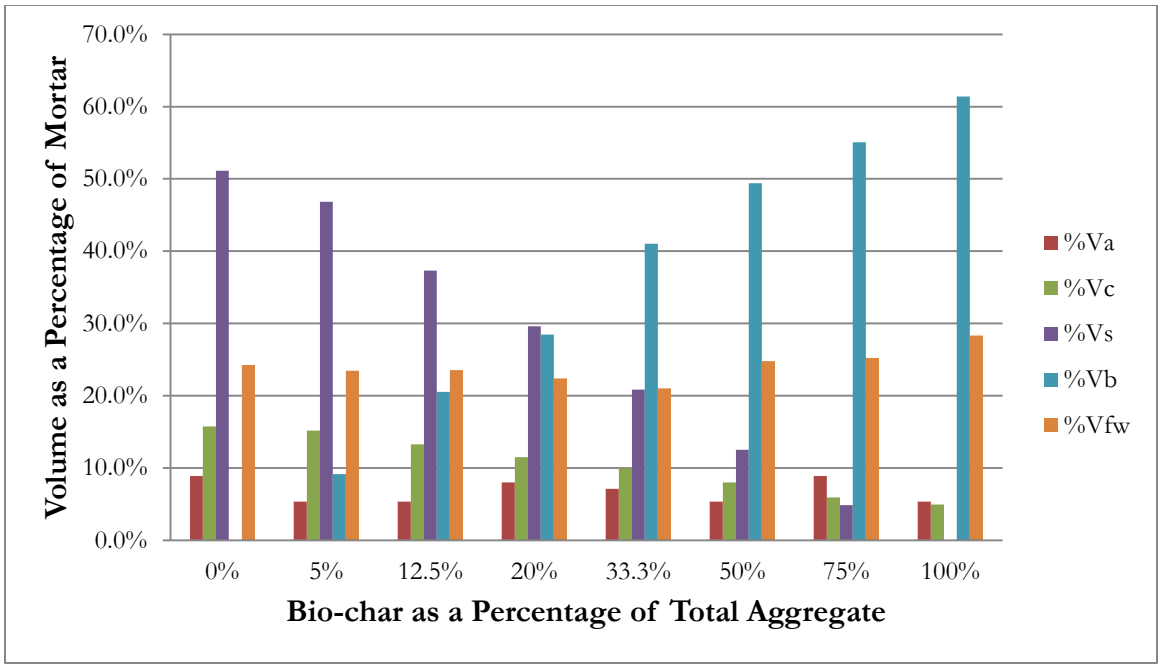

Figure 6.7(f) Volume Percentage of Each Ingredient When E.A = 150%

In Figures 6.7(g) and (h), the data are plotted on log-scale axes, where the linear correlation between log of strength and log of "$\%V_{fw}$" is shown. In both figures, the first regression equation at the top presents the compressive and splitting tensile strength as a power function of "$\%V_{fw}$" when "Effective Absorption" is taken as 0%. The second, third and fourth equation are for mortar strength when "Effective Absorption" is taken as 100%, 125% and 150%". The correlation coefficient (R^2) in these regression analyses is in range of 0.25 to 0.97 for compressive strength and 0.25 to 0.95 for splitting tensile strength. As "Effective Absorption" is taken to be greater than 125%, the data no longer fits the log-log linear correlation.

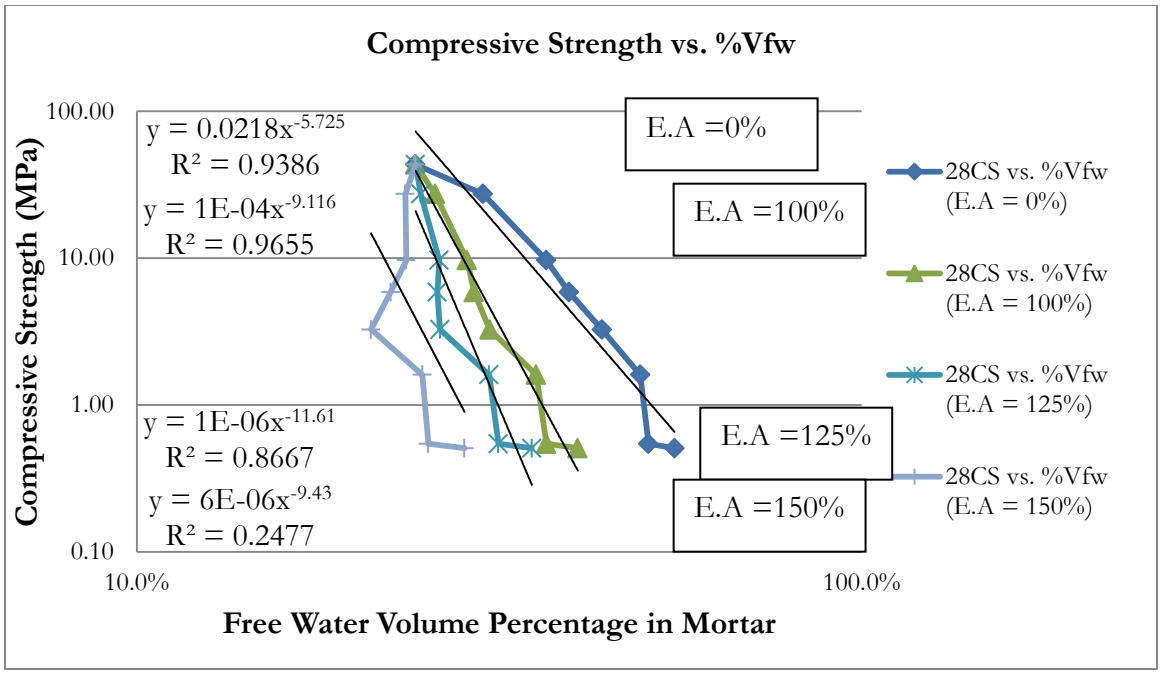

Figure 6.7(g) Compressive Strength vs. $\%V_{fw}$ with Regression Equation in Log Scale

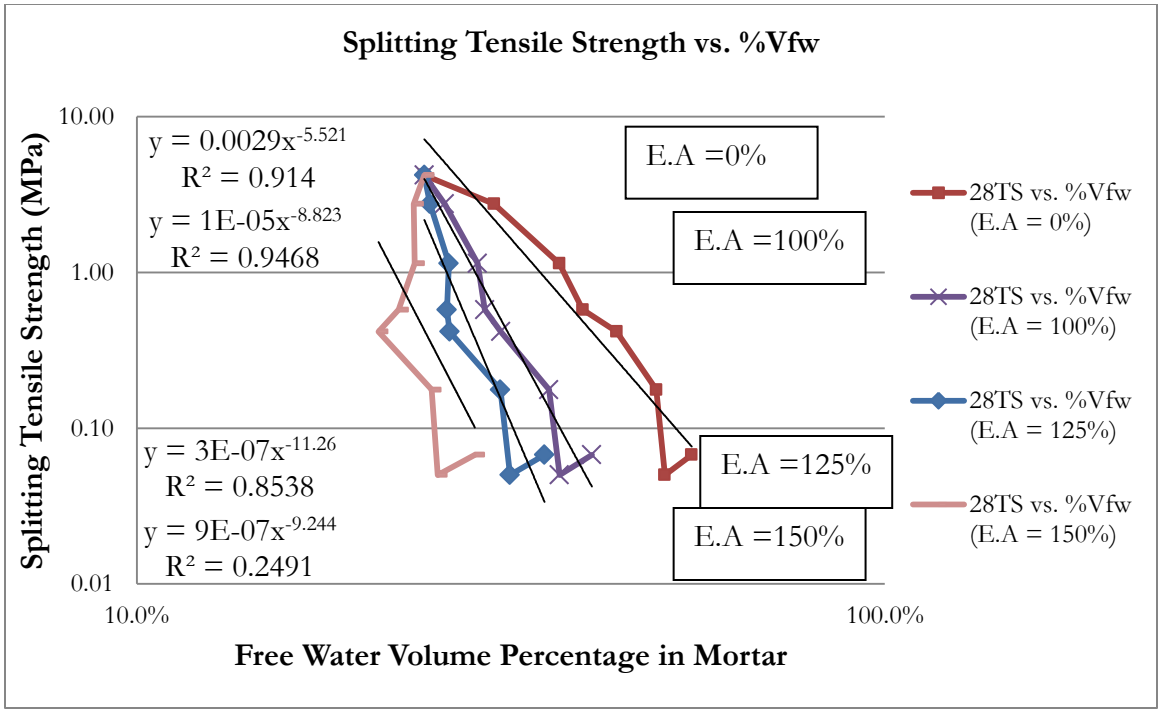

Figure 6.7(h) Splitting Tensile Strength vs. $\%V_{fw}$ with Regression Equation in Log Scale

6.3.3.5 Strength vs. $\%V_c$

As reported in Chapter 2, the setting and hardening of concrete/mortar are the result of chemical and physical processes that take place between cement and water, which results in strength increase in concrete/mortar [Mindess & Young, 1981].

In Figures 6.8(a) and (b), compressive strength and splitting tensile strength at the test age of 28-days are plotted against cement content (as a volume percentage of mortar).

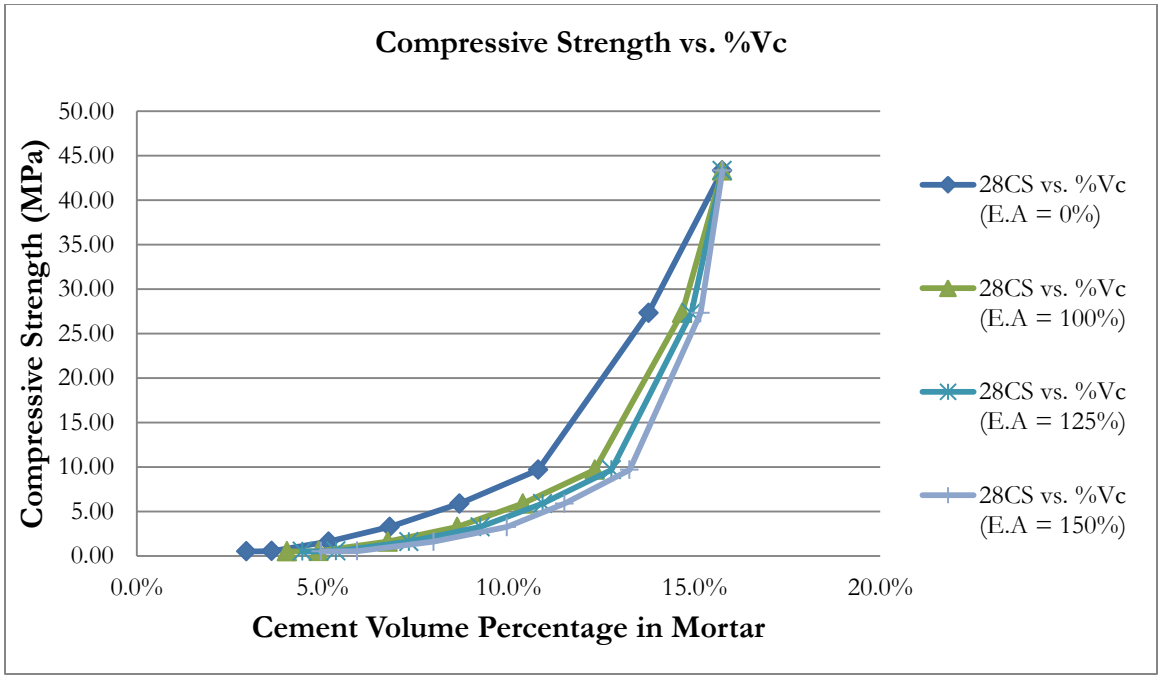

Figure 6.8(a) Compressive Strength vs. $\%V_c$

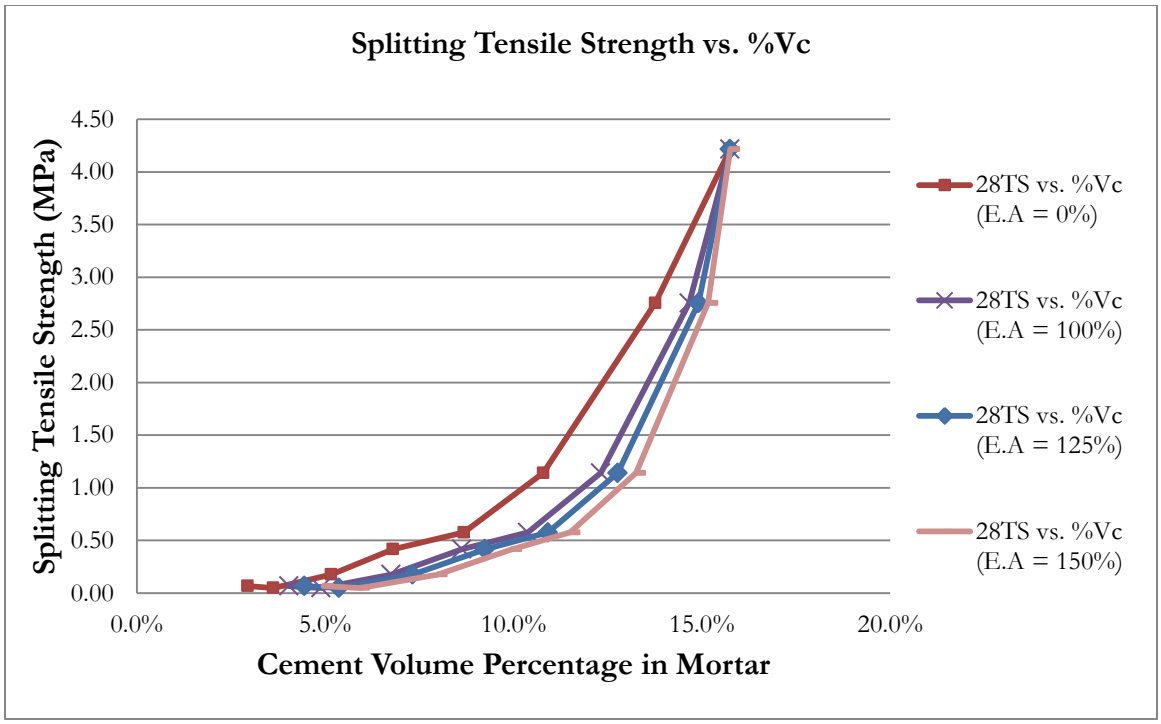

Figure 6.8(b) Splitting Tensile Strength vs. $\%V_c$

In Figures 6.8(c) and (d), the data are plotted on log-scale axes, where the linear correlation between log of strength and log of "$\%V_c$" is shown. In both figures, the first regression equation at the top presents the compressive and splitting tensile strength as a power function of "$\%V_c$" when "Effective Absorption" is taken as 0%. The second, third and fourth equation are for mortar strength when "Effective Absorption" is taken as 100%, 125% and 150%". The correlation coefficient (R^2) in these regression analyses is in range of 0.95 to 0.98 for compressive strength and 0.95 to 0.97 for splitting tensile strength.

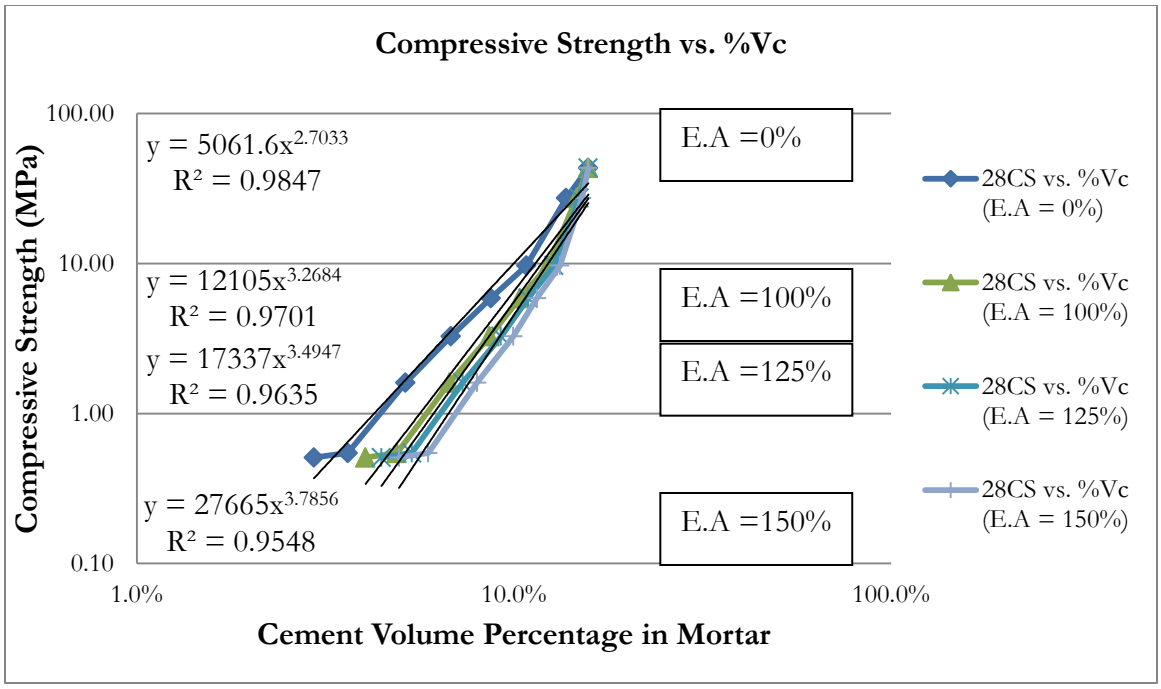

Figure 6.8(c) Compressive Strength vs. $\%V_c$ with Regression Equation in Log Scale

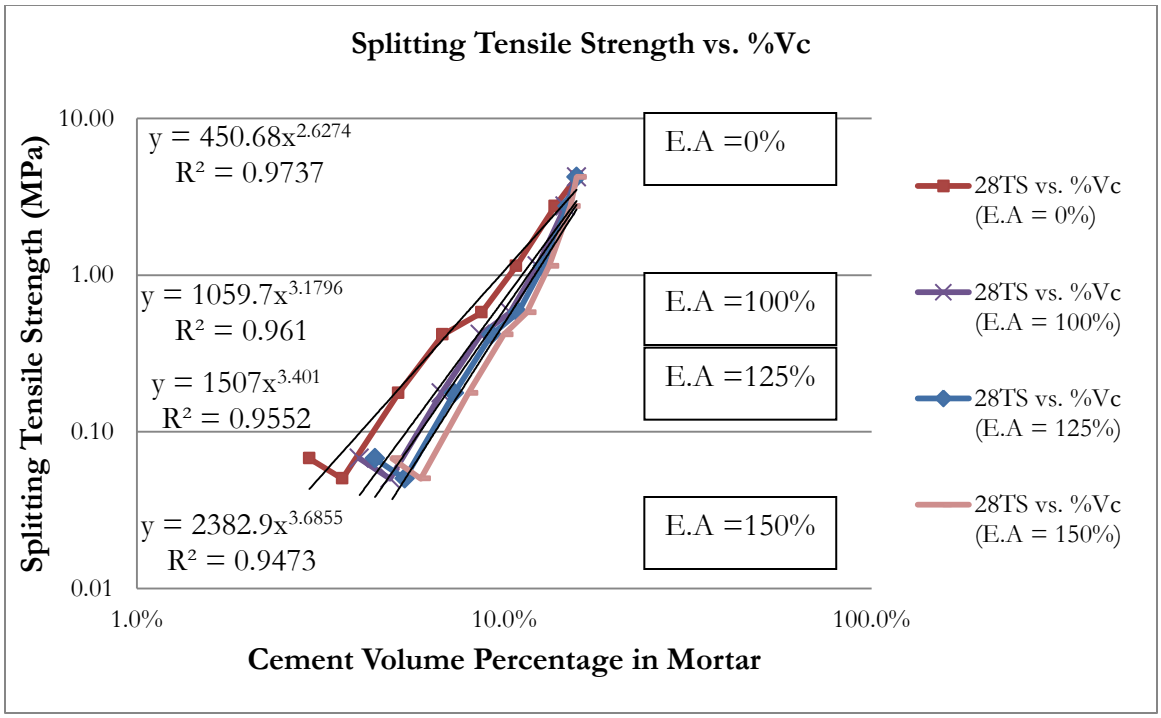

Figure 6.8(d) Splitting Tensile Strength vs. $\%V_c$ with Regression Equation in Log Scale

6.3.4 Combinations of Factors

In Section 6.3.3, the individual factors are compared to the mortar strength at the test age of 28-days. In this section, the combined effects of individual factors are explored.

Table 6.5 Combinations of Individual Factors Affecting Mortar Strength

Symbol	Variable Name	Equation
$\%V_{a+b+fw}$	"Total voids" is taken as the sum volume percentage of total mortar that has been occupied by air, bio-char, and free water.	$\frac{V_{air} + V_{bio-char} + V_{free\ water}}{V_{mortar}}$
c/v	Cement voids ratio (c/v) is the ratio between the volume of cement used in a mortar mixture and the volume of void in a mortar mixture that consists of free water, air and bio-char.	$\frac{V_{cement}}{V_{air} + V_{bio-char} + V_{free\ water}}$

6.3.4.1 Strength vs. $\%V_{a+b+fw}$ (Total Voids Model)

In Figures 6.9(a) and (b), compressive strength and splitting tensile strength at the test age of 28-days are plotted against "Total voids" (as a volume percentage of mortar).

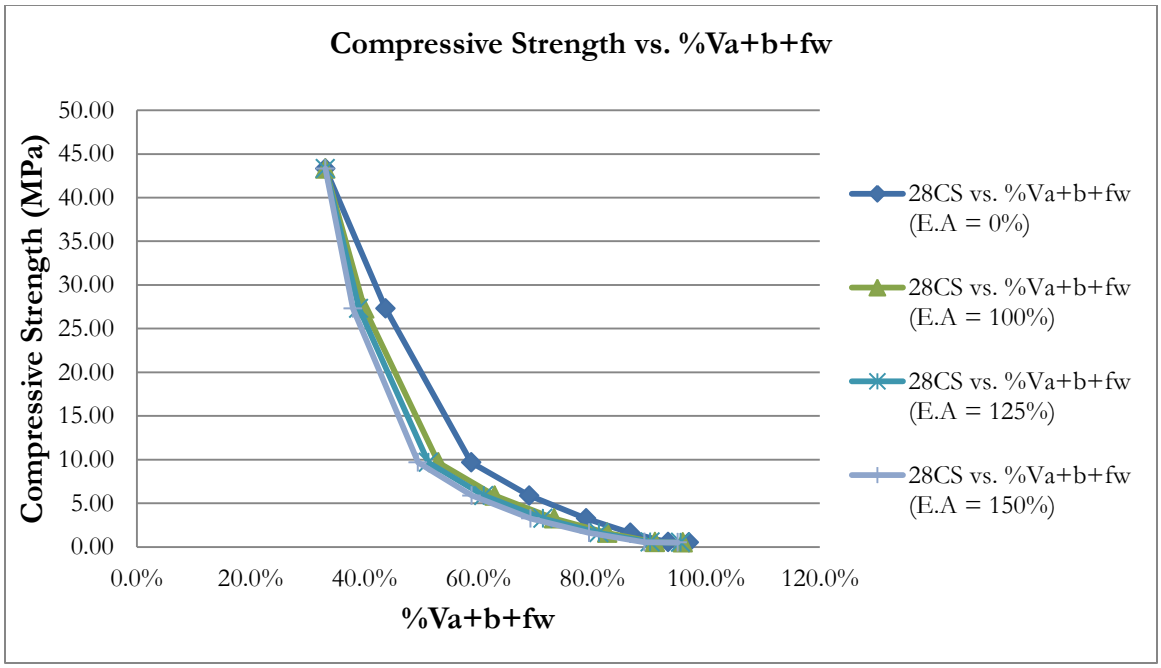

Figure 6.9(a) Compressive Strength vs. $\%V_{a+b+fw}$

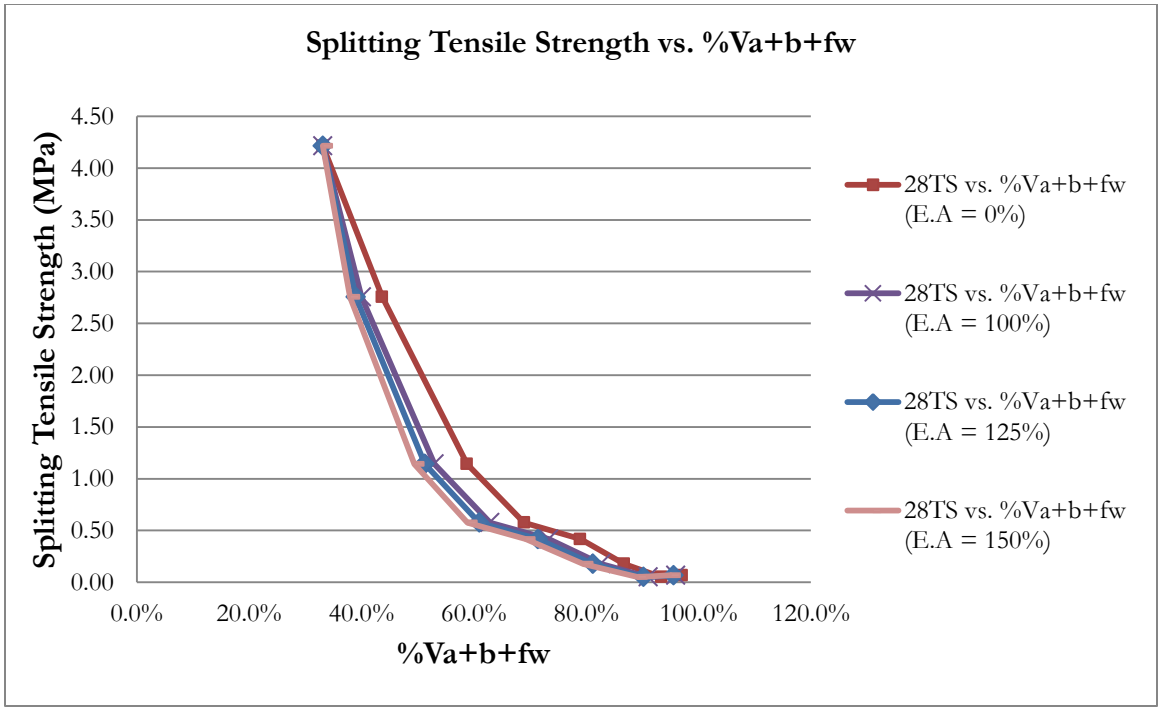

Figure 6.9(b) Splitting Tensile Strength vs. $\%V_{a+b+fw}$

In Figures 6.9(c) and (d), the data are plotted on log-scale axes, where the linear correlation between log of strength and "Total voids" is shown. In both figures, the first regression equation at the top presents the compressive and splitting tensile strength as an exponential function of "Total voids" when "Effective Absorption" is taken as 0%. The second, third and fourth equation are for mortar strength when "Effective Absorption" is taken as 100%, 125% and 150%. The correlation coefficient (R^2) in these regression analyses is in range of 0.97 to 0.99 for compressive strength and 0.96 to 0.98 for splitting tensile strength.

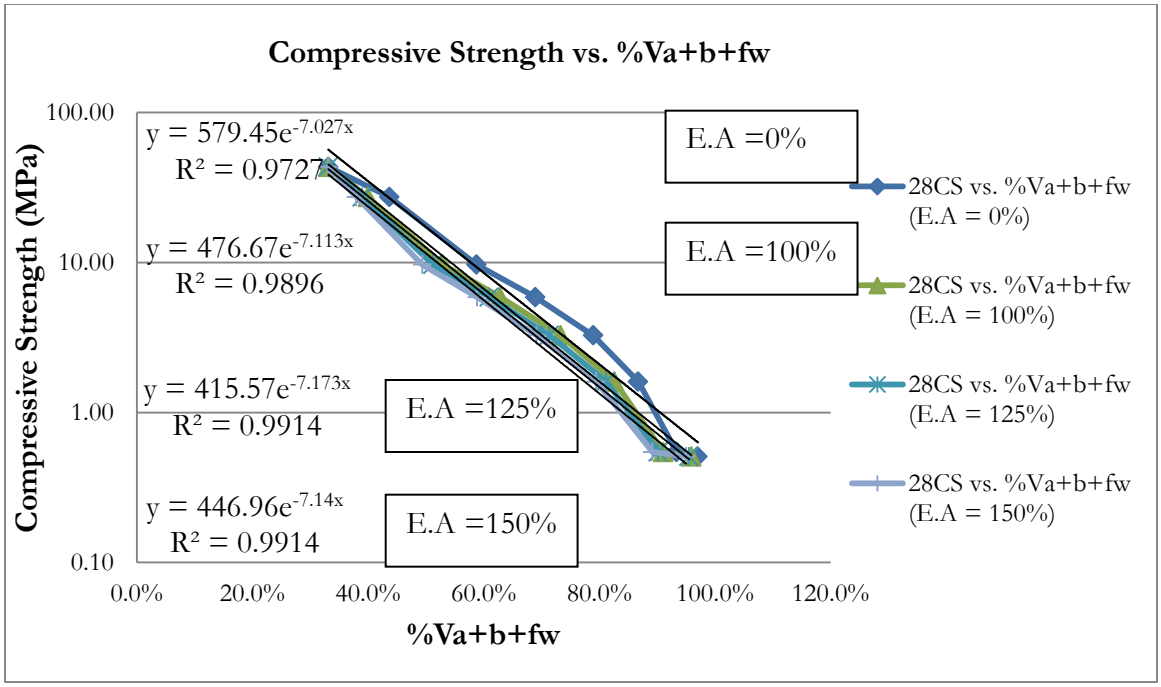

Figure 6.9(c) Compressive Strength vs. $\%V_{a+b+fw}$ with Regression Equation in Log Scale

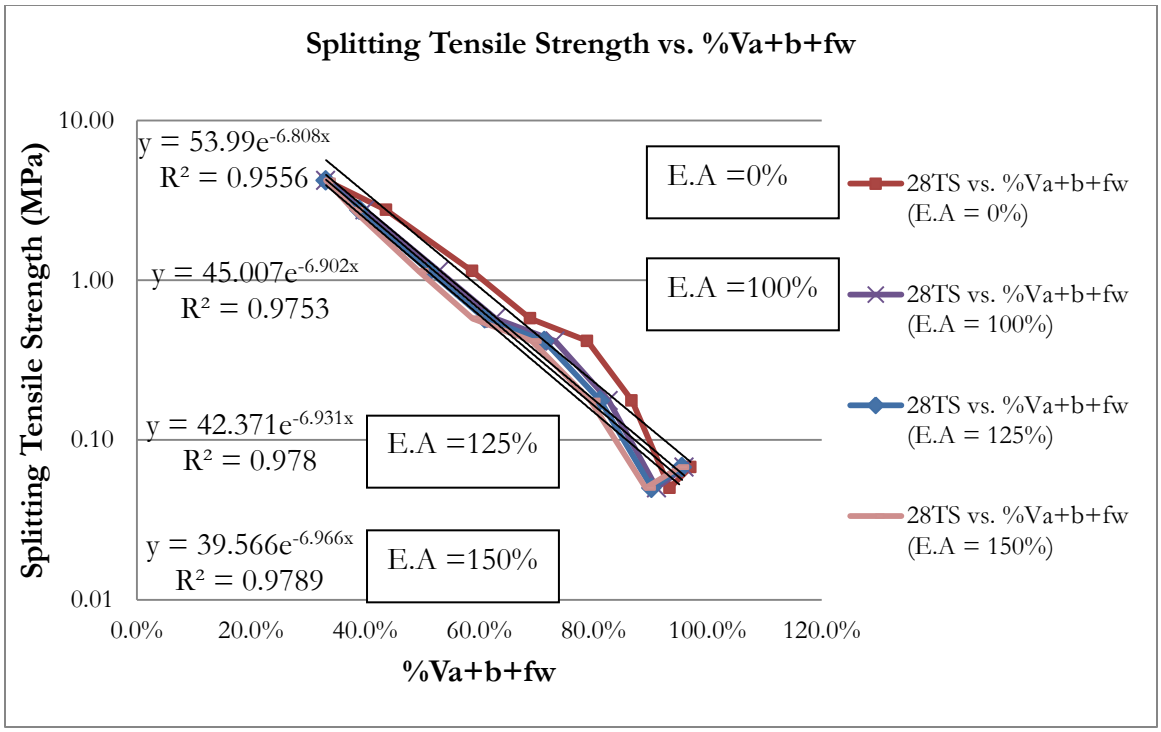

Figure 6.9(d) Splitting Tensile Strength vs. $\%V_{a+b+fw}$ with Regression Equation in Log Scale

6.3.4.2 Strength ~ $\%V_a$, $\%V_b$ and $\%V_{fw}$ (Weighted Total Voids Model)

As reported in Sections 6.3.3.2, 6.3.3.3 and 6.3.3.4, the increasing bio-char and free water content (as volume percentages of mortar) adversely affected the strength of the mortar mixtures. The air content alone did not show a consistent tendency to affect the strength of the mortar mixtures. However, as reported in Chapter 2, the air content (as a part of the void space in mortar) typically reduces strength at a given water-cement ratio. Free water content likewise generates void volume inside the fresh and hardened mortar. In this analysis it was hypothesized that the soft bio-char particles may themselves act as void space rather than as "solid" aggregate particles. As will be shown, the resulting correlation supports this general hypothesis.

The linear regression model evaluated is:

$$\ln(28CS) = \alpha_0 + \alpha_1 \%V_a + \alpha_2 \%V_b + \alpha_3 \%V_{fw}$$

$$\ln(28TS) = \beta_0 + \beta_1 \%V_a + \beta_2 \%V_b + \beta_3 \%V_{fw}$$

These models not only enable the prediction of mortar strength, but also provide insight to how an individual component of total void space may affect mortar strength.

In the regression analyses for this "total voids" model, the adjusted correlation coefficient (R^2) is 0.99 for compressive strength, and 0.97 for splitting tensile strength. In Tables 6.6(a) and (b), the regression coefficients and P-values of regression are listed.

Table 6.6(a) Regression for Weighted Total Voids Model on ln(28CS) When E.A = 0% and 100%

E.A	0%		100%	
Regression	Cofficient	P-value	Cofficient	P-value
Intercept	α_0 = 11.0	0.00080496	α_0 = 7.7	0.00183628
$\%V_a$	α_1 = -15.7	0.01670785	α_1 = -11.2	0.0563161
$\%V_b$	α_2 = 7.0	0.14574835	α_2 = -5.5	0.01315137
$\%V_{fw}$	α_3 = -24.3	0.00688708	α_3 = -12.6	0.0374436
Adjusted R^2	0.9901		0.9886	

Table 6.6(b) Regression for Weighted Total Voids Model on ln(28CS) When E.A = 125% and 150%

E.A	125%		150%	
Regression	Cofficient	P-value	Cofficient	P-value
Intercept	α_0 = 6.9	0.00267674	α_0 = 6.1	0.00420844
$\%V_a$	α_1 = -10.1	0.0858152	α_1 = -8.9	0.13396521
$\%V_b$	α_2 = -6.7	0.00101932	α_2 = -7.2	4.841E-05
$\%V_{fw}$	α_3 = -9.7	0.07390036	α_3 = -6.7	0.15988122
Adjusted R^2	0.9873		0.9855	

Table 6.6(c) Regression for Weighted Total Voids Model on ln(28TS) When E.A = 0% and 100%

E.A	0%		100%	
Regression	Cofficient	P-value	Cofficient	P-value
Intercept	β_0 = 9.2	0.00557589	β_0 = 6.0	0.01620
$\%V_a$	β_1 = -20.5	0.02116616	β_1 = -16.2	0.05463
$\%V_b$	β_2 = 8.0	0.21851134	β_2 = -5.0	0.05383
$\%V_{fw}$	β_3 = -25.1	0.01977086	β_3 = -13.5	0.08161
Adjusted R^2	0.9796		0.9757	

Table 6.6(d) Regression for Weighted Total Voids Model on ln(28TS) When E.A = 125% and 150%

E.A	0%		100%	
Regression	Cofficient	P-value	Cofficient	P-value
Intercept	β_0 = 5.2	0.02402897	β_0 = 4.4	0.03793074
$\%V_a$	β_1 = -15.0	0.07354909	β_1 = -13.9	0.10084861
$\%V_b$	β_2 = -6.3	0.00452479	β_2 = -7.0	0.00019603
$\%V_{fw}$	β_3 = -10.7	0.13327215	β_3 = -7.9	0.22775618
Adjusted R^2	0.9738		0.9712	

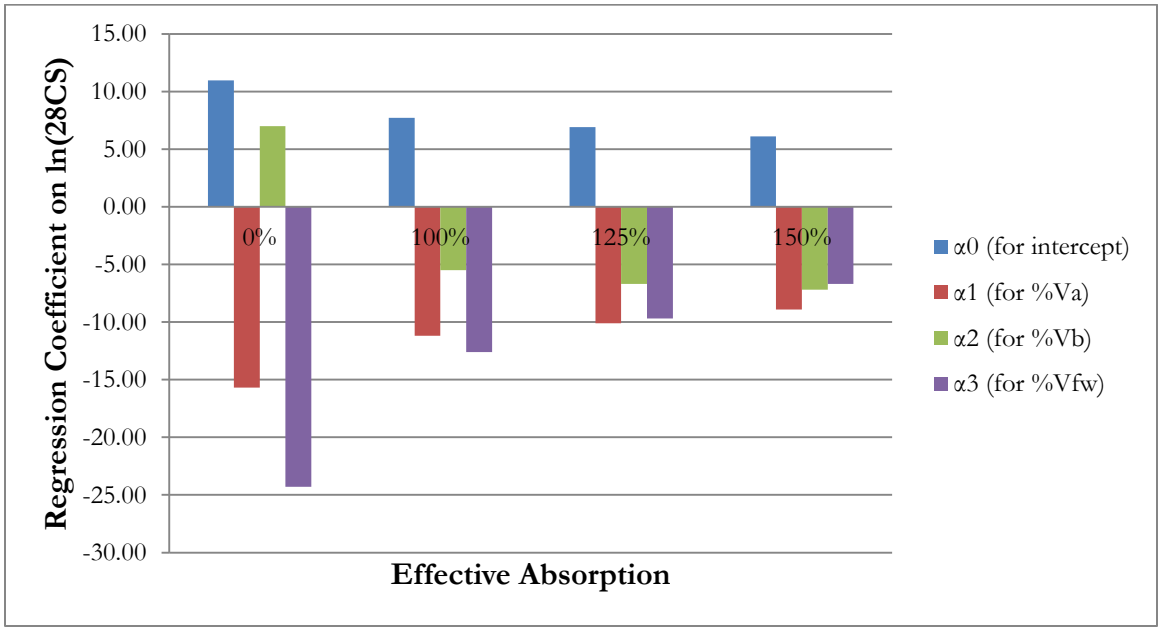

Figure 6.10(a) Regression Coefficient for Weighted Total Voids Model on ln(28CS)

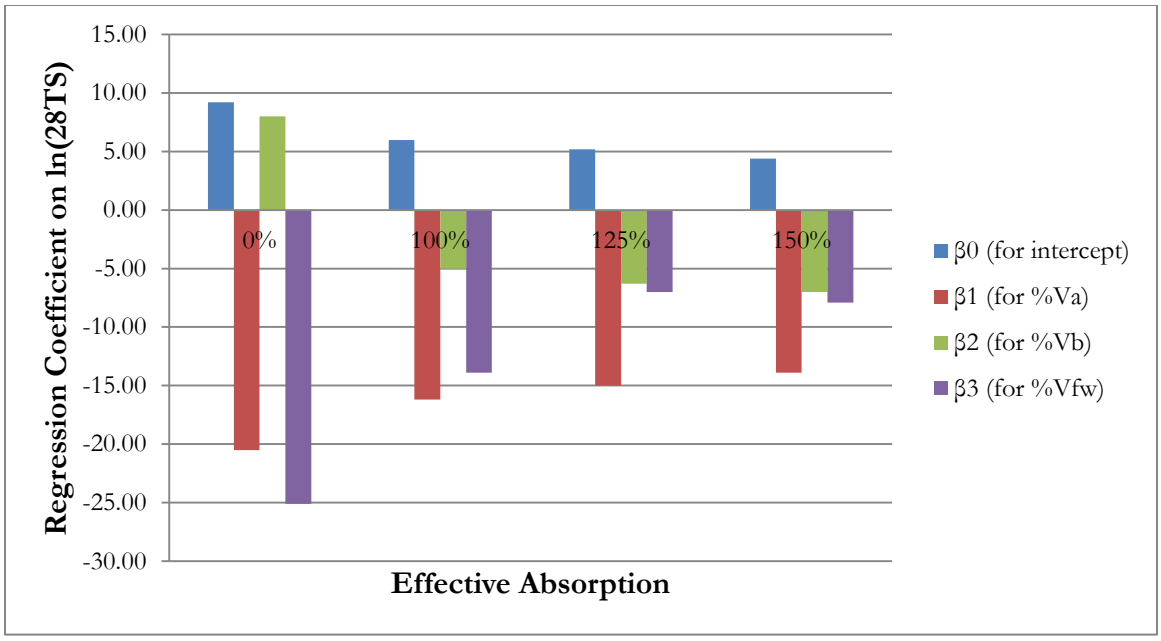

Figure 6.10(b) Regression Coefficient for Weighted Total Voids Model on ln(28TS)

As is observed in Tables 6.6(a) and (b), Figures 6.10(a) and (b), when "Effective Absorption" increases, the absolute value of regression coefficient for $\%V_a$ and $\%V_{fw}$ decreases, indicating the negative impact on strength due to air and free water void is less dominant when bio-char is assumed to be capable of absorbing more water. Except for the case that the regression coefficient for $\%V_b$ is positive when "Effective Absorption" is taken as 0%, the decreasing negative value of regression coefficient for $\%V_b$, indicating the presence of bio-char adversely affects the mortar strength. As the "Effective Absorption" increases, the strength reduction due to bio-char "void" is more apparent. When "Effective Absorption" is taken as 100%, 125% and 150%, the magnitude of regression coefficients indicating that the presence of air void damages the mortar most, followed by free water and bio-char void. Figures 6.10(a) and (b) demonstrate a reliable pattern of values of the coefficients and the assumed value of E.A.

6.3.4.3 Strength ~ $\%V_{a+b+fw}$ and $\%V_c$ (Advanced Total Voids Model)

Based on the regression results in Section 6.3.4.2, the advanced models are provided as follow:

$$\ln(28CS) = a_0 + a_1\,\%V_{a+b+fw} + a_2\log(1/\%V_c)$$

$$\ln(28TS) = b_0 + b_1\%V_{a+b+fw} + b_2\log(1/\%V_c)$$

which are also expressed as:

$$28CS = \frac{e^{a_1(\%V_{a+b+fw})+a_0}}{(\%V_c)^{a_2}}$$

$$28TS = \frac{e^{b_1(\%V_{a+b+fw})+b_0}}{(\%V_c)^{b_2}}$$

In the revised regression analysis, both "Total voids" and cement content are accounted for, such that all ingredients of void and solid part in the mixture are included. One can automatically deduct the volume percentage of sand in the mortar mixtures for the fact that the sum volume of air, bio-char, free water, cement and sand (as percentages of mortar) is 100%.

The regression results are reported in Tables 6.7(a) and (b). The surface plot of the regression is also provided in Figure 6.10.

Table 6.7(a) Regression for Advanced Total Voids Model on ln(28CS) When E.A = 0% and 100%

E.A	0%		100%	
Regression	Cofficient	P-value	Cofficient	P-value
Intercept	a_0 = 8.0	2E-36	a_0 = 7.4	2.01E-26
$\%V_{a+b+fw}$	a_1 = -2.5	6.19E-07	a_1 = -4.8	2.1E-11
$\log(1/V_c)$	a_2 = -1.8	2.01E-13	a_2 = -1.2	5.61E-05
R^2	0.9915		0.9900	

Table 6.7(b) Regression for Advanced Total Voids Model on ln(28CS) When E.A = 125% and 150%

E.A	125%		150%	
Regression	Cofficient	P-value	Cofficient	P-value
Intercept	a_0 = 6.8	1.47E-20	a_0 = 6.4	9.66E-18
$\%V_{a+b+fw}$	a_1 = -6.1	7.27E-13	a_1 = -6.7	2.38E-13
$\log(1/V_c)$	a_2 = -0.6	0.072368	a_2 = -0.30	0.42
R^2	0.9885		0.9877	

Table 6.7(c) Regression for Advanced Total Voids Model on ln(28TS) When E.A = 0% and 100%

E.A	0%		100%	
Regression	Cofficient	P-value	Cofficient	P-value
Intercept	b_0 = 5.6	9.4E-22	b_0 = 5.2	3.02E-14
$\%V_{a+b+fw}$	b_1 = -1.9	0.007254	b_1 = -4.0	7.42E-06
$\log(1/V_c)$	b_2 = -2.0	1.76E-08	b_2 = -1.4	0.001013
R^2	0.9768		0.9760	

Table 6.7(d) Regression for Advanced Total Voids Model on ln(28TS) When E.A = 125% and 150%

E.A	125%		150%	
Regression	Cofficient	P-value	Cofficient	P-value
Intercept	b_0 = 4.7	2.97E-10	b_0 = 4.4	1.92E-08
$\%V_{a+b+fw}$	b_1 = -5.3	2.45E-07	b_1 = -5.8	6.78E-08
$\log(1/V_c)$	b_2 = -0.9	0.061479	b_2 = -0.6	0.22
R^2	0.9747		0.9740	

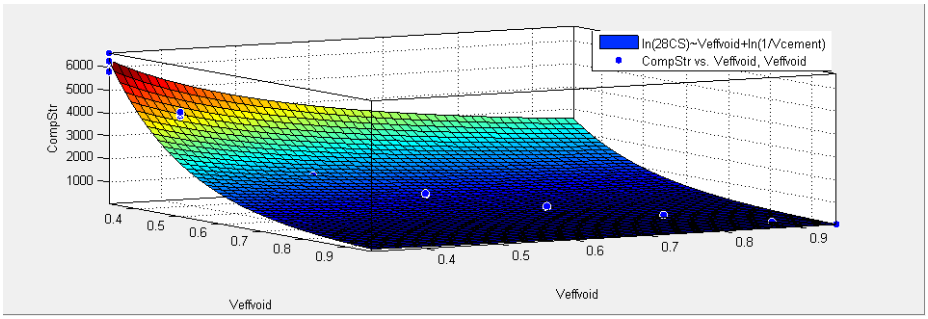

Figure 6.11 Surface fit for Advanced Total Voids Model on Compressive Strength When E.A = 125%

6.3.4.4 Strength vs. Cement-Voids Ratio (Cement-voids Ratio Model)

As suggested in "Concrete Manual" by Department of Transportation, State of Minnesota [Technical Service Division, 1968], the cement-void ratio positively affects the concrete/mortar strength.

In Figures 6.12(a) and (b), compressive strength and splitting tensile strength at the test age of 28-days are plotted against cement-void ratio.

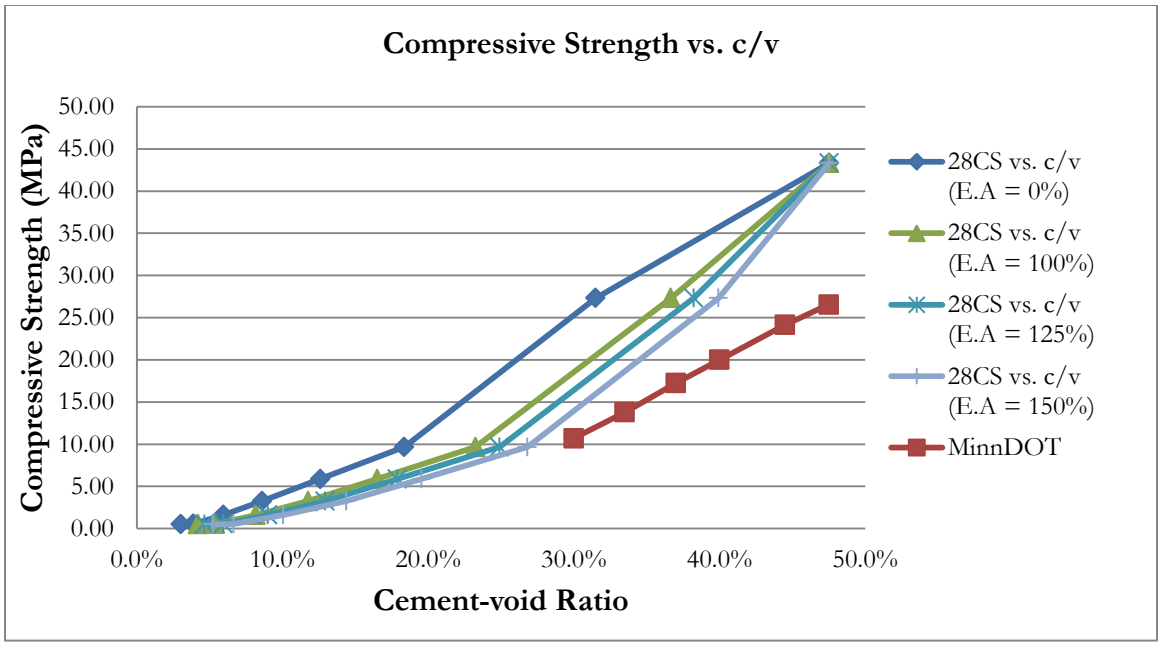

Figure 6.12(a) Compressive Strength vs. c/v

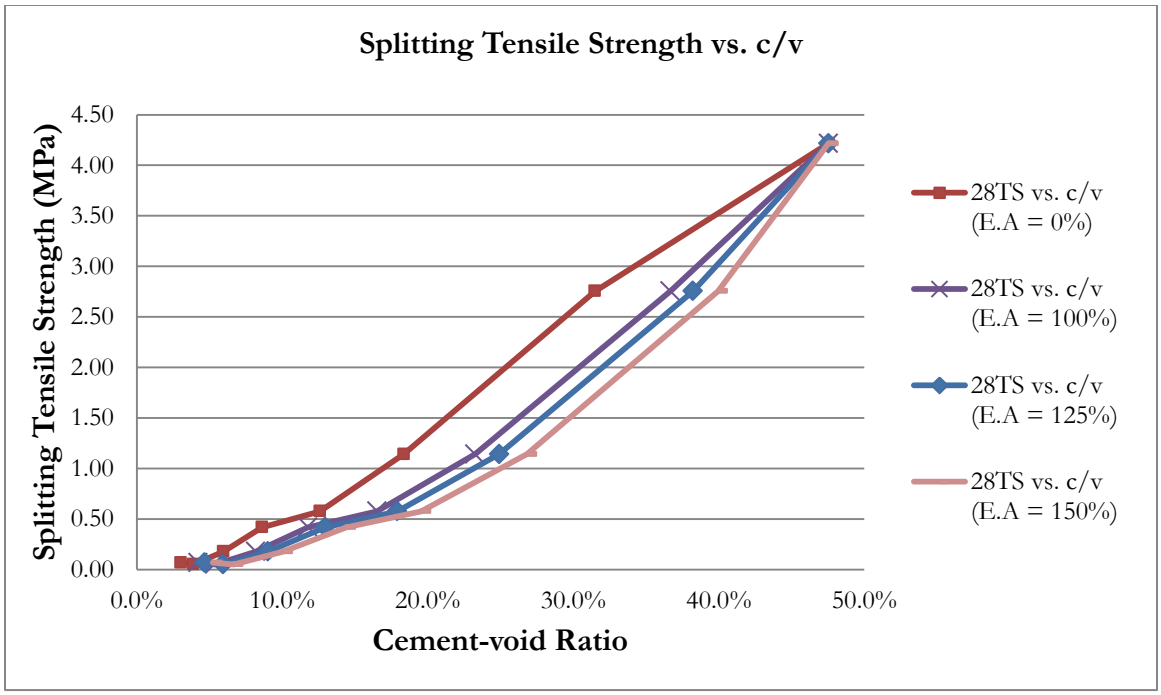

Figure 6.12(b) Splitting Tensile Strength vs. c/v

In Figures 6.12(c) and (d), the data are plotted on log-scale axes, where the linear correlation between log of strength and log of "c/v" is shown. In both figures, the first regression equation at the top presents the compressive and splitting tensile strength as a power function of cement-void ratio when "Effective Absorption" is taken as 0%. The second, third and fourth equation are for mortar strength when "Effective Absorption" is taken as 100%, 125% and 150%. The correlation coefficient (R^2) in these regression analyses is 0.99 for compressive strength and 0.98 for splitting tensile strength.

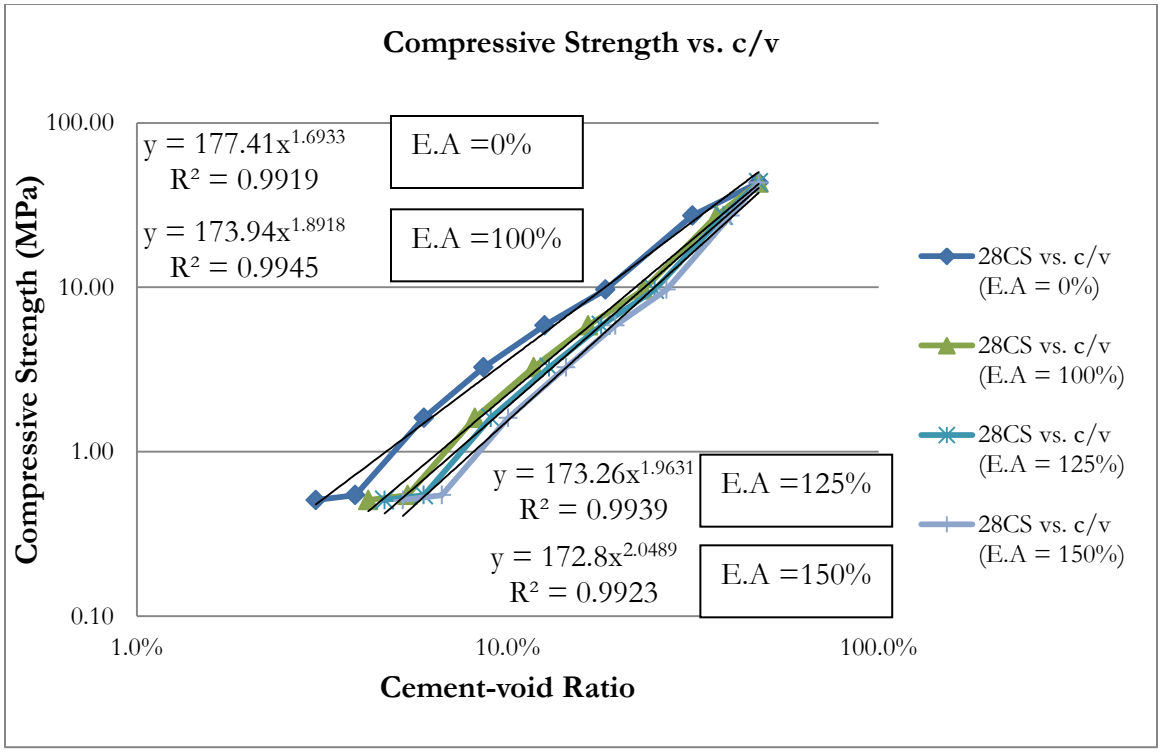

Figure 6.12(c) Compressive Strength vs. c/v with Regression Equation in Log Scale

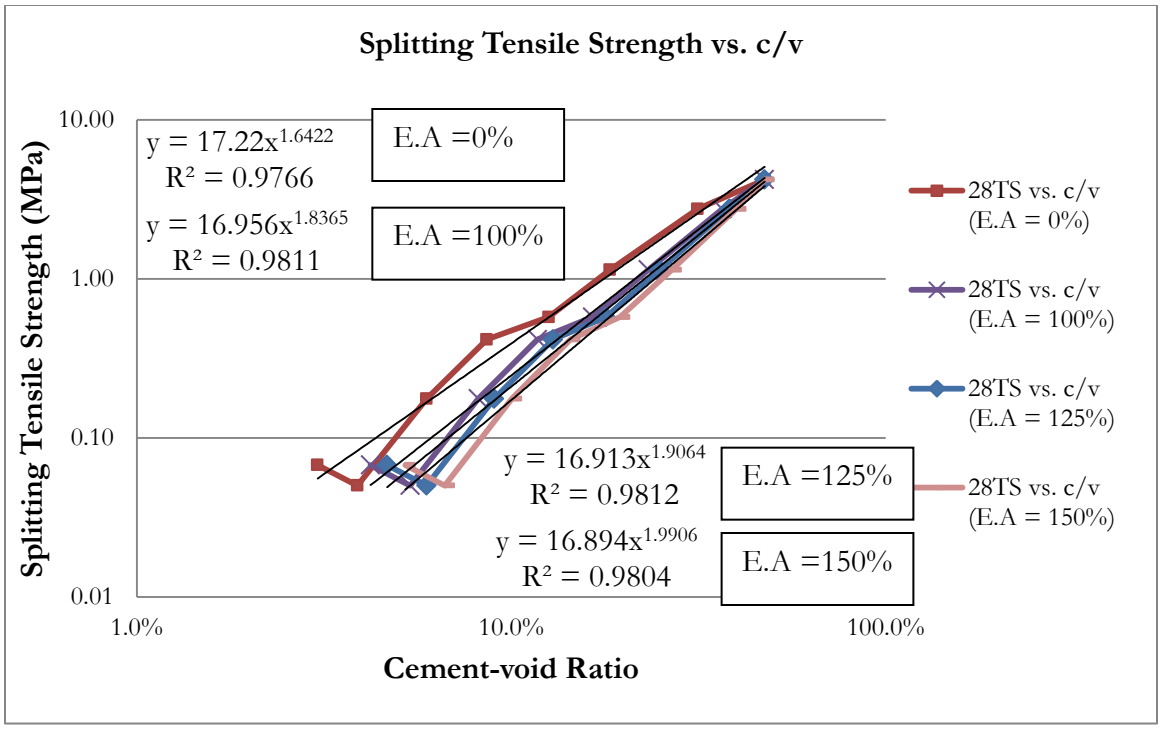

Figure 6.12(d) Splitting Tensile Strength vs. c/v with Regression Equation in Log Scale

6.3.5 Recommendation on Strength Prediction

In the section, the similarities between the behavior of bio-char mortar and traditional mortar theories are summarized. Then in the context of this bio-char experiment (where initial w/c is 0.485, mass ratio of cement to total aggregate (sand and bio-char) is 0.36, bio-char "dust" from "Bio-Char Now", mortar flow is 110±5%, and sealed cylinders were cured at room temperature until testing), the recommendations on strength prediction model based on simplicity and reliability/accountability are provided. Last but not least, a recommendation is suggested for a strength-prediction model based on applicability to other bio-char mortars with conditions other than studied here.

6.3.5.1 Similarity to Traditional Mortar Theories

There are trends that appear to apply to the bio-char mortar that are also generally as expected for typical cementitious materials, such as

- The linear correlation between compressive and splitting tensile strength of bio-char mortar is almost identical to traditional cementitious materials that splitting tensile strength is about 1/10 of the compressive strength.
- The regression analysis that strength as a function of age (ACI 209) is applicable to bio-char mortar, with all 8 correlation coefficients greater than 0.92.
- The regression analysis for mortar strength as a function of water-cement ratio (Abram's Law) is marginally applicable to bio-char mortar, with all 8 correlation coefficient s greater than 0.79. (The chief difficulty is the inability to confidently know the actual w/c because of the unknown effective absorption of the bio-char during the mixing and casting period.)
- Other individual factors such as cement volume, free water volume (as a percentage of mortar) shows similar impacts on bio-char mortar strength that normallypretain to traditional cementitious materials.

6.3.5.2 Simplicity (Within This Study)

In this study, "%bio-char" is bio-char content as a mass percentage of total aggregate, a defining variable around which the experimental program was designed. In the author's opinion, the "strength vs. %bio-char" is the simplest yet straightforward prediction model in the context of this study for the reason that:

- "%Bio-char" is not only the defining variable for the experimental program, but also is not influenced by the specific properties of bio-char, especially its absorption (given that water is added to maintain flow).
- The "strength vs. %bio-char" model exhibits a one-to-one relationship between (both compressive- and splitting tensile-) strength of bio-char mortar and the rate of bio-char replacement of sand, and the trend clearly indicates that the increasing of bio-char content adversely affects the strength of mortar, which leads to the suggestion that bio-char might function more as a "void" than "solid" constituent.

6.3.5.3 Accountability (Within This Study)

To further investigate how bio-char affects mortar strength, prediction models including individual variables and combinations of variables were reported in Section 6.3.3 and 6.3.4. All models in Section 6.3.3 and 6.3.4 have taken the "Effective Absorption" of bio-char into consideration.

In author's opinion, the "Cement-voids ratio model" is the most reliable prediction model to account for mortar behavior in the context of this study for the reason that

- The "Cement-voids ratio model" includes all degrees of freedom exhibited in mixture proportions. Both "Total voids" (arithmetic sum of air, bio-char and free water content as a volume percentage of mortar) and cement content (as a volume percentage of mortar) are accounted for, such that all voids and solid constituents are included. One can automatically account for the volume percentage of sand in the mortar mixtures for the fact that the sum volume of air, bio-char, free water, cement and sand (as percentages of mortar) is 100%.

- Although both "Cement-voids ratio model" and "Advanced total voids model" include all degrees of freedom, the equation of "Cement-voids ratio model" requires less algebraic transformation.
- The precedent of the cement-voids ratio theory was recognized by The Department of Transportation, State of Minnesota, as published in their "Concrete Manual" [Technical Service Division, 1968]. The difference in curve shape, however, is evident in the comparison of bio-char curves and the v c/v concrete curve in Figure 6.12(a). Nevertheless, in both cases, an increase in the "cement-void ratio" likewise increases mortar strength. The difference in the shapes of curve may suggest that although the presence of bio-char reduces the strength of mortar, bio-char is not as damaging as air or free water voids. This is also supported by the model in "Weighted total voids model".

6.3.5.4 Applicability for Other Bio-char-mortar Studies

Considering the applicability of prediction models on other bio-char-mortar studies that may not share the same experimental design and testing program, perhaps the most generically applicable model for future exploration is the "strength vs. cement-void ratio" for the reason that:

- The data from this study is well-represented by the "Cement-void ratio model" established by Minnesota Department of Transportation [Technical Service Division, 1968].
- One outcome of this study is the concept that the volume of bio-char, an admittedly soft yet solid material, can be modeled as void volume. The more complicated model introduced here assigned weighting factors to the various "void" components, thus opening the options of dealing with the bio-char over a spectrum of voids to solid volume as appropriate.

CHAPTER 7

CONCLUSION

7.1 Conclusion on Bio-char and Bio-char Mortar

This chapter presents the conclusions that were drawn about the physical properties of bio-char, including its density, absorption and surface area. This chapter also includes the summary of the behavior of fresh and hardened bio-char mortar, and their similarities and differences when compared to traditional cementitious materials. Last but not least, the author's current understanding of the roleof bio-char in mortar behavior and carbon sequestration potential is summarized.

Figure 7.1 Bio-char Mortar Cylinders of Each Mixture Proportion

7.1.1 Physical Properties of Bio-char

7.1.1.1 Density

The determination of the density of bio-char was necessary before the final experimental program. With the assistance of CT scan technique, the bio-char particle density was measured to be 0.7 g/ml, which was an essential value for mixture proportioning. With the value of particle density of bio-char, one could determine the cumulative volume of bio-char particles. The value of density is also essential in the algebraic process of determining the absorption of bio-char.

7.1.1.2 Absorption

The absorption and time dependency of bio-char absorption are the key issues in this study. By combining the derived mathematical relationships with experimental results, the value of bio-char absorption was calculated to be approximately 125%. The rate of absorption and the actual quantity of water being absorbed during mixing and casting however remained unknown. To deal with this problem, the term "Effective Absorption" is helpful in considering a wider range of possibility (0%, 100%, 125% and 150%) of the instantaneous absorption of bio-char, which affects the subsequent analysis, especially when volume of free water is involved. The soaking experiment indicated that bio-char "dust" has an absorption of at least 125%, and all water of 125% of bio-char's own oven-dry mass can be absorbed by itself within 7-days.

7.1.1.3 Surface Area of Bio-char

After the mixing and casting, it was identified that for some mixtures more than 1.25 gram of additional water was required per gram of bio-char to maintain flow. Through the material

characterization of bio-char, it was recognized that the bio-char "dust" used in this study consisted of particles that are about 100 times finer than sand in terms of surface area per unit mass. Due to the increasing surface area when bio-char replaces sand in the mortar mixtures, an increased paste content would be required to coat the surface of all bio-char particles. This additional paste volume would therefore require additional water, fully independent of any water absorbed into the bio-char particles, to maintain the workability. This surface area-effect was not quantified within the scope of this project.

7.1.2 Bio-char Mortar Reflects Some Behaviors of Traditional Cementitious Composite Material

There are observable trends reflect that bio-char mortar exhibits similar behavior of traditional cementitious materials. The splitting tensile strength is linearly correlated to the compressive strength, and is about 1/10 of compressive strength, which is generally expected for typical cementitious materials. It is also shown in the bio-char mortar that strength is growing as a function of time in accordance with the ACI 209 strength-time model. Other individual factors such as the influence of water-cement ratio, cement volume, free water volume (as a percentage of mortar volume) influence bio-char mortar strength as would be expected with traditional cementitious materials.

7.1.3 Function of Bio-char as an Effective Void in Lieu of a Solid

As reported in section 6.3.2.1 and 6.3.3.3, although bio-char was originally perceived as "solid" aggregate particles and as a sand-replacement, the results clearly show that increasing the amount of

bio-char consistently and predictably reduces both compressive and tensile strength as would be expected as the volume of voids (such as air voids) increases. The hypothesis was discussed in Section 6.3.4.1 and 6.3.4.2 whereby the soft bio-char particles may themselves act as effective void space rather than as "solid" aggregate particles. Regression results generally support this hypothesis, where the weighting factors suggest that bio-char volume is less detrimental to strength than either air or free-water voids, however.

7.1.4 Bio-char Mortar Sequestration Potential

As reported in Section 5.2.5, the ability of carbon sequestration of each mixture in this research project is quantified and summarized in Table 5.14 and Figure 5.17. Based on the experimental result, carbon sequestration potential increases at the expense of mortar strength decreasing exponentially. The study did not evaluate the long-term ability to inhibit or prevent oxidation of the carbon sequestered within the mortar, however. Permeability or diffusivity of oxygen (into) or CO_2 (out from) mortar remains to be studied.

7.2 Recommendation and Application

This section presents an assessment of the application of bio-char mortar in the mortar industry.

7.2.1 Interpretation of 3D Plots

Three-dimensional surface (Figure 5.13(a)) and column (Figure 5.13(b)) plots shown in Section 5.2.4 summarize the experiment data, and demonstrate how the mass fraction of bio-char to total

aggregate and curing duration influence the compressive strength of the mortar tested mixture in this study.

The plots demonstrate the bio-char mixture proportions required for a given specific strength requirement. For instance, if one requests bio-char mortar that can provide the strength of 20.7-MPa (3000-psi), the producer would advise no more than 5%-bio-char/sand replacement with at least 7-days curing.

7.2.2 Structural Material

Perhaps bio-char mortar is not a structural material per se, unless one is satisfied to only replace 5% bio-char for sand, which could in return have a compressive strength of 4000psi at the test age of 28-days, with a limited environmental advantage.

7.2.3 CLSM with Geo-type Application

Controlled Low-Strength Material (CLSM) is one possible application for bio-char mortar that requires compressive strength of 1200 psi or less. The American Concrete Institute [ACI, 2005]defines CLSM as having a compressive strength less than 8.3-MPa (1200-psi), however most current CLSM applications require unconfined compressive strengths of less than 2.1-MPa (300-psi) [ACI, 2005]. Twelve and a half percent of bio-char mixtures at the test age of 28-days meet the minimum strength requirement of 8.3-MPa (1200-psi), and meanwhile the carbon sequestration potential is zero so that the mortar is a carbon-neutral cementitious material. CLSM is typically used for non-structural purposes such as backfill or road bases as a soil substitute. Considering the

absorption ability of carbon from bio-char, the bio-char mortar might even be able to serve as in-ground filters, or as in-ground absorbers to intercept contaminants.

According to a report by National Cooperative Highway Research Program [2008], 90 percent of the 3,000 ready-mixed concrete producers in the United States produce some type of flowable fill (CLSM) [U.S. EPA, 1998]. The benefits of using CLSM as a backfill material are recognized by at least forty-two state DOTs

7.2.4 Masonry Mortar

Masonry mortar is another possible application. The minimum 28-days compressive strength required for Type M mortar is 17.2-MPa (2500-psi), for Type S mortar is 12.4-MPa (1800-psi), for Type S mortar is 5.2-MPa (750-psi) and for Type O mortar is 2.4-MPa (350-psi). [Farny, Melander, & Panarese, 2008] The mortar mixtures with less than 50% bio-char replacement satisfy the minimum strength requirement for Type O mortar.

7.3 Future Work

Based on this research, the author recommends the following as areas for future work:

- Examine the surface area effect due to the introduction of fine bio-char "dust", and how the surface area effect of bio-char influences workability of bio-char mortar.
- Determine the extent that bio-char function as a void in mortar, and quantitatively evaluate the bio-char void-effect compared to traditional air and free water void. Likewise consider

the advantages of such void volume as an absorbed-water reservoir to sustain continued hydration of the cement, promoting "Internal Curing" [Ferrara, Cortesi & Ligabue, 2015].

- Explore the minimum strength of bio-char mortar that corresponds to the mortar's ability to effectively sequester carbon. Strength may thus t be an index to the properties critical for sequestration. The possible approach to this problem is to measure oxygen permeability or diffusivity in and CO_2 permeability or diffusivity out, and associate these properties with strength of mortar.
- Explore the possibility that bio-char mortar can function as a high carbon, in-ground barriers to block or absorb contaminants (i.e., in-ground, stabilized bio-char filters)
- Explore use of bio-char mortar as a controlled low-strength material (CLSM), primarily for geotechnical applications.

Appendix A. Acquire Density Value from CT Scans

A.1 Import Image Sequences in ImageJ

To acquire density value from CT scans, ImageJ was the image processing tool that helped interpreting the image data.

First, CT scan files were imported as in image sequence.

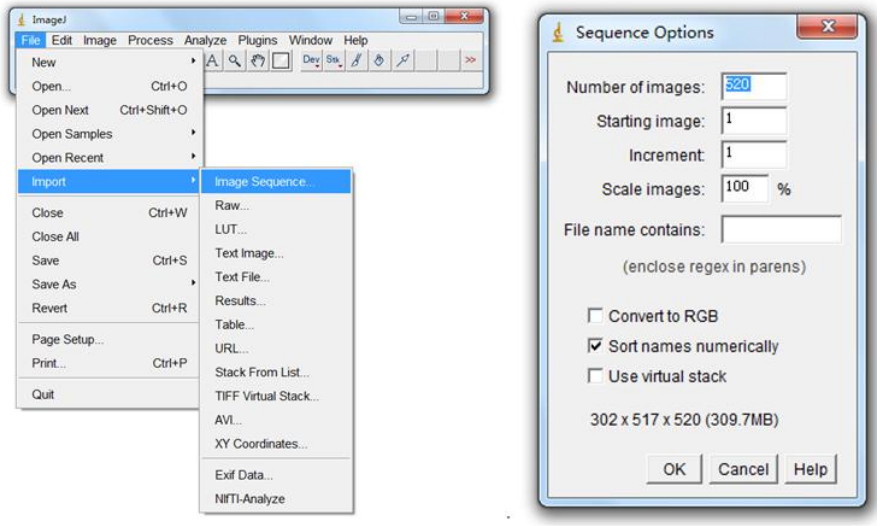

Figure A.1 Import Image Sequence

A.2 Stack to 3D Project

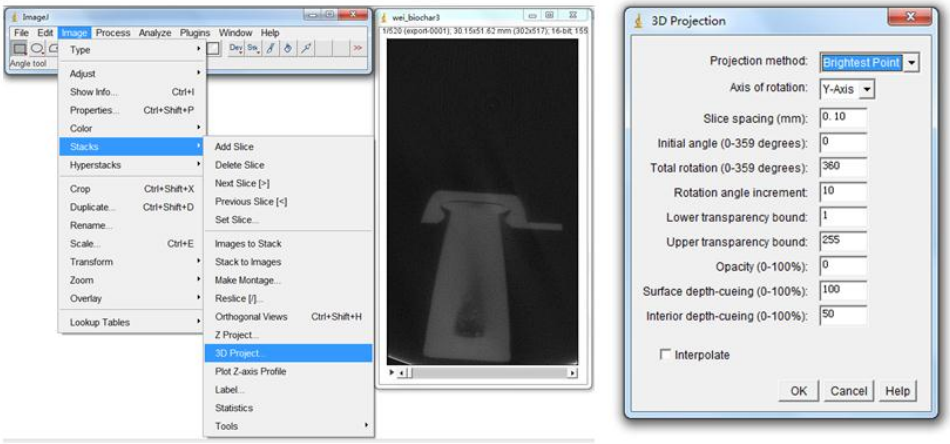

Figure A.2 Stack to 3D Project

A.3 Define and Select Target

These white dots (bio-char "dust") are the target. Use polygon selection to define the target boundary.

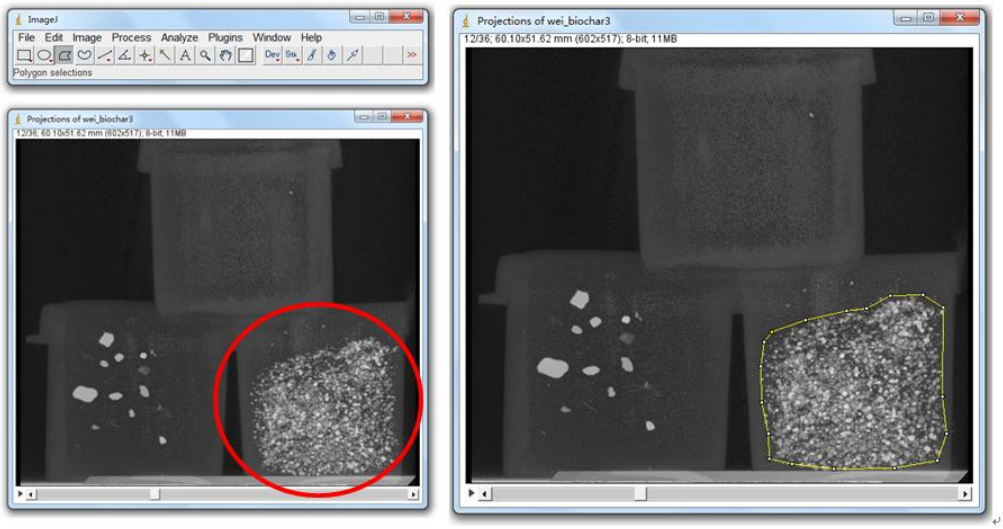

Figure A.3 Define the Target Boundary

A.4 Generate Histogram for Selected Boundary

Select 'No', only create histogram for the current image

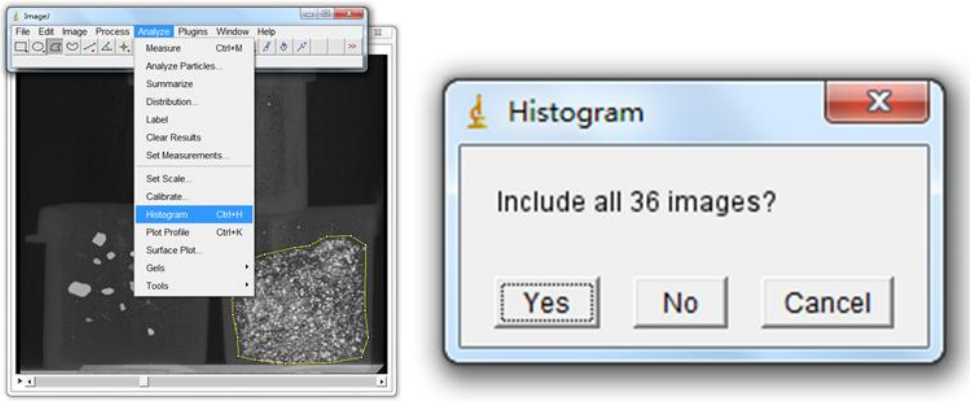

Figure A.4 Create histogram for Selected Boundary

A.5 Data Transmission

Select 'List', copy all data, and then paste to Excel

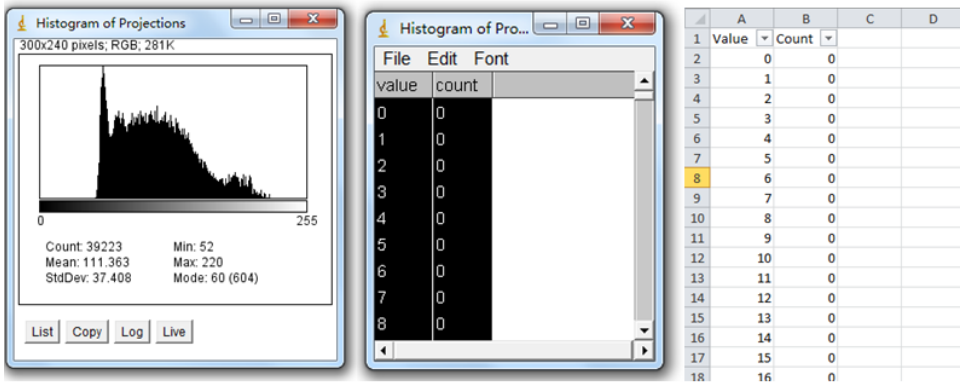

Figure A.5 Transmit Data to Excel

A.6 Filter Background Noise

The average assigned color value for background noise (the vessel that holds bio-char) is 69.25.

Filter out the color value that is below 69.25 in the excel data list

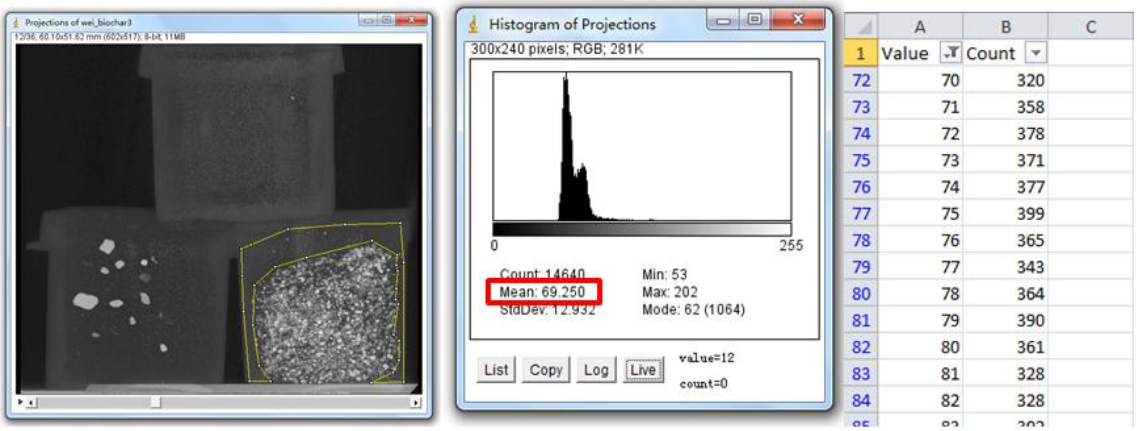

	A	B	C
1	Value	Count	
72	70	320	
73	71	358	
74	72	378	
75	73	371	
76	74	377	
77	75	399	
78	76	365	
79	77	343	
80	78	364	
81	79	390	
82	80	361	
83	81	328	
84	82	328	

Figure A.6 Filter Background Noise

A.7 Calculate Weighted Average Color Value

Calculate weighted average color value within selected boundary after filtering out the noise

$$\text{Weighted avg.} = \frac{\sum(\text{value} * \text{count})}{\sum \text{count}}$$

The weighted average color value is **119.9** within the selected boundary for current image.

A.8 Find Reference Color Value

One bone of known density was used as reference to determine the target density. The average assigned color value for reference is **189.62**.

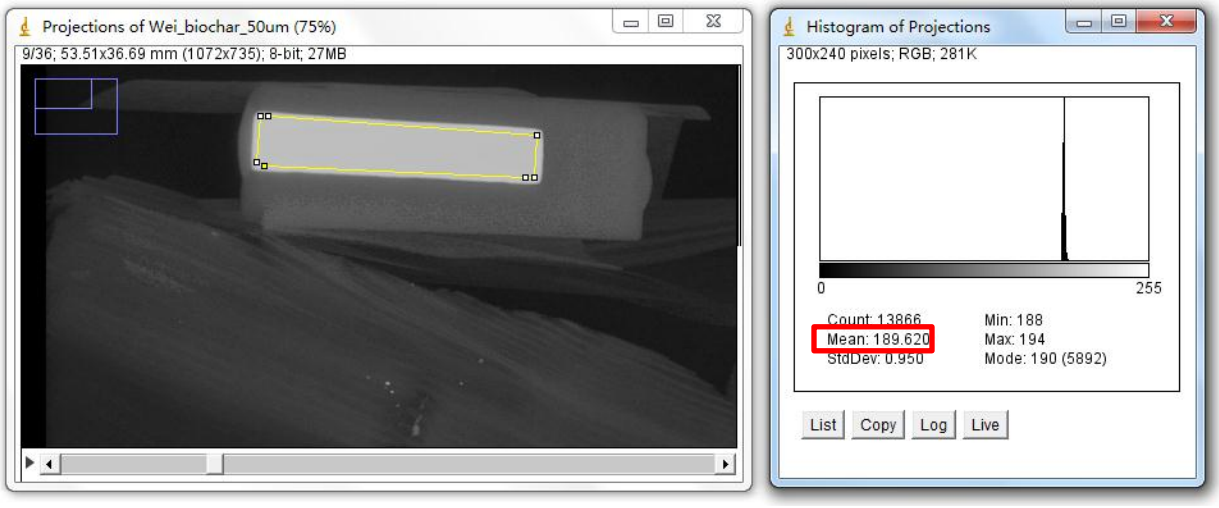

Figure A.7 Reference Scan

A.9 Calculate Target Density

Calculate Target Density of the target (bio-char "dust") within the selected boundary

The average assigned color value for reference is **189.62**.

The density of that piece of bone is **1.07 g/ml**

The weighted average color value is **119.9** within the selected boundary for current image.

And therefore, by proportion, the density of the target within the selected boundary is

1.07/189.62*119.9 = **0.68 g/ml**

A.10 Repeat

Sample from the remaining images from CT scans for more density value, then average the target density value.

Appendix B. Derivation of Absorption

B.1 Hypothesized Model of Bio-char Particle Structure

Table B.1 Hypothesized Bio-char Particle Structure

	Mass and volume of a single, solid, non-porous carbon element of the "carbon frame."
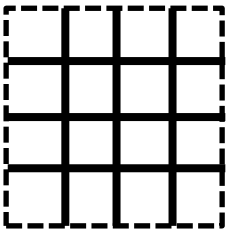	Solid lines represent the carbon structure or "frame" of the bio-char particle. The mass of the particle is the cumulative mass of the carbon frame elements. The bulk volume of the particle is represented by the dashed lines at the perimeter. The bulk volume of the particle includes the solid volume of the carbon frame elements, and the volume of empty pore space within that frame. The density of the particle as a whole, including the volume frame and all pores, is taken to be **0.70 g/ml** based on CT scan analysis.
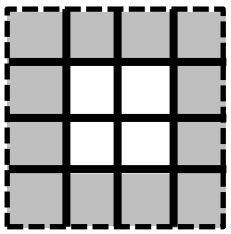	Void spaces shaded in gray represent pores that are accessible from the exterior surface of the particle, often called the permeable pores. Such voids can be 0 to 100% full of liquids or gases. At oven-dry state (OD) they are full of air. At saturated state they are full of water. At damp or wet state they are intermediate.

Void space shaded in white represents pores that are NOT accessible to gases and liquids from the exterior surface of the particle. Such voids are always considered to be 100% full of air, regardless of exposure to moisture.

The 'Absorption' of a particle is defined as the mass of water contained in the 'permeable' pores when saturated, divided by the oven-dry mass of the particle.

$$\text{Absorption} = \frac{W_{\text{absorbed water at saturation}}}{W_{\text{OD particle}}}$$

The volume of absorbed water at saturation = "Absorption of particle" × "Mass of OD particle" / "Density of water".

$$V_{\text{absorbed water}} = \frac{\text{Absorption} \times W_{\text{OD particle}}}{\rho_{\text{water}}}$$

The moisture content of a particle is defined as the mass of water contained in the permeable pores at the current condition (may or may not be saturated), divided by the oven-dry mass of the particle.

$$\text{Moisture content} = \frac{W_{\text{water in permeable pores at current condition}}}{W_{\text{OD particle}}}$$

B.2 Define Variables

Table B.2 Variable Definition

Symbol	Definition	Explanation
x	Absorption of bio-char	This is a particle property. It is a characteristic of the assembly of the particle.
y	Frame density of bio-char	This is a characteristic of the solid component of the particle. Multiple configurations at various values of absorption of particles could be constructed from the same carbon structure. A particle could have a high or low absorption with the same frame density.
y'	Specific gravity of bio-char frame; $y' = y/\varrho_{water}$	The ratio between frame density of bio-char and density of water
k	V_{pore}/V_{frame},	This is the ratio between V_{pore} and V_{frame}, where V_{pore} is the volume of total pore space in the particle, both 'permeable' pores and 'impermeable' pores included; Vf_{rame} is the volume of carbon frame itself in the particle
p	$V_{permeable\ pore}/V_{pore}$	This is the ratio between $V_{permeable\ pore}$ and V_{pore}, where $V_{permeable\ pore}$ is the volume of permeable pore space only in the particle

α	Particle density (bulk density) of OD bio-char, $W_{frame}/(V_{frame}+V_{pore})$	The value of α is provided by CT scan; α = 0.70 g/ml
α'	Specific gravity of bio-char particle; $\alpha' = \alpha / \varrho_{water}$	The ratio between particle density of bio-char and density of water

B.3 Derivation from Definition

The mass unit in the following derivation is gram. The volume unit is milliliter. The density unit is gram/milliliter.

α is the particle density of OD bio-char:

$$\alpha = \frac{W_{frame}}{V_{frame} + V_{pore}} = \frac{\frac{W_{frame}}{V_{frame}}}{1 + \frac{V_{pore}}{V_{frame}}}$$

$$\alpha = \frac{y}{1 + k} \quad \text{Eq. (1)}$$

x is the absorption of bio-char:

$$x = \frac{W_{absorbed\ water\ at\ saturation}}{W_{OD\ particle}} = \frac{W_{water}}{W_{frame}}$$

$$x = \frac{\rho_{water} \times V_{permeable\ pore}}{\rho_{frame} \times V_{frame}} = \frac{\rho_{water}}{\rho_{frame}} \times \frac{\frac{V_{permeable\ pore}}{V_{pore}}}{\frac{V_{frame}}{V_{pore}}}$$

$$x = \frac{p}{y' k^{-1}} \quad \text{Eq. (2)}$$

Combine Eq.(1) and Eq.(2):

$$\begin{cases} \alpha = \dfrac{y}{1+k} \\ x = \dfrac{p}{y'k^{-1}} \end{cases}$$

$$y = \frac{p\alpha}{p - x\alpha} \quad \text{Eq. (3)}$$

B.4 Derivation from Experiment Data

From 8 sets of bio-char mixtures, a unique set of data including mass of batched material, mortar density and air content percentage. These data led to the relationship between x (absorption) and α (particle density).

The algebraic derivation is demonstrated by using the data set of 5% bio-char-mortar mixture as an example. The data is from Chapter 4 of the thesis.

Table B.3 Summary of 5% Bio-char-mortar Mixture

	Mass (g)	Density (g/ml)	Volume (ml)
Cement	7700	3.15	2444
Sand (SSD)	20085	2.66	7551
Bio-char (OD)	1035	α	1035/α
Water	5334	1	5334-1035x
Air	-	-	5.3%ΣV
Mortar mixture	34154	2.24	ΣV

Summing the volume column:

$$2444 + 7551 + \frac{1035}{\alpha} + 5334 - 1035x + 5.3\%\Sigma V = \Sigma V$$

$$15329 + \frac{1035}{\alpha} - 1035x = 94.7\%\Sigma V \quad \text{Eq. (4)}$$

Also,

$$\Sigma V = \frac{W_{\text{batched material}}}{\rho_{\text{mortar}}} = \frac{34154}{2.24} = 15247\text{ml}$$

Simplify Eq.(4), and input the value of ΣV,

$$\frac{1}{\alpha} - x = -0.852 \quad \text{Eq. (5)}$$

Eq. (5) is derived from the experiment data of 5% bio-char-mortar mixture. Each group of mixture with different proportion of bio-char generates a unique equation in such form:

$$c = \frac{1}{\alpha} - x$$

c is a constant determined by the unique set of data of each mixture, including mass of batched material, mortar density and air content percentage. For 8 sets of bio-char-mortar mixture, there are 7 different value of c.

Table B.4 Value of c

Bio-char as a percentage of total aggregate	c
0%	-
5%	-0.852
12.5%	0.003
20%	0.181
33.3%	0.174
50%	0.311
75%	0.298
100%	0.410

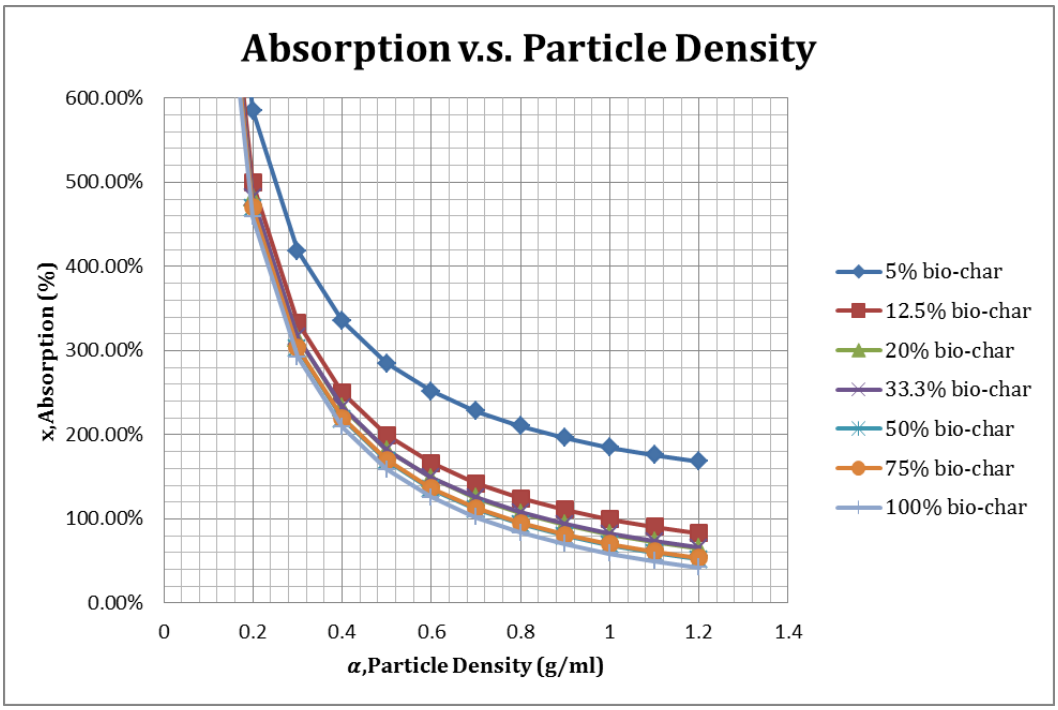

Figure B.1 Plot of c=1/α-x

The value of α is provided by CT scan: α = 0.70 g/ml, and therefore the value of x can be calculated for each mixture proportion.

Table B.5 Value of α

Bio-char as a percentage of total aggregate	x
0%	-
5%	228%
12.5%	143%
20%	125%
33.3%	125%
50%	112%
75%	113%
100%	102%

The average value of bio-char absorption of 7 values is 160%.

The average value of bio-char absorption after excluding the outlier of 5% and 100% bio-char-mortar mixture is 125%.

Appendix C. Developing Vibration System

The vibration system includes two parts:

- Vibration table

  The machine consists of a flat top table and motors inside. It allows periodic and repetitive mechanical vibration.

- Vibration box

  The vibration box was tailor-made to hold those 2" by 4" cylindrical molds. It constituted 2 pieces of plywood that was drilled with 16 circular holes with a diameter of 2" and 4 short corner columns. The diameter of the holes on the top plywood was made to be slightly more than 2 inches. These holes on the top were designed to make the insertion of cylindrical molds convenient, and at the same time it does not make the cylinder unstable and tilting during the vibration.

  The vibration box was attached to the vibration table by 2 c-clamps. The clamps were located diagonally to keep the vibration box still to the vibration table during vibration movement.

  The vibration protocol described in the section 7, chapter 4 was tested through the trial runs. The mortar after mixing from one single batch was placed in the cylinder molds. The cylinder molds were vibrated with the procedure described in the Section 8, Chapter 4. The mass of the mortar in the cylinder molds was weighed, and the result is displayed as follow.

Table C.1 Result of Vibration Protocol Test Run

#	Mass of Cylinder (g)	Mass of Cylinder and Mortar (g)	Mass of Mortar (g)
1	26.7	507.3	480.6
2	27.1	507.2	480.1
3	27.1	503.9	476.8
4	27.1	509.7	482.6
5	26.7	505.2	478.5
6	27.1	503.8	476.7
7	27.1	502.5	475.4
8	26.8	504	477.2
9	27.0	507.5	480.5
10	27.1	505.6	478.5
11	26.8	500.6	473.8
12	27.1	505	477.9
13	27.1	507.2	480.1
14	27.1	510.7	483.6
15	26.8	505	478.2
16	27.2	508.1	480.9

In total 16 counts of samples, the average mass of mortar was 478.8 gram. The standard deviation of samples was 2.585, and the covariance was 0.54%, which suggests the mass variance of mortar in the cylinders caused by vibration was minimal.

Appendix D. Validity of Air Indicator Conversion Table

The conversion table from the operation manual for instrument indicates that for mortar (without coarse aggregate), every one stem reading implies 1.78% air content by volume of mortar.

A set of measurements was conducted to verify the accuracy of the conversion table.

The dimension of air indicator was measured by a caliper. The diameter of the stem was 3.85 mm, and the depth per reading was 4.45 mm, and therefore the volume per reading was

$$\frac{1}{4} \times \pi \times 3.85^2 \times 4.45 = 51.8\, mm^3$$

The diameter of the cup was 19.81 mm, and the depth of the cup was 11.63 mm, and therefore the volume per reading was

$$\frac{1}{4} \times \pi \times 19.81^2 \times 11.63 = 3582.8\, \text{mm}^3$$

The air percentage per reading by measurement of dimension of air indicator was

$$\frac{51.8}{3582.8} = 1.45\ \%$$

Another alternative measurement was conducted by filling both stem and cup with water. The mass of water that was held in 11 readings was 0.8 gram, and therefore 0.073 gram per reading. The mass of water that was held in the cup was 3.6 gram.

The air percentage per reading by measurement of mass of water was

$$\frac{0.073}{3.6} = 2.03\ \%$$

The 1.78% air content per reading was in the range of the verification measurement (1.45% and 2.03%).

REFERENCE

ASTM C33, "Standard Specification for Concrete Aggregates", ASTM C33/C33M-16, Annual Book of ASTM Standard, vol.4.02, American Society of Testing and Materials, 2016

ASTM C39, "Standard Test Method for Compressive Strength of Cylindrical Concrete Specimens", ASTM C39/C39M-16, Annual Book of ASTM Standard, vol.4.02, American Society of Testing and Materials, 2016

ASTM C109, "Standard Test Method for Compressive Strength of Hydraulic Cement Mortars (Using 2-in. or [50-mm] Cube Specimens)", ASTM C109/C109M-16a, Annual Book of ASTM Standard, vol.4.01, American Society of Testing and Materials, 2016

ASTM C128 "Standard Test Method for Relative Density (Specific Gravity) and Absorption of Fine Aggregate", ASTM C128-15, Annual Book of ASTM Standard, vol.4.02, American Society of Testing and Materials, 2016

ASTM C136 "Standard Test Method for Sieve Analysis of Fine and Coarse Aggregates", ASTM C136/C136M-14, Annual Book of ASTM Standard, vol.4.02, American Society of Testing and Materials, 2016

ASTM C150 "Standard Specification for Portland Cement", ASTM C150/C150M-16, Annual Book of ASTM Standard, vol.4.01, American Society of Testing and Materials, 2016

ASTM C192 "Standard Practice for Making and Curing Concrete Test Specimens in the Laboratory", ASTM C192/C192M-16, Annual Book of ASTM Standard, vol.4.02, American Society of Testing and Materials, 2016

ASTM C230 "Standard Specification for Flow Table for Use in Tests of Hydraulic Cement", ASTM C230/C230M-14, Annual Book of ASTM Standard, vol.4.01, American Society of Testing and Materials, 2016

ASTM C305 "Standard Practice for Mechanical Mixing of Hydraulic Cement Pastes and Mortars of Plastic Consistency", ASTM C305-14, Annual Book of ASTM Standard, vol.4.01, American Society of Testing and Materials, 2016

ASTM C496 "Standard Test Method for Splitting Tensile Strength of Cylindrical Concrete Specimens", ASTM C496/C496M-11, Annual Book of ASTM Standard, vol.4.02, American Society of Testing and Materials, 2016

ASTM C1231 "Standard Practice for Use of Unbonded Caps in Determination of Compressive Strength of Hardened Cylindrical Concrete Specimens", ASTM C1231/C1231M-15, Annual Book of ASTM Standard, vol.4.02, American Society of Testing and Materials, 2016

ASTM C1437 "Standard Test Method for Flow of Hydraulic Cement Mortar", ASTM C1437-15, Annual Book of ASTM Standard, vol.4.01, American Society of Testing and Materials, 2016

American Concrete Institute Committee 229, (2005), "Controlled Low-Strength Materials"

Peyvandi, A., Soroushian, P., and Nassar, R. (2014) "Recycled Glass Concrete, Milled Waste Glass Used in Mixtures for Flatwork Construction on the Campus of Michigan State University", Concrete International, vol 35, issue 1, pp29-32

Bennett, D., (2010), Sustainable Concrete Architecture, RIBA publishing, London

Brown, R. A., Kercher, A. K., Nguyen, T.H., Nagle, D. C. and Ball, W.P. (2006), "Production and characterization of synthetic wood chars for use as surrogates for natural sorbents", Organic Geochemistry, vol 37, pp321-333

Byrne, C. E. and Nagle, D. C., (1997), "Carbonization of Wood for Advanced Materials Applications", Carbon, vol 35, issue 2, pp259-266

Choi, W.C., Yun, H.D., and Lee, J. Y., (2012), "Mechanical Properties of Mortar Containing Bio-char from Pyrolysis", Journal of the Korea Institute for Structural Maintenance and Inspection, vol 16, issue 3, pp67-74

Emmett, P. H. (1948), "Adsorption and Pore-size Measurements on Charcoal and Whetlerites", Chemical Reviews, vol 43, pp69–148

Environmental Information Administration, (2008), "EIA Annual Energy Outlook with Projections to 2030", DOE/EIA-0383

Farny, J.A., Melander, J.M., and Panarese, W.C., (2008), Concrete Masonry Handbook for Architects, Engineers, Builders, sixth edition, Portland cement association, Illinois

Ferrara;L, Cortesi,L. Ligabue,O, (2015), "Internal Curing of Concrete with Presaturated LWA: a Preliminary Investigation", ACI Special Publication 305, Paper No. 12

Froeschle, L. M., (1999), "Environmental Assessment and Specification of Green Building Materials", The Construction Specifier, p.53

Glaser, B., Haumaier, L., Guggenberger,G. And Zech,W. (2001), "The Terra Preta phenomenon: A model for sustainable agriculture in the humid tropics", Naturwissenschaften, vol 88, pp37–41

Hover, K. C., (2015), "Class Material of CEE6750 Concrete Materials and Construction", New York

International Biochar Initiative, "IBI Biochar Certification Program Manual", World Wide Web: http://www.biochar-international.org/sites/default/files/IBI_Biochar_Certification_Program_Manual_V2.1_Final.pdf; last access: April 2016

Jankowska, H., Swiatkowski, A. and Choma, J. (1991), "Active Carbon", Ellis Horwood, New York

Kim J. J, (1998), "Sustainable Architecture Module: Introduction to Sustainable Design", National Pollution Prevention Center for Higher Education, Ann Arbor MI

Laine, J., Simoni, S. and Calles, R. (1991), "Preparation of Activated Carbon from Coconut Shell in a Small Scale Concurrent Flow Rotary Kiln", Chemical Engineering Communications, vol 99, pp15–23

Lehmann, J., and Joseph, S., (2009), Bio-char for Environmental Management Science and Technology, Earthscan

Mehta, P.K., and Monteiro, P.J.M., (2006), Concrete, Microstructure, Properties and Materials, McGraw-Hill Inc. New York

Mindess, S., and Young, J.F., (1981), Concrete, Prentice-hall, Inc., New Jersey

Morley, J. (1927), "Following through with Grass Seeds", The National Greenkeeper, vol 1, no 1, p15

Najjar, W.S., Aderhold, H.C., and Hover, K.C., (1986), "The Application of Neutron Radiography to the Study of Microcracking in Concrete, Cement, Concrete, and Aggregates", CCAGDP Vol. 8, No. 2, pp. 103-109

National Cooperative Highway Research Program, (2008), "Development of a Recommended Practice for Use of Controlled Low-Strength Material in Highway Construction", NCHRP Report 597

National Ready Mixed Concrete Association, (2008), "Concrete CO2 Fact Sheet", NRMCA Publication Number 2PCO2

Neville, A.M., (1981), Properties of Concrete, Pitman Publishing Inc., Great Britain

Nisbet, M. A, Marceau, M. L., and Van Geem, M. G.,(2003), "Environmental Life Cycle Inventory of Portland Cement Concrete", PCA R&D Serial No. 2137a, a report on Concrete: Sustainability and Life Cycle, PCA CD033

Oberlin, A. (2002), "Pyrocarbons – Review", Carbon, vol 40, pp7–24

Organic Material Review Institute, "OMRI Policy Manual: Policies for the Review of Products Intended for Use in Certified Organic Production or Processing", World Wide Web: http://www.omri.org/sites/default/files/app_materials/16PolicyManual_pubversion1F.pdf; last access: April 2016

O'Brien, M., Wallbaum, H., and Bleischwitz, R., (Eds.), (2011), "Eco-Innovation Observatory Thematic Report", World Wide Web: http://wupperinst.org/uploads/tx_wupperinst/EIO_WP4_ResEff_Constr_Report.pdf; last access: April 2016

Ozyildirim, C., (2010), "Use of Slag Cement for Improved Durability in Virginia Department of Transportation Structures", Concrete International, Special Publication, vol 269, pp49-56

Pastor-Villegas, J., Pastor-Valle, J. F., Meneses Rodriguez, J. M., and Garcia Garcia, M., (2006), "Study of Commercial Wood Charcoals for the Preparation of Carbon Adsorbents", Pyrolysis, J. Anal., pp103-108

Schmidt, M.W. I. and Noack, A.G., (2000), "Black Carbon in Soils and Sediments: Analysis, Distribution, Implications, and Current Challenges", Global Biogeochemical Cycles, vol 14, pp777–794

Slag Cement Association, (2002), "Slag Cement and Fly Ash"

Spiegel, R., and Meadows, D., (1999), Green Building Materials: A Guide to Product Selection and Specification, John Wiley & Sons, Inc., New York

Sustainable Concrete and Carbon Storage Group, Princeton University, World Wide Web: http://white.princeton.edu/research/materials.html; last access: April 2016

Technical Service Division, Department of Transportation, State of Minnesota, (1968), "Concrete Manual", Office of Engineering Standards, Minnesota

UNFCCC COP9 Report, (2004), "Delivering the Kyoto baby, Refocus", International Renewable Energy Magazine, 52–53.

U.S. Department of Agriculture, "USDA Bio-based Product Certification Step", World Wide Web: http://www.biopreferred.gov/BioPreferred/faces/pages/DocumentBrowser.xhtml; last access: April 2016

U.S. Environmental Protection Agency (EPA), (1995), Complication of Air Pollutant Emission Factors, Volume 1, Fifth Edition, CH 11.6

U.S. Environmental Protection Agency (EPA), (1998), "Back Document for Proposed CPG III and Draft RMAN III", EPA Report EPA530-R-98-003, Washington, D.C., 31 p.

Wildman, J. and Derbyshire, F., (1991), "Origins and Functions of Macroporosity in Activated Carbons from Coal and Wood Precursors", Fuel, vol 70, pp655–661

Woolf, D., Lehmann, J., Fisher, E. M, and Angenent, L.T., (2014), "Biofuel from Pyrolysis in Perspective: Trade-offs between Energy Yields and Soil-Carbon Additions", Environ. Sci. Technol., 48 (11), pp 6492–6499